CANADIAN THESES ON MICROFICHE

I.S.B.N.

THESES CANADIENNES SUR MICROFICHE

National Library of Canada
Collections Development Branch

Canadian Theses on
Microfiche Service

Ottawa, Canada
K1A 0N4

Bibliothèque nationale du Canada
Direction du développement des collections

Service des thèses canadiennes
sur microfiche

NOTICE

The quality of this microfiche is heavily dependent upon the quality of the original thesis submitted for microfilming. Every effort has been made to ensure the highest quality of reproduction possible.

If pages are missing, contact the university which granted the degree.

Some pages may have indistinct print especially if the original pages were typed with a poor typewriter ribbon or if the university sent us a poor photocopy.

Previously copyrighted materials (journal articles, published tests, etc.) are not filmed.

Reproduction in full or in part of this film is governed by the Canadian Copyright Act, R.S.C. 1970, c. C-30. Please read the authorization forms which accompany this thesis.

THIS DISSERTATION
HAS BEEN MICROFILMED
EXACTLY AS RECEIVED

AVIS

La qualité de cette microfiche dépend grandement de la qualité de la thèse soumise au microfilmage. Nous avons tout fait pour assurer une qualité supérieure de reproduction.

S'il manque des pages, veuillez communiquer avec l'université qui a conféré le grade.

La qualité d'impression de certaines pages peut laisser à désirer, surtout si les pages originales ont été dactylographiées à l'aide d'un ruban usé ou si l'université nous a fait parvenir une photocopie de mauvaise qualité.

Les documents qui font déjà l'objet d'un droit d'auteur (articles de revue, examens publiés, etc.) ne sont pas microfilmés.

La reproduction, même partielle, de ce microfilm est soumise à la Loi canadienne sur le droit d'auteur, SRC 1970, c. C-30. Veuillez prendre connaissance des formules d'autorisation qui accompagnent cette thèse.

LA THÈSE A ÉTÉ
MICROFILMÉE TELLE QUE
NOUS L'AVONS REÇUE

NL-339 (r. 82/08)

Canada

National Library
of Canada

Canadian Theses Division

Ottawa, Canada
K1A 0N4

Bibliothèque nationale
du Canada

Division des thèses canadiennes

0-315-06129-4

54049

PERMISSION TO MICROFILM — AUTORISATION DE MICROFILMER

- Please print or type — Écrire en lettres moulées ou dactylographier

Full Name of Author — Nom complet de l'auteur
KAROL EDWARD SZKLARZ

Date of Birth — Date de naissance FEB. 12, 1952	Country of Birth — Lieu de naissance CANADA

Permanent Address — Résidence fixe
76 FLINT CRES.
ST. ALBERT, ALTA.
T8N 1Y8

Title of Thesis — Titre de la thèse
SEGREGATION AND SOLUBILITY
IN FERROMAGNETIC IRON

University — Université
UNIVERSITY OF ALBERTA

Degree for which thesis was presented — Grade pour lequel cette thèse fut présentée
Ph. D.

Year this degree conferred — Année d'obtention de ce grade 1981	Name of Supervisor — Nom du directeur de thèse M. L. WAYMAN

Permission is hereby granted to the NATIONAL LIBRARY OF CANADA to microfilm this thesis and to lend or sell copies of the film.

The author reserves other publication rights, and neither the thesis nor extensive extracts from it may be printed or otherwise reproduced without the author's written permission.

L'autorisation est, par la présente, accordée à la BIBLIOTHÈQUE NATIONALE DU CANADA de microfilmer cette thèse et de prêter ou de vendre des exemplaires du film.

L'auteur se réserve les autres droits de publication; ni la thèse ni de longs extraits de celle-ci ne doivent être imprimés ou autrement reproduits sans l'autorisation écrite de l'auteur.

Date August 14, 1981	Signature K. E. Szklarz

NL-91 (4/77)

THE UNIVERSITY OF ALBERTA

SEGREGATION AND SOLUBILITY IN FERROMAGNETIC IRON

by

© KAROL E. SZKLARZ

A THESIS
SUBMITTED TO THE FACULTY OF GRADUATE STUDIES AND RESEARCH
IN PARTIAL FULFILMENT OF THE REQUIREMENTS FOR THE DEGREE
OF DOCTOR OF PHILOSOPHY
IN
METALLURGY

DEPARTMENT OF MINERAL ENGINEERING

EDMONTON, ALBERTA
FALL 1981

THE UNIVERSITY OF ALBERTA

RELEASE FORM

NAME OF AUTHOR KAROL E. SZKLARZ

TITLE OF THESIS SEGREGATION AND SOLUBILITY IN FERROMAGNETIC IRON

DEGREE FOR WHICH THESIS WAS PRESENTED DOCTOR OF PHILOSOPHY

YEAR THIS DEGREE GRANTED FALL 1981

Permission is hereby granted to THE UNIVERSITY OF ALBERTA LIBRARY to reproduce single copies of this thesis and to lend or sell such copies for private, scholarly or scientific research purposes only.

The author reserves other publication rights, and neither the thesis nor extensive extracts from it may be printed or otherwise reproduced without the author's written permission.

(SIGNED) K. E. Szklarz

PERMANENT ADDRESS:

76 Flint Cres.
St. Albert, Alberta

DATED August 4 1981

THE UNIVERSITY OF ALBERTA

FACULTY OF GRADUATE STUDIES AND RESEARCH

The undersigned certify that they have read, and recommend to the Faculty of Graduate Studies and Research, for acceptance, a thesis entitled SEGREGATION AND SOLUBILITY IN FERROMAGNETIC IRON submitted by KAROL E. SZKLARZ in partial fulfilment of the requirements for the degree of DOCTOR OF PHILOSOPHY in METALLURGY.

M L Wayman

Supervisor

B M Patchett

R. F. Egerton

S.A. Bradford

G C Weatherly

External Examiner

Date August 4, 1981

DEDICATION

To Marie, without whom this work would not be possible.

ABSTRACT

The effect of ferromagnetism on intergranular segregation and solid solubility in Fe was theoretically investigated and the solid solubility of P in alpha Fe was experimentally investigated.

For the solubility measurements, a special apparatus was constructed to produce high purity iron phosphide from elemental iron and phosphorus. The iron phosphide and pure iron were vacuum arc-melted to produce high purity alpha Fe-P alloys. These alloys were aged at temperatures between 800 C and 500 C and EPMA techniques were used to determine the equilibrium solubility of P. The results agreed with recently published data by Nishizawa et al. Nishizawa's explanation of anomalous solid solubility in alpha iron binaries below the Curie temperature by considering non-linear magnetic components of thermodynamic functions was confirmed.

In the theoretical part of the work empirical magnetic components of thermodynamic functions for alpha iron were calculated from data in the literature. These thermodynamic functions were applied to confirm Nishizawa's predicted behavior of solute solubility in an alpha iron binary. The formalism was then extended to predict equilibrium vacancy concentration in alpha iron. In addition Guttmann's approach to grain boundary solute segregation for alpha iron binaries and ternaries was treated using magnetic components. It is thereby predicted that most non-magnetic solute in iron is

expected to segregate to grain boundaries in larger amounts at higher temperatures than predicted by a purely non-magnetic analysis. Unexpected magnetic transitions within the grain boundary are also predicted to occur.

A consequence of this treatment is that because of its ferromagnetic nature, alpha iron is more susceptible to intergranular segregation and thus intergranular embrittlement than an equivalent non-magnetic alloy.

ACKNOWLEDGEMENTS

The author is indebted to Dr. M. L. Wayman for providing guidance and encouragement over the span of my graduate studies.

My thanks to Dr. F. H. Vitovec and Dr. T. Etsell for their advice and comments on problems encountered in this research. I would also like to extend my appreciation to Mr. T. Forman, Mr. G. Cameron, Mr. B. Konzuk, Mr. B. Snider, Ms. C. Barker and Ms. F. Sutherland for their able technical assistance.

This work was supported by Grant #A6074 to Dr. M. L. Wayman from the Natural Sciences and Engineering Research Council of Canada.

The microprobe facilities in the Department of Geology at the University of Alberta are partially supported by Grant #A4254 to Dr. D. G. Smith from the Natural Sciences and Engineering Research Council of Canada.

Table of Contents

Chapter Page

1. INTRODUCTION 1

2. BACKGROUND 7

  2.1 The Development of Segregation Theory 7

  2.2 The Solubility of Phosphorus in alpha Iron 13

3. EXPERIMENTAL PROCEDURES 16

  3.1 The Production of 'Pure' alpha Fe-P Alloys 16

    3.1.1 Sources of Iron and Phosphorus 16

    3.1.2 Production of an Iron Phosphide 18

    3.1.3 Production of Final alpha Fe-P Alloys 26

  3.2 Heat Treatment of alpha Fe-P Alloys 31

  3.3 Metallographic Specimen Preparation, Examination, and Chemical Analysis 33

  3.4 Theoretical Techniques 43

    3.4.1 Equipment 43

    3.4.2 Numerical Analysis 43

4. RESULTS AND DISCUSSION 47

  4.1 The Free Energy Function for alpha Iron 47

  4.2 The alpha Fe-X Solid Solution 57

  4.3 Chemical Potentials of alpha Fe-X Solid Solutions 64

  4.4 Limit of Solubility for X in alpha Fe-X Solid Solution 74

    4.4.1 Alpha Fe-X Solid Solutions 74

    4.4.2 The Limit of Solubility For P in alpha Fe-P 84

  4.5 Vacancy Concentrations in alpha Iron 89

    4.5.1 A Hypothetical Iron Solution 89

4.5.2 Predicted Vacancy Concentrations from alpha Iron Self-Diffusion Data 91

4.6 The Thermodynamics of Equilibrium Grain Boundary Segregation 94

4.7 Grain Boundary Segregation in Binary alpha Fe-X Solid Solutions 102

4.7.1 Case I: Grain Boundary Free Energy Without Magnetic Terms 102

4.7.2 Case II: Segregation when Grain boundaries may be Ferromagnetic 114

4.8 The Magnetic State of the Boundary Phase 126

4.9 The Thermodynamics of Dilute alpha Fe-M-X Solid Solutions 129

4.10 Chemical Potentials For Alpha Fe-M-X 133

4.11 The Solid solubility of X in Alpha Fe-M-X Solid Solutions 136

4.12 Vacancy Concentration in alpha Fe-X 150

4.13 Grain Boundary Segregation in Alpha Fe-M-X Solid Solutions 154

4.13.1 Case I: Grain Boundary Free Energy Without Magnetic Terms 157

4.13.2 Case II: Grain Boundaries May Be Ferromagnetic 164

4.14 Predicted Grain Boundary States in Certain Ternary Systems 172

4.15 Non-linear Changes in Curie Temperature 179

4.16 A Calculated Magnetic Parameter 181

4.17 Applicability of the model 183

5. CONCLUSIONS 186

6. FUTURE WORK 189

BIBLIOGRAPHY 191

APPENDIX 1 195

APPENDIX 2 198

List of Tables

Table		Page
3.1	Compositions of 'pure' irons used (in wt%)	19
3.2	Ageing temperature and times for final samples	32
4.1	The magnetic thermodynamic functions of alpha iron [40]	51
4.2	Magnetic parameters of solute in alpha iron calculated from solubility data [44]	78
4.3	Experimental results of bulk phosphorus content	85
4.4	Interaction parameters for M-P calculated from solubility data [64]	143

List of Figures

Figure Page

2.1 The solubility of phosphorus in alpha iron 15

3.1 A sketch of the experimental apparatus for producing iron phosphides 22

3.2 A schematic of experimental procedures used in alloy production 27

4.1 The magnetic heat capacity of alpha iron. 53

4.2 The magnetic entropy of alpha iron (+ denotes data [40]) 55

4.3 The magnetic enthalpy and Gibbs free energy of alpha iron (+ denotes data [40]) 56

4.4 The shift in the magnetic free energy of alpha iron...61

4.5 The magnetic chemical potential of Fe in alpha Fe-X. 69

4.6 The effect of magnetic parameter on the chemical potential of Fe in alpha Fe-X (A = -2000 K, B = -1000 K, C = 0 K, D = 1000 K). 70

4.7 The effect of the magnetic parameter on the chemical potential of X in alpha Fe-X (A = -2000 K, B = -1000 K, C = 0 K, D = 1000 K). ...72

4.8 The effect of bulk solute concentration on the chemical potential of X in alpha Fe-X (A = 0.001, B = 0.01, C = 0.1). 73

4.9 A schematic of free energy for two phases in equilibrium. 75

4.10 The effect of the magnetic parameter on the free energy of solution (A = -2000 K, B = -1000 K, C = 0 K, D = 1000 K). 79

4.11 Calculated Curie temperatures for various alpha Fe-X binaries 80

4.12 The effect of magnetic parameter on predicted solid solubility in Fe (A = -2000 K, B = -1000 K, C = paramagnetic, D = 0 K, E = 1000 K). 82

4.13 Examples of solid solubility for X in alpha Fe. 83

Figure Page

4.14 An example concentration profile from T550 86

4.15 The experimental limit of solubility for P in alpha Fe (□ denotes data). 87

4.16 Experimental self-diffusion data for alpha Fe [53-56,respectively]. 92

4.17 Predicted magnetic free energy of vacancy formation in alpha Fe. 95

4.18 Predicted equilibrium vacancy concentration in alpha Fe. 96

4.19 Typical McLean segregation curves. 101

4.20 Free energy of segregation for P in alpha Fe (dilute bulk approximation). 105

4.21 The effect of the segregation free energy on intergranular solute concentration (A = non-magnetic, B = magnetic). 107

4.22 Predicted grain boundary solute concentrations for the alpha Fe-P system according to case I. 109

4.23 The magnetic component of the segregation free energy according to Case I (A = 1000 K, B = 0 K, C = -1000 K, D = -2000 K). 111

4.24 Predicted grain boundary solute concentration according to Case I (A = 1000 K, B = 0 K, C = -1000 K, D = -2000 K). 112

4.25 The effect of bulk solute content on predicted grain boundary solute concentration according to Case I (A = 0.00001, B = 0.0001, C = 0.001, D = 0.01). 113

4.26 The magnetic component of segregation free energy according to Case II (A = 1000 K, B = 0 K, C = -1000 K, D = -2000 K). 118

4.27 Predicted grain boundary solute concentrations according to Case II (A = 1000 K, B = 0 K, C = -1000 K, D = -2000 K). 120

4.28 The effect of bulk solute content on the magnetic segregation free energy according to Case II (A = 0.00001, B = 0.0001, C = 0.001, D = 0.01). ...121

Figure Page

4.29 The effect of bulk solute content on predicted grain boundary solute concentrations according to Case II (A = 0.00001, B = 0.0001, C = 0.001, D = 0.01). 122

4.30 The effect of the non-magnetic segregation free energy on the magnetic segregation free energy according to Case II (A = 20 KJ/mole, B = 30 KJ/mole, C = 40 KJ/mole, D = 50 KJ/mole). ..124

4.31 The effect of the non-magnetic segregation free energy on the grain boundary solute concentration according to Case II (A = 20 KJ/mole, B = 30 KJ/mole, C = 40 KJ/mole, D = 50 KJ/mole). ..125

4.32 Case I and Case II segregation curves for the alpha Fe-P system. 127

4.33 The effect of bulk solute content on the boundary Curie temperature 130

4.34 The effect of the magnetic parameter of M on the magnetic chemical potential of X (A = -1000 K, B = 0 K,C = 1000 K). 137

4.35 The effect of the content of M on the magnetic chemical potential of X (A = 0.001, B = 0.01, C = 0.1). 138

4.36 The effect of the magnetic parameter of M on phosphorus solid solubility in alpha Fe-0.01M-P (A = -2000 K, B = -1000 K, C = 0 K, D = 1000 K). ..144

4.37 The effect of the content of solute M on phosphorus solid solubility in alpha Fe-M-X (A = 0.1, B = 0.01, C = 0.001, D = 0.0001). 145

4.38 The effect of I′ on the solubility of phosphorus in alpha Fe-0.01M-P (A = 100 KJ/mole, B = 75 KJ/mole, C = 50 KJ/mole, D = 25 KJ/mole). ..146

4.39 The experimental solid solubility of phosphorus for selected ternaries [23]. 147

4.40 The predicted solubility of phosphorus in selected alpha Fe-0.01M-P ternaries (1 = Fe-Mo-P, 2 = Fe-V-P, 3 = Fe-Cr-P, 4 = Fe-Mn-P, 5 = Fe-Ni-P, 6 = Fe-P). 149

4.41 The predicted solubility of P in Fe-0.01Mo-P 151

Figure Page

4.42 The predicted solubility of P in alpha Fe-0.01V-P .152

4.43 The effect of I′ on the segregation free energy for alpha Fe-0.01M-P (A = 20 KJ/mole, B = 40 KJ/mole, C = 60 KJ/mole). 155

4.44 The effect of I′ on the boundary solute content for alpha Fe-0.01M-P (A = 20 KJ/mole, B = 40 KJ/mole, C = 60 KJ/mole). 156

4.45 The effect of the magnetic parameter of M on the magnetic segregation free energy of X according to Case I (A = -1000 K, B = 0 K, C = 1000 K). 160

4.46 The effect of the magnetic parameter of M on boundary solute contents (A = -1000 K, B = 0 K, C = 1000 K). 162

4.47 The effect of bulk content of M on the boundary solute contents according to Case I (A = 0.1, B = 0.01, C = 0.001). 163

4.48 The effect of the magnetic parameter of M on the magnetic segregation free energy according to Case II (A = -1000 K, B = 0 K, C = 1000 K). 166

4.49 Predicted grain boundary solute contents for alpha Fe-0.01M-X according to Case II (A = -1000 K, B = 0 K, C = 1000 K). 168

4.50 The effect of bulk content of solute M on the magnetic segregation free energies according to Case II (A = 0.1, B = 0.01, C = 0.001). 169

4.51 The effect of bulk content of M on grain boundary segregation according to Case II (A = 0.1, B = 0.01, C = 0.001). 170

4.52 The effect of the non-magnetic segregation free energy of M on grain boundary solute content acccording to Case II (A = 50 KJ/mole, B = 40 KJ/mole, C = 30 KJ/mole). 171

4.53 The effect of bulk content of M on the equilibrium grain boundary Curie temperature (A = 0.1, B = 0.01, C = 0.001). 173

4.54 Predicted grain boundary content of P in alpha Fe-Ni-P according to Case II (C = chemical only, M = magnetic only, B = chemical and magnetic). 174

Figure Page

4.55 Predicted grain boundary content of P in alpha Fe-Mn-P according to Case II (C = chemical only, M = magnetic only, B = chemical and magnetic). 176

4.56 Predicted grain boundary content of P in alpha Fe-Cr-P according to Case II (C = chemical only, M = magnetic only, B = chemical and magnetic). 177

4.57 Equilibrium Curie temperature curves for alpha Fe-Cr-P corresponding to Figure 4.56 (C = chemical only, M = magnetic only, B = chemical and magnetic). 178

4.58 Predicted grain boundary content of X in alpha Fe-X with a linear and non-linear magnetic parameter according to Case II. 180

List of Plates

Plate Page

3.1 An X-ray spectrum from an inclusion in Armco iron ..20

3.2 Pyrex reaction tube for producing iron phosphides ..23

3.3 Experimental apparatus for producing iron phosphides 24

3.4 The vacuum arc furnace used to produce final alloys 28

3.5 Specpure iron cylinders and plugs with locking taper 30

3.6 An example of final alloy (buttons) produced 34

3.7 Microstructure of produced iron phosphide, X520 36

3.8 A typical X-ray spectrum for the produced iron phosphide 37

3.9 Precipitation in T700C, X520 38

3.10 A typical X-ray spectrum from the bulk solid solution of T700C 39

3.11 Precipitation in T600C, X480 40

3.12 Precipitation in T500C, X480 42

1. INTRODUCTION

Two processes which can act simultaneously in an iron alloy are grain boundary solute segregation and second phase precipitation. Both can affect the structure and certain properties of the alloy. One such property is intergranular cohesion, a decrease in which can result in intergranular fracture. In many iron alloys this intergranular embrittlement is associated with certain heat treatments (causing temper embrittlement) and is generally manifest as a reduction in impact strength and fracture toughness [1].

Segregation is defined as the non-uniform distribution of elements in a material. Frequently used in reference to castings, where segregation occurs during solidification of a melt, intergranular segregation in the present context refers to the solid state thermal redistribution of species between the matrix and interfaces. It is also necessary to distinquish between two types of solid state segregation phenomena. A non-equilibrium type of segregation may be connected with the dragging of solute species by a flux of vacancies toward the interface [2] during cooling from a high temperature or during irradiation [3]. Another non-equilibrium type of segregation involves the rejection of solute during precipitate growth.

However, the omnipresent form of intergranular segregation is a reversible equilibrium segregation [4]. For a polycrystalline alloy, held isothermally, there will be an enrichment of surface active species at interfaces. The extent of this enrichment is determined only by the system parameters at equilibrium and not by their history. Therefore, as the temperature of the alloy is changed, there are compositional and perhaps structural changes at the grain boundaries. From this point the word *segregation* will be used to denote this phenomenon.

The *precipitation* process in a material requires the nucleation and growth of a second phase from a super-saturated solid solution. The second phase may be nucleated heterogeneously at grain boundaries and interfaces, dislocations and other structural defects, or homógeneously within the matrix. However, at equilibrium for a given temperature, there is a limit of solubility for each solute species present in the material.

The present project stems from the postulate that precipitation and intergranular segregation in iron must be simultaneous consequences of the tendency of the iron to reject foreign atoms from its matrix. This rejection of solute atoms, which is reflected in the limit of solid solubility and in grain boundary segregation, is best treated by applying conditions of thermodynamic equilibrium to the system. Of special interest in iron alloys are the so called 'impurity elements' (S,P,As,Sb,Sn etc.) which are highly surface active and are associated with temper embrittlement phenomena.

It is well known that the solubility of element X is very sensitive to the relative position of the free energy curve of the precipitate (containing species X) with respect to the free energy curve of the matrix. Guttmann [5] has recently shown that equilibrium grain boundary segregation is also very sensitive to the relative position of the free energy curve of the segregated interface with respect to the free energy curves of the bulk phases. This correlation between solubility and intergranular segregation implies that the energetic properties of a boundary are related to the energetic properties of all the matrix phases.

Therefore, material properties and external conditions affecting precipitation in a given material should also affect grain boundary segregation although the exact nature of the effect is not obvious. This is very important in that data on precipitation in simple systems is relatively easily available while good segregation data for simple systems is difficult to obtain and consequently scarce.

When specifically considering iron, the one obvious but often ignored material property is its ferromagnetic nature. The following 3 paragraphs have been compiled from references [6-8] as a brief description of ferromagnetism in iron.

The 3d shell of the Fe atom is responsible for its ferromagnetic behaviour. The 3d shell may have up to 10 electrons, gradually filling from scandium to copper across the first row of transition elements. For each electron within the shell and along some specified direction, there is a component of orbital angular momentum which must be an integral multiple of $h/2\pi$. In addition, each electron has an intrinsic angular momentum, called spin, due to a rotation about its own axis; this spin can be either $+1/2(h/2\pi)$ or $-1/2(h/2\pi)$ along the specified direction. The spin of a charged particle is associated with a magnetic moment. A fundamental principle of atomic structure, Pauli's exclusion principle, states that no two electrons in a given shell may have identical components of orbital angular momentum with identical components of spin. However, the manner in which electrons are added to a shell as the atomic number increases is important. Hund's rule states that within a given shell, the maximum number of electrons have spins pointing in the same direction, consistent with Pauli's exclusion principle. There is a coupling of exchange energy between electrons with parallel spins; this exchange energy is negative for electrons in the same atom and leads to a minimum energy when the maximum number of spins are parallel.

When a number of atoms are associated, as in a crystal, this internal interaction is called the exchange field, molecular field, or Weiss field (after Pierre Weiss). The exchange field gives an appropriate representation of the quantum mechanical exchange interaction. It has been shown that the energy of interaction w_{12} of atoms 1, 2 bearing spins s_1, s_2 contains a term

$$w_{12} = - j\, s_1 \cdot s_2 \qquad (1.1)$$

(Heisenberg model)

where j is the exchange integral and is related to the overlap of the charge distribution of the atoms.

The outer shells of an isolated Fe atom are $3d^6 4s^2$ and the 3d shell contains 4 coupled electrons (antiparallel electrons cancel each other). In general, the parallel spin arrangement will be energetically favoured over the antiparallel one. This condition exists in the electronic (conduction) band of iron, cobalt and nickel. The density of levels within the band is so high that the negligible gain in kinetic energy required for an electron to move from a filled level to an unfilled one is more than offset by the lowering of electrostatic energy. This is responsible for the alignment of electron-spin magnetic moments that constitute the spontaneous magnetization existing within domains of ferromagnetic materials. Below a critical temperature (material dependent) called the Curie temperature, there is a ferromagnetic coupling between electrons with parallel spins, but above this temperature, the coupling is destroyed by thermal energy (paramagnetism).

The above description is included for completeness but it is not the intent of the present work to delve further into the quantum mechanical aspects of ferromagnetism. Rather, an equilibrium, macroscopic thermodynamic approach will be considered. Empirical thermodynamic functions obtained from solid solubility data in alpha iron will be used to predict grain boundary segregation behavior of selected solute species in alpha iron.

2. BACKGROUND

The purpose of this chapter is to provide a brief historical background to the present work. The development of grain boundary segregation theory is presented with some reference to the segregation of phosphorus in alpha iron. Excellent reviews of grain boundary segregation have been published by Inman and Tipler [9] and by Hondros and Seah [4]. As the experimental determination of phosphorus solubility in alpha iron was part of this project, a brief review of previous investigations into P solubility is also presented.

2.1 The Development of Segregation Theory

The driving force for interfacial segregation must be the lowering of interfacial energy. The theory applies to all interfaces but the major interest, at present, is in grain boundaries. Grain boundaries, which form due to the geometrical discontinuity between two adjacent lattices, are distorted and more or less disordered areas where the orientation and magnitude of atomic bonds are different from those in the bulk crystal. It can be considered to be a discontinuity large in two-dimensional extent but only a few atomic diameters thick. Within this volume, it can be treated as distorted lattice containing compressed and expanded lattice sites.

About one hundred years ago Gibbs [10] developed a thermodynamic treatment of surfaces that included such considerations as adsorption, heat and mechanical surface effects, and grain boundaries. This is the framework for all modern thermodynamic theory. For a surface in a binary system with components 1 and 2, Gibbs derived the following:

$$(d\gamma/d\mu_1)_{T,P} = -[\Gamma_2 - \frac{X_2}{X_1}\Gamma_1] \tag{2.1}$$

where γ is the surface energy of the interface,

μ_1 is the chemical potential of 1,

X_i is the bulk atomic fraction of i, and

Γ_i is the excess surface concentration of i.

This familiar Gibbs adsorption isotherm is the starting point of segregation theory.

The earliest segregation calculations were made in the development of a theory of yield-point behavior in metals by Cottrell [11]. He considered that the binding energy, E, between a solute atom and a dislocation could be evaluated by considering the release of strain energy on segregation to the dislocation[1], such that in a dilute case,

$$C = C_0 \exp(E/RT) \tag{2.2}$$

where C is the local concentration of the solute and

Co is the average bulk concentration of solute.

---

[1] For example, E for nitrogen in alpha iron was estimated at 50 KJ/mole.

In the mid 1950's McLean [12] considered equilibrium segregation in terms of the lattice distortion energy around solute atoms in the crystal bulk. A solute atom larger than the site it occupies in the solvent lattice should fit easily in an expanded boundary site causing less lattice distortion. Likewise, a smaller solute atom should fit more easily into a compressed site. Generally, large energies are required to alter the volume occupied by atoms in a metal. For example, an elastic ~10% expansion in the alpha iron lattice requires approximately 62.7 KJ/mole. The solution of atoms different in size from the solvent requires strain energy which can be relieved by segregation of the solute to distorted sites. In this way, a large amount of the distortion energy of the entire system can be released by segregation.

McLean produced the useful expression

$$\frac{X^{\phi}}{1-X^{\phi}} = \frac{X^{\alpha}}{1-X^{\alpha}} \exp(E/RT) \qquad (2.3)$$

where X^{ϕ} = the boundary solute content

X^{α} = the bulk solute content

E = the binding energy of the solute. This model shows that segregation rises as the bulk solute content rises or as the temperature falls. Segregation will occur in nearly all solid solutions. However, it would be noticeable only when the temperature, time and diffusion coefficient are such that a large grain boundary concentration can build up. To grain boundary segregation it is necessary to quench from a temperature high enough to disperse solute to one low enough to prevent significant diffusion.

McLean's model has the same behavior as described by the simple Langmuir theory of gas adsorption on a solid surface. That is, there is a single layer, a single adsorbate and no site-to-site interaction. There are very few grain boundary results for iron binaries that are sufficiently complete to be properly interpreted in terms of McLean-Langmuir type theories [13,14].

Hondros and Seah [13] have invoked other solid state analogues of theories developed for gas adsorption on solid surfaces, adopting the concepts and analytical treatments commonly used in classical free surface adsorption. One of these is the BET theory of multilayer gas adsorption [15], given by

$$\frac{X_1^{\phi}}{X^{\phi}} \frac{X^{\alpha}}{X_1^{\alpha}-X^{\alpha}} = \frac{1}{K} + \frac{K-1}{K} \frac{X^{\alpha}}{X_1^{\alpha}} \qquad (2.4)$$

where K = exp(E/RT)

E = the difference between the energy of adsorption of the first layer and the free energy of condensation of successive layers

X^{ϕ} = boundary solute content

X_1^{ϕ} = boundary solute content of a layer

X^{α} = bulk solute content

X_1^α = maximum bulk solute content

In this model it was assumed that atoms adsorbing in the first monatomic layer have a different free energy of adsorption than those in successive layers. The adsorbate atoms have no lateral interaction in the layer and each layer does not have to be complete before the next is started. A truncated BET model[2] is very similar to the McLean model.

The above theories neglect site-to-site interactions and chemical interactions. Site-to-site interactions are mutual interactions between the same solute in neighboring boundary sites and chemical interactions are element-element interactions found in systems with multicomponent segregation. In the Fowler model [16] there is a single layer, a single segregating solute species, and site-to-site interaction. For the gas adsorption models, the assumption that a filled site does not affect the probability of one of z neighbouring sites being filled can be removed by allowing an interaction energy r between pairs of nearest neighbours. The solid state analogue is

$$\frac{X^\phi}{1-X^\phi} = X^\alpha \exp(\{E-rz[X^\phi/X_1^\phi]\}/RT) \tag{2.5}$$

If r is positive the atoms are mutually repulsive and if negative vice versa. With r negative the temperature dependence of segregation deviates from that given by McLean by showing a sharper rise in segregation as temperature falls.

---

[2] The boundary conditions are the same as in the McLean model.

In the recent work, Guttmann [17] has developed a thermodynamic treatment of multi-component segregation. His model is used in the present work and it will therefore be discussed fully in chapter 4.

The particular system of major interest here is alpha Fe-P. There has been a great deal of experimental work concerning P segregation in steels[3] as P is a potent intergranular embrittling element, but little on pure alpha Fe-P binaries. The reason is that it is difficult to temper embrittle pure iron binaries sufficiently so that intergranular fracture may occur and the surface may be studied. In the late 1950's Inman and Tipler [18] carried out a study of P segregation in Fe by using radioactive P. The occurrence of segregation was conclusively shown but the resolution was poor since a sectioning technique was used. More recent investigations [14,19] have used Auger Electron Spectrometer (AES) techniques. However, the results are scattered with widely varying saturation levels and do not seem to fit a simple McLean-type model.

---

[3] For example, see the work of McMahon at the University of Pennsylvania.

2.2 The Solubility of Phosphorus in alpha Iron

Alpha iron forms a substitutional solid solution with phosphorus to a maximum solubility of 2.55 wt% at ~1050 C. Phase diagrams and a compilation of early works are given by Hansen [20] and Vol [21]; these demonstrate an interest in the Fe-P system since before the turn of the century.

The solid solubility of P in alpha Fe decreases with decreasing temperature. Before the advent of quantitative Electron Probe Microanalysis (EPMA), the most accurate solubility determinations were by metallographic analyses[4] [22,23]. Temperatures from 1000 C to 600 C were investigated but the most reliable values lie above the Curie temperature of iron (1043 K).

In the 1960's Hornbogen [24-26] investigated the factors that govern precipitation from alpha Fe substitutional solid solutions. Phosphorus was chosen because of its small atomic size as compared to iron and the lack of chemical and crystallographic similarity between the two elements. He reported that high P alloys tended to show extensive intergranular brittleness. The phosphorus precipitated from alpha Fe as Fe_3P when equilibrium was reached. This phosphide which has a tetragonal body-centered unit cell containing 32 atoms, forms precipitates parallel to a high index plane of alpha Fe (1,4,12). Hornbogen also found that phosphides nucleate from alpha iron in the sequence: at high angle boundaries, at low angle boundaries and dislocations, and in the matrix.

---

[4] Resistivity measurements and lattice parameter determinations by X-ray techniques were not very successful [23].

More recent determinations of P solubility [27-29] have involved the use of EPMA and are shown in Figure 2.1. Hofmann et al. [27] were among the first to notice an anomalous decrease in the solubility of P and in its diffusion coefficient in iron below the Curie temperature. More recently, Doan et al. [28] in investigating the Fe-Ni-P system noticed a much more pronounced anomalous decrease in P solubility. While the present project was in progress, Nishizawa et al. [29] published an even more striking decrease in P solubility below the Curie temperature, and related it to the ferromagnetism of alpha iron (see Chapter 4). It is very interesting that, as EPMA techniques have improved and more time allowed for alloys at temperature to reach equilibrium, the experimentally measured solubility of P in alpha iron has been continously decreasing.

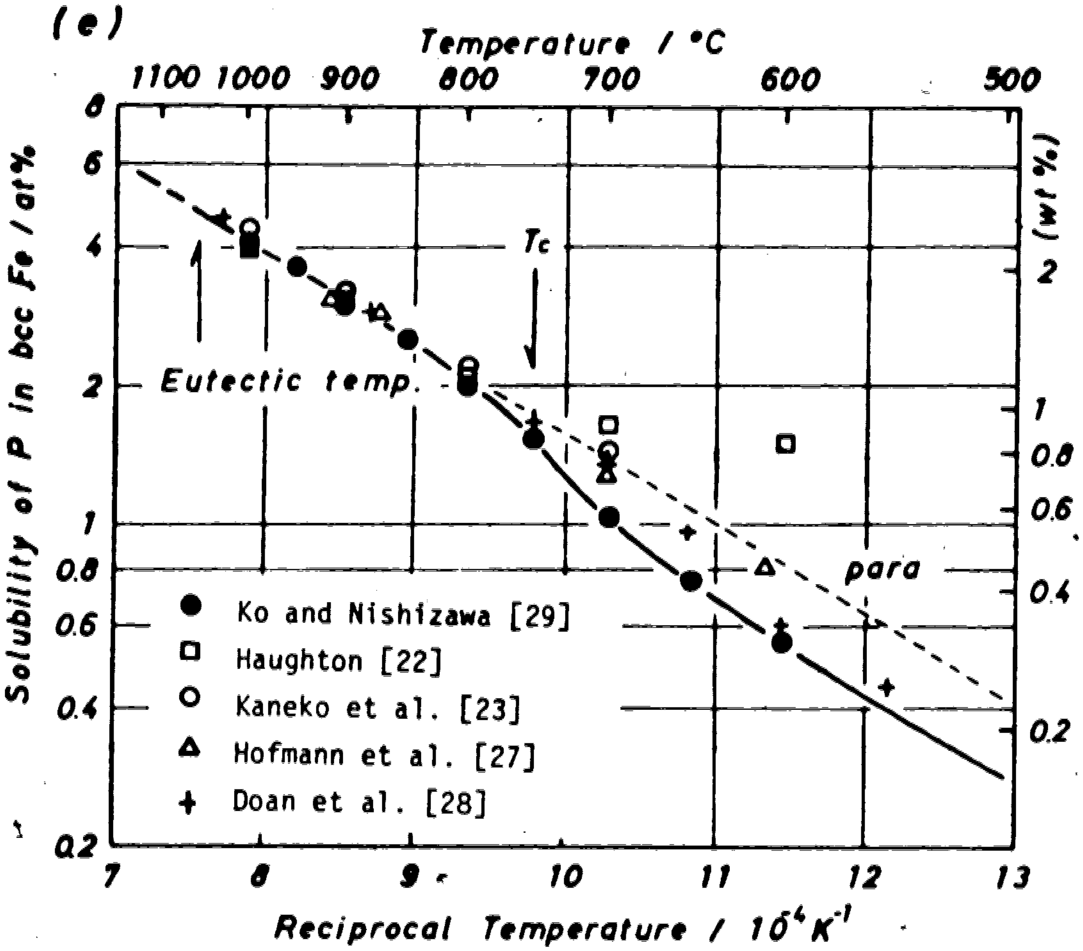

Figure 2.1 The solubility of phosphorus in alpha iron

3. EXPERIMENTAL PROCEDURES

Although this thesis is primarily theoretical some initial experimental work was performed. This experimental work was quite difficult and so the procedures used are described in extensive detail in this section.

3.1 The Production of 'Pure' alpha Fe-P Alloys

The production of 'pure' alloys containing only iron and phosphorus was necessary in order to determine the equilibrium limit of solid solubility of phosphorus in alpha iron. The presence of additional elements could affect the behavior of the alloys. For example, at higher temperature, small quantities of a similar atom such as Ni are tolerable for experimental purposes whereas small quantities of Mo are not. This is illustrated by some of the results obtained (see e.g. section 4.11). The first step in the production of the 'pure' alpha Fe-P alloys must be the procurement of the proper raw materials.

3.1.1 Sources of Iron and Phosphorus

An initial decision that was faced was whether to use phosphorus in the elemental form or as a compound. In the elemental form, phosphorus exists in a number of allotropes including white (yellow), red, and black (violet). White phosphorus burns spontaneously in air producing a pentoxide which is very poisonous (.50 mg fatal dose). However, when heated in its own vapour to 250 C, white phosphorus is converted to the red variety. This form is fairly stable, does not ignite in air but sublimes with a vapour pressure of 1 atm at 417 C. For the present project, red phosphorus (99.9+ wt%) was obtained from Fisher Scientific Co. This material was kept sealed under argon gas as much as possible to minimize oxygen contamination.

The only phosphorus-containing compounds suitable for production of alloys for this project are iron phosphides. Ferrophosphorus is used as an alloying addition by the steel industry. This material has a high phosphorus content (~25 wt%); however, it also contains varying and unacceptable amounts of carbon, silicon, manganese and chromium. Commercially, there are very few sources of phosphides available. ICN Pharmaceuticals, Inc. sells a ferric phosphide, FeP, but only guarantees purity to greater than 95 wt%. A quantity of this commercial FeP was obtained; however, upon obtaining a qualitative X-ray spectrum of this material using an Energy Dispersive Spectrometer (EDS), peaks denoting significant quantities of Cr and Mn were clearly visible. Therefore, this 'pure' commercial iron phosphide was not used. Instead 'pure' iron phosphide was produced from 'pure' iron and 'pure' phosphorus.

Several commercial sources of 'pure' iron are available. Three materials were considered as the possible iron base for the alpha Fe-P alloys:

1. High Purity Armco iron in the form of 0.017 in. thick

sheet was tried, but rejected due to the impurities present. For example, Plate 3.1 shows an X-ray spectrum from one of many inclusions.

2. Analysed reagent grade iron wire was obtained from J. T. Baker Chemical Co. This material was somewhat better than Armco iron and was used for preliminary tests and initial production of iron phosphides.
3. Specpure iron 0.25 in. diameter rod (spectrographically standardized) was obtained from Johnson Matthey Chemicals Limited. This material is extremely pure and expensive and therefore was used only for the final samples.

Table 3.1 contains the compositions of the above iron materials.

3.1.2 Production of an Iron Phosphide

There are several possible techniques for producing iron phosphide of a desired composition from iron and phosphorus, including the following:

1. A special vacuum furnace may be constructed such that above a particular temperature pure iron is surrounded by and thus reacts with phosphorus vapour. The inner lining of the furnace must resist attack from the phosphorus vapour. There is normally a large loss of P with this method.
2. An ordinary vacuum furnace may be used if the amount of P is small compared to the iron. This allows the P to be

Table 3.1 Compositions of 'pure' irons used (in wt%)

Element	1. Armco	2. Wire	3. Specpure
Ag			1 ppm
Ca			1 ppm
Mg			1 ppm
C	0.007		-
Mn	0.010		1 ppm
P	0.020	0.010	-
S	0.002	0.004	-
Cu	0.130		<1 ppm
Ni	0.042		-
Cr	0.003		<1 ppm
Cb	0.005		-
Mo	0.006		-
Si	0.001	0.005	<1 ppm
Co	0.009		-
Pb	0.001		-
Sn	0.010		-
Al	0.003		-
Fe	balance	99.9+	balance

A blank signifies the element was analysed for; whereas "-" indicates a concentration below the limit of detectability.

Plate 3.1 An X-ray spectrum from an inclusion in Armco iron

enclosed within the iron and to be kept away from the furnace lining.

In the present work a master alloy (nominally 20 wt% P) was produced by reacting iron with red phosphorus in a weight ratio of 4 to 1. This was carried out in the special apparatus shown in Figure 3.1. A pyrex glass tube, see Plate 3.2, was fitted with a fretted quartz glass disc. Iron, in the form of powder, turnings, or sectioned sheet and rod was placed inside the tube above the disc. When the tube was in a vertical position, the disc kept solid material at a specific position (reaction chamber) but allowed passage of gases. The tube was placed within a vertical furnace, see Plate 3.3. The bottom of the tube (below the furnace) was connected by a 2-way valve to a cylinder of ultra-high purity hydrogen gas and a rotary-diffusion vacuum pump combination.

The top of the tube (above the furnace) was also connected by a 2-way valve to a bubbler and to an upper container of red phosphorus which was directly connected to an argon cylinder. The pyrex tubes had a reduced internal diameter on either side of the reaction chamber to allow for easy sealing of the tube with a torch.

The use of the apparatus is summarized as follows:

1. Iron was first pickled in HCl to remove surface contamination and placed in the reaction chamber. Phosphorus was positioned in the upper chamber under argon. The tube was then inserted in the furnace.

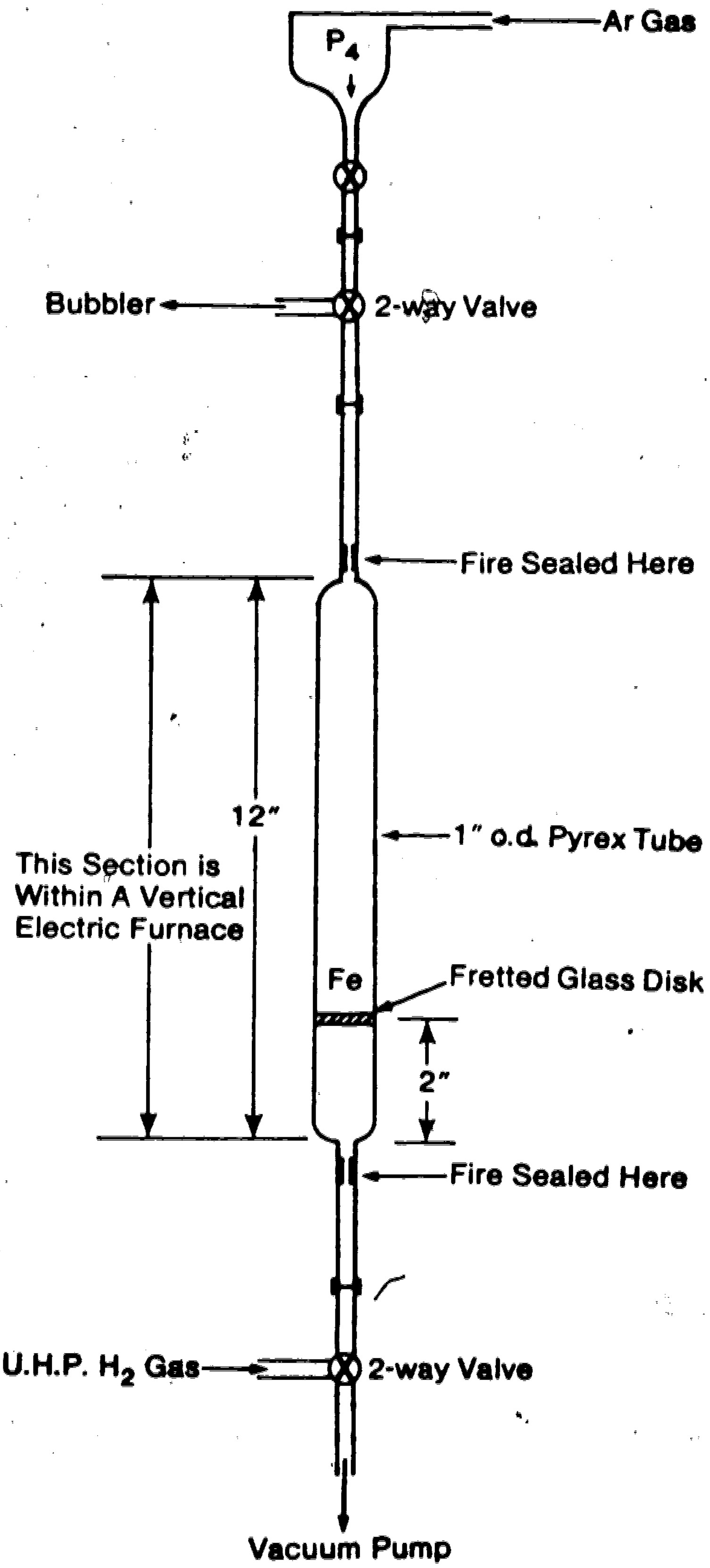
Ar Gas
P_4
Bubbler
2-way Valve
Fire Sealed Here
12"
This Section is Within A Vertical Electric Furnace
1" o.d. Pyrex Tube
Fe
Fretted Glass Disk
2"
Fire Sealed Here
U.H.P. H_2 Gas
2-way Valve
Vacuum Pump

Figure 3.1 A schematic of the apparatus developed for iron phosphide production.

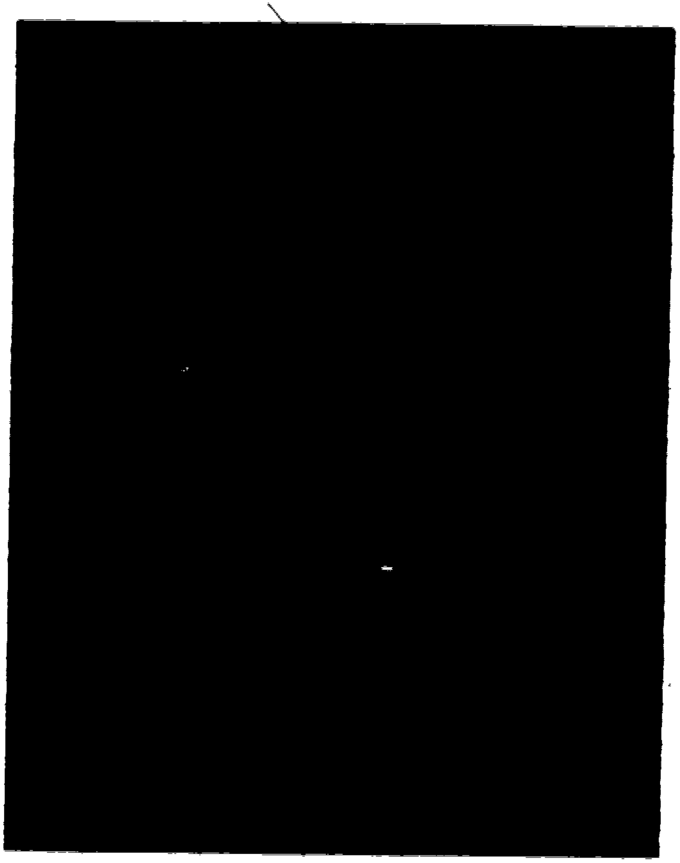

Plate 3.2 Pyrex reaction tube for producing iron phosphides

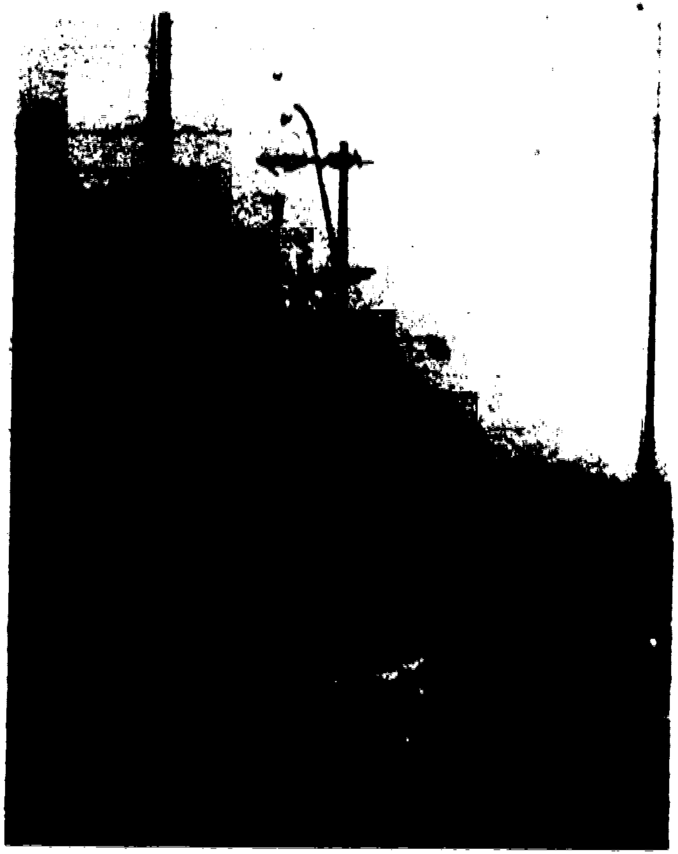

Plate 3.3 Experimental apparatus for producing iron phosphides

2. Hydrogen gas was passed through the tube to the bubbler at approximately 1 bubble per second. The furnace was then raised to 585 C and held for up to 24 hours. This procedure was to reduce iron oxides, eliminating oxygen and other impurities [30].
3. When the tube had cooled to room temperature, the hydrogen gas was shut off, the top valve closed and the tube evacuated by the pump. By opening the top valve to the phosphorus, the powder was 'sucked' into the reaction chamber.
4. The evacuated reaction chamber (tube) was then sealed by torch at the reduced section.
5. The tube was removed from the vertical furnace, checked for vacuum integrity using a Tesla coil, and shaken to mix the iron and phosphorus contents.
6. The tube was then placed completely within a horizontal furnace, slowly raised to 585 C and held for 8 hours.[5] During this treatment the iron and phosphorus reacted to giving mainly FeP with some remaining Fe.
7. When cool, the tube was carefully broken under an inert atmosphere and the iron and phosphide removed. Each tube was thus used only once.

Although the phosphorus has a very high vapour pressure and the pyrex tube is at the point of softening at the temperatures mentioned, the glass tube did not bulge or explode because the iron and phosphorus combined very rapidly, preventing the occurrence of high phosphorus vapor pressure.

---

[5] Although Fe-P alloys have been sintered in the past [31], the present conditions were determined by trial.

Some of the produced phosphide was ground to a powder and analysed by X-ray diffraction methods. This showed that most of the phosphorus was present as FeP with minor amounts of Fe_2P. It also became apparent that unless the phosphide powder was kept under an inert atmosphere, it oxidized. An oxide was particularly noticeable when the phosphide powder was vacuum arc-melted into 'buttons'. However, if melted into buttons immediately, only stable phophides were present and oxidation was not a problem.

3.1.3 Production of Final alpha Fe-P Alloys

All final phosphides (master alloys) and alpha Fe-P alloys were vacuum arc-melted into 'buttons' using a Materials Research Corporation V-4 Series vacuum arc furnace, Plate 3.4. A partial vacuum of argon was used. The gas passed through a dessicator, over hot Cu turnings (600 C), and through a cold trap before reaching the alloys. Melting was carried out on a water-cooled copper hearth using a tungsten rod electrode. All gases from the vacuum chamber were vented to a fume hood to prevent accidental exposure to phosphorus pentoxides. Figure 3.2 shows a schematic of experimental procedures used in alpha Fe-P alloy production. As the figure shows, the Specpure iron rods were machined into cylinders 2.50 cm. long, a hole

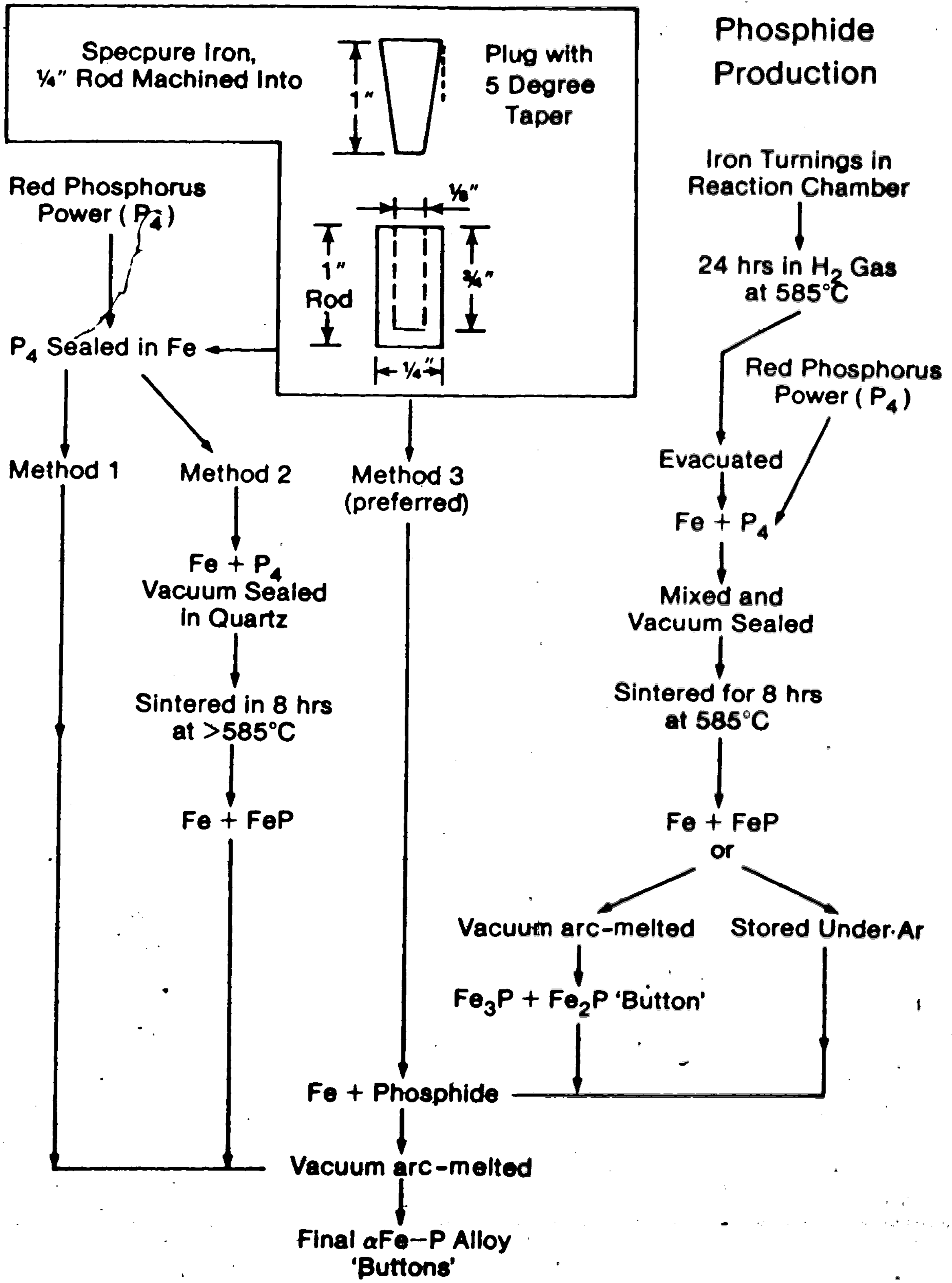
Phosphide Production
Specpure Iron, ¼" Rod Machined Into
1"
Plug with 5 Degree Taper
⅛"
1" Rod
¾"
¼"
Red Phosphorus Power (P_4)
P_4 Sealed in Fe
Method 1
Method 2
Method 3 (preferred)
Fe + P_4 Vacuum Sealed in Quartz
Sintered in 8 hrs at >585°C
Fe + FeP
Iron Turnings in Reaction Chamber
24 hrs in H_2 Gas at 585°C
Red Phosphorus Power (P_4)
Evacuated
Fe + P_4
Mixed and Vacuum Sealed
Sintered for 8 hrs at 585°C
Fe + FeP or
Vacuum arc-melted
Stored Under Ar
Fe_3P + Fe_2P 'Button'
Fe + Phosphide
Vacuum arc-melted
Final αFe–P Alloy 'Buttons'

Figure 3.2 A schematic of procedures developed for the production of αFe–P alloys.

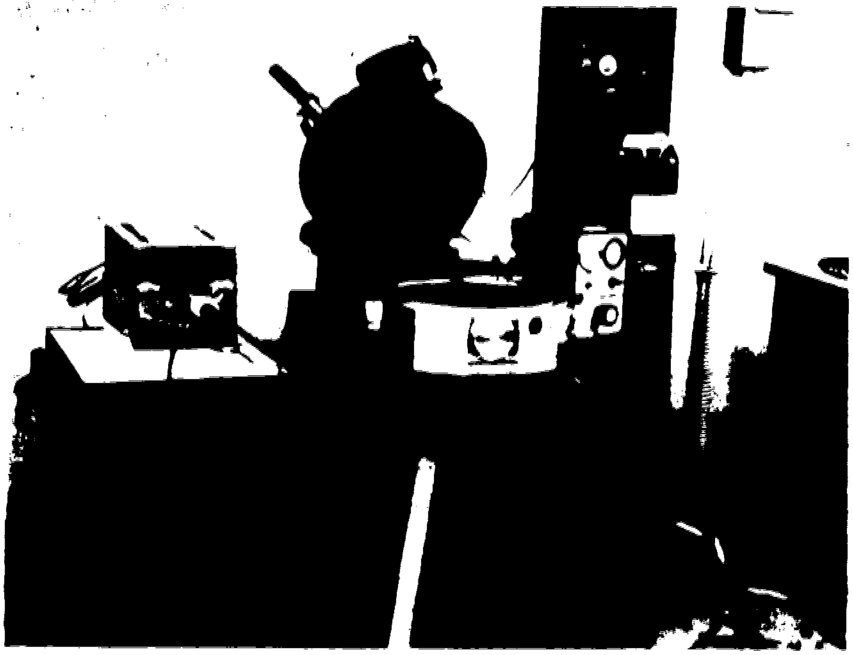

Plate 3.4 The vacuum arc furnace used to produce final alloys

0.318 cm. i.d. was drilled into each cylinder to contain either phosphorus or phosphide, and 2.50 cm. long plugs with a 5 degree locking taper were used to seal the compartment. The cylinders and plugs are shown in Plate 3.5. These configurations allowed three successful methods of final alloy production:

1. Red phosphorus was enclosed within the iron cylinders and directly vacuum arc-melted. This method produced clean alloys but the phosphorus had to be packed and sealed under an inert atmosphere. A limited amount of powder could be packed and at least 1/3 of the phosphorus was lost on melting (larger cylinders were difficult to handle and melt). This resulted in alloys containing less than 1 wt% P.
2. This method was identical to the above except that the sealed iron cylinders were also encapsulated in quartz and annealed at greater than 600 C for 24 hours before melting. This resulted in a lower phosphorus loss.
3. The method preferred and the one actually used required that the turnings from the machining of the Specpure iron rods were produced into phosphide buttons as described in section 3.1.2. Alloys of any phosphorus concentration could then be made simply by arc-melting a portion of the phosphide button with the Specpure iron rod and atmosphere was not a problem.

All alpha Fe-P specimens produced were nominally 1.5 wt% P. The specimens were marked by a letter and a temperature,

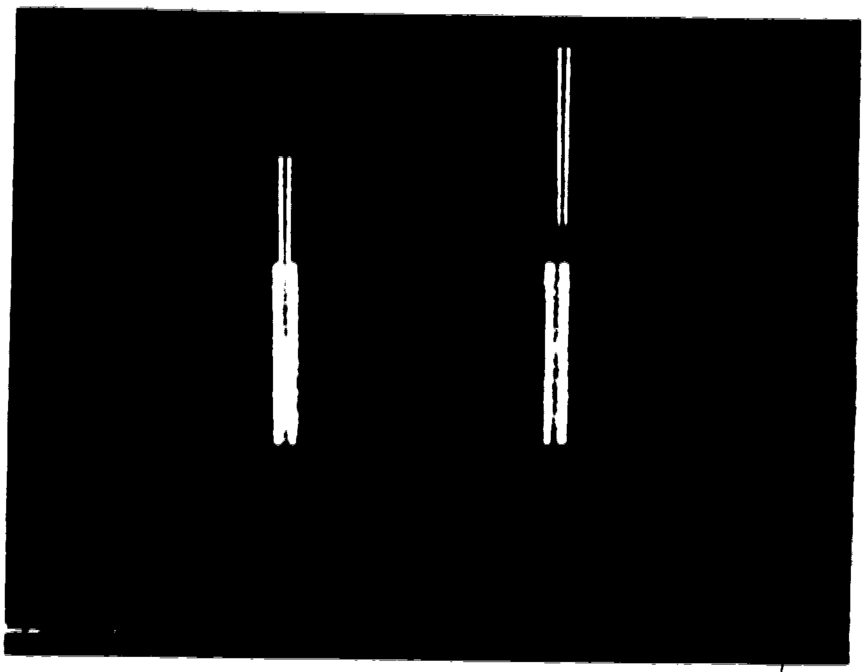

Plate 3.5 Specpure iron cylinders and plugs with locking taper

e.g. T800 C. T was the designation used for the final, completely successful series using Specpure iron.

3.2 Heat Treatment of alpha Fe-P Alloys

As previously stated, the solubility limit of P in Fe above the Curie temperature (770 C) has been well documented. Therefore, an investigation range of 800 C to 500 C was chosen. All furnace temperatures mentioned were maintained within five degrees of the temperature stated. The heat treatments for the T series were:

1. A number of samples were sealed together in an evacuated quartz ampoule, solution heat treated at 1050 C for 24 hours, and cold water quenched, breaking the quartz ampoule under water.
2. The samples were then individually sealed in evacuated quartz ampoules aged as indicated in Table 3.2, and quenched in cold water.

The length of ageing was determined by assuming that the square of distance the solute travels is approximately equal to the diffusion coefficient for the solute times the time available. In all cases a phosphorus atom was allowed on average to move at least one micron, based on a low temperature extrapolation of a high temperature diffusion coefficient [32]. The paramagnetic diffusion coefficient may be used for higher temperatures, but extremely long times are necessary at low temperatures due to a diminished

Table 3.2 Ageing temperature and times for final samples

Sample	Ageing Time (hrs)	Diffusion Distance (microns)
T800C	240	43.0
T750C	504	33.4
T700C	960	23.1
T650C	1896	15.1
T600C	3840	9.1
T550C	4272	3.7
T500C	4920	1.3

the Curie temperature (see section 4.11).

3.3 Metallographic Specimen Preparation, Examination, and Chemical Analysis

All samples (buttons) were sectioned using a Buehler Low Speed Saw with a diamond blade. Examples of buttons are shown in Plate 3.6. The sectioned samples were then mounted in a 1 in. mold using a copper-filled thermo-setting epoxy; this allowed the mount to conduct electrons, a useful property when viewing with a Scanning Electron Microscope (SEM).

After mounting, all samples were polished in the following sequence using a Buehler Minimet Automatic Polisher:

1. 420 grit silicon carbide paper and water,
2. 600 grit silicon carbide paper and water,
3. 6 micron diamond paste and oil on Buehler AB Texmet paper,
4. 3 micron diamond paste and oil on Buehler AB Texmet paper,
5. 1 micron diamond paste and oil on Buehler AB Texmet paper.

A final polish with Linde B alumina was attempted but the specimens were found to pit excessively. All specimens were given a final 10 second etch with a 2% Nital solution.

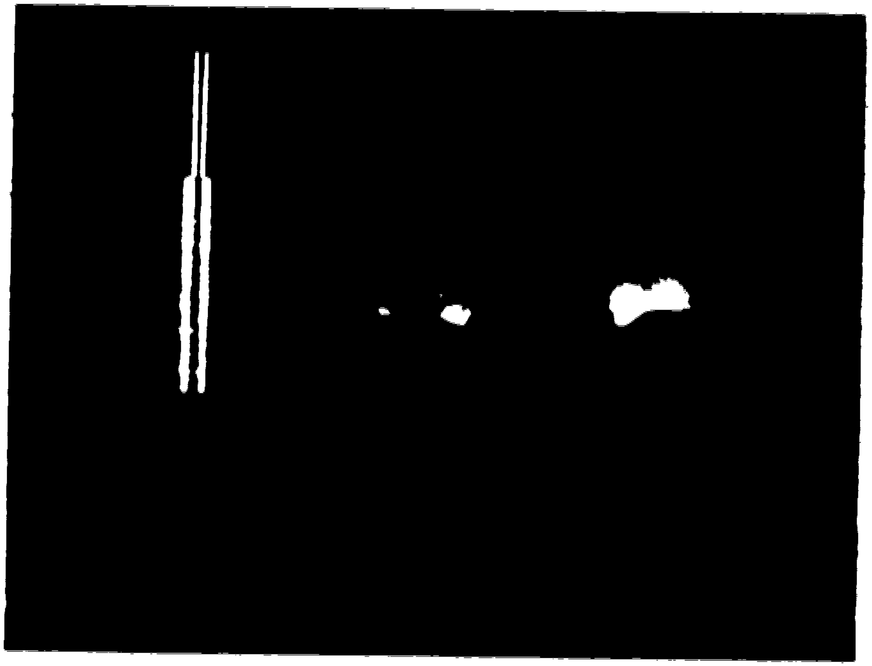

Plate 3.6 An example of final alloy (buttons) produced

Micrographs were taken of the sample microstructures at various magnifications using a Zeiss Ultraphot III Metallograph. The samples were also viewed with much greater resolution using an ISI 60 Scanning Electron Microscope (SEM). This SEM is fitted with a National Semiconductor Energy Dispersive Spectrometer (EDS) and a Tracor Northern TN-1710 multichannel analyser. These instruments produce an X-ray spectrum of the elements present under the electron beam, permitting a qualitative chemical analysis.

Following are a few examples of the specimen microstructures and X-ray spectra. Plate 3.7 shows the microstructure of the produced iron phosphide after vacuum arc-melting into a button. The nominal 20 wt% P present would place this alloy in the Fe_3P-Fe_2P range. Grains with higher P content are characterized by their rectangular morphology. Plate 3.8 shows a typical X-ray spectrum from this phosphide. As is evident, no impurities are detectable. Plate 3.9 shows a representative microstructure of T700C. The phosphide precipitates appear as plates and needles along specific crystallographic planes and directions [24]. Also present are grain boundary allotriomorphs as described by Aaronson and co-workers [33,34]. Plate 3.10 shows a representative X-ray spectrum from the bulk solid solution of T700C. The large peak is an iron K-alpha peak. Other than iron and phosphorus there are no detectable elements.

Plate 3.11 shows a representative microstructure of T600C. This plate is similar to Plate 3.9, with all relevant

Plate 3.7 Microstructure of produced iron phosphide, X520

Plate 3.8 A typical X-ray spectrum for the produced iron phosphide

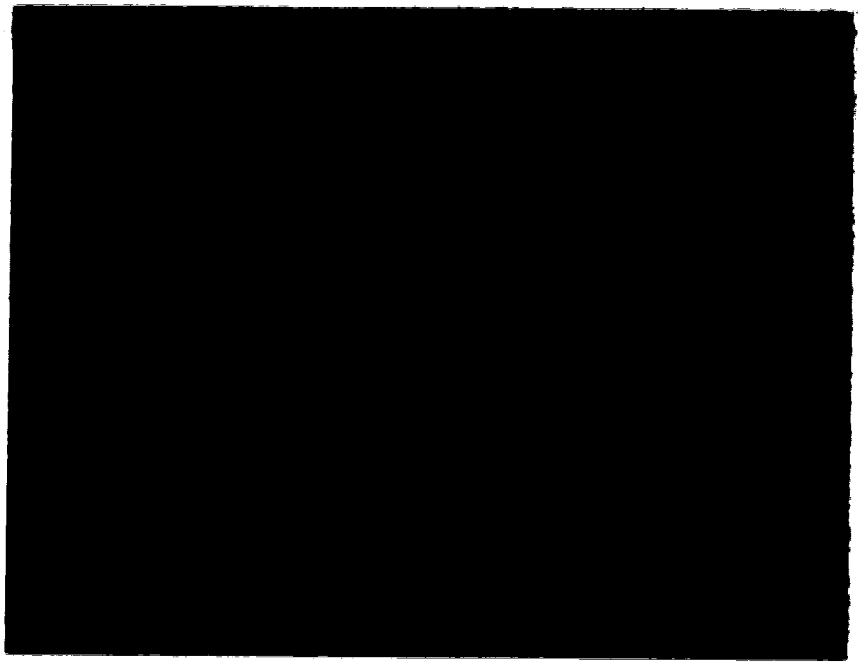

Plate 3.9 Precipitation in T700C, X520

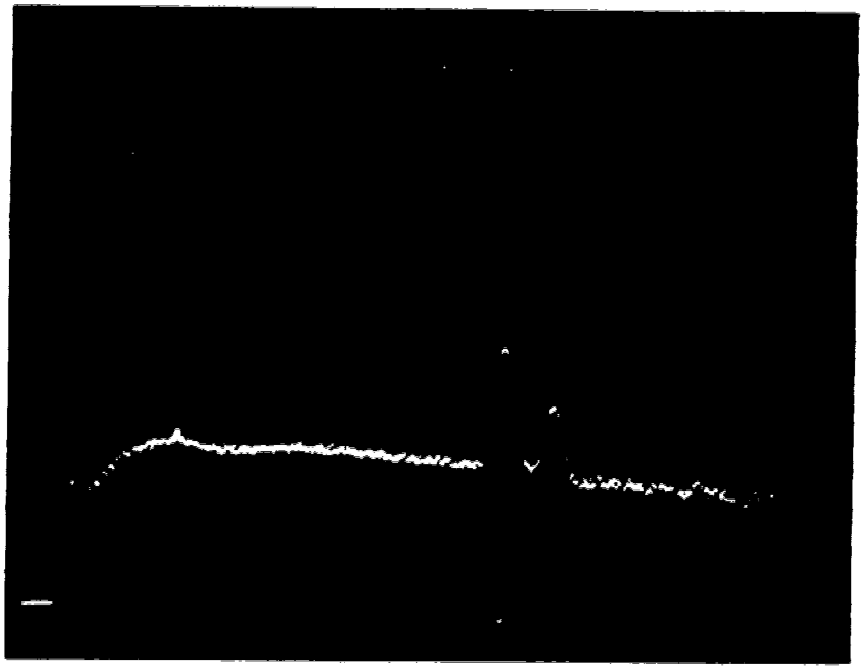

Plate 3.10 A typical X-ray spectrum from the bulk solid solution of T700C

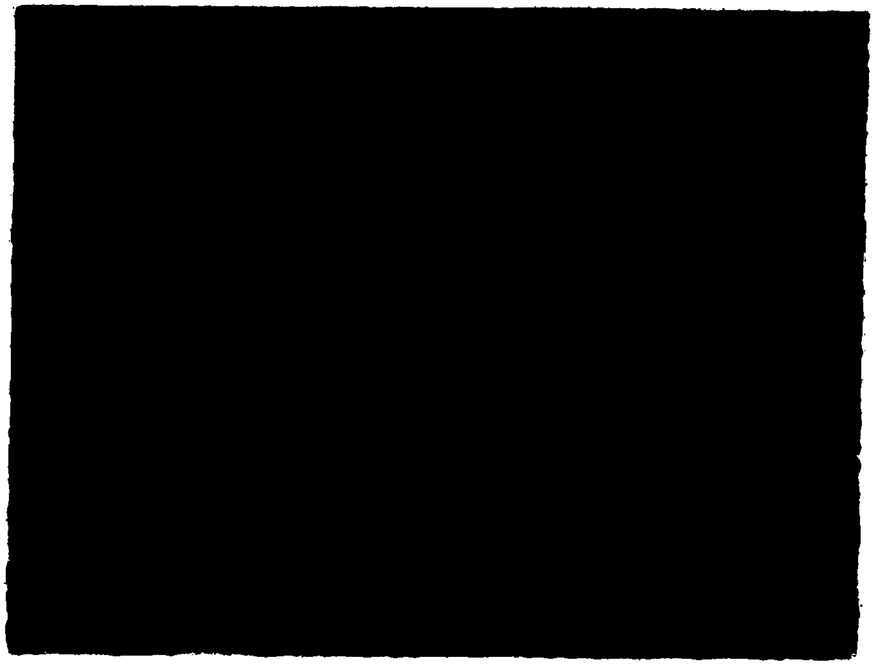

Plate 3.11 Precipitation in T600C, X480

features the same. However, the precipitates are smaller and less widely spaced. This is as expected since the diffusion coefficient of P decreased more rapidly than the time available for diffusion increased. Plate 3.12 shows the microstructure of sample T500C. Here the precipitates have had insufficient time to grow therefore they are very small and finely spaced. This may be explained by considering the very recent work of Luckman et al. [35] which shows that P diffusivity decreases more rapidly than predicted from high temperature extrapolation.

A quantitative chemical analysis of the specimens was carried out on an ARL electron microprobe in the Department of Geology, by courtesy of Dr. D. G. W. Smith. Established experimental techniques, technical assistance and data analyses were provided. An EDS system was first used to determine the purity of the samples. Then, because only the two elements needed analysis, a Wavelength Dispersive Spectrometer (WDS) was used for all quantitative analyses. The resulting raw data (X-ray counts for K-alpha peak and background for each element) were analysed by an iterative Atomic Number-Atomic Absorption-Fluorescence correction program called EDATA2. Sensitivity of the system was better than 0.02 at% of P.

The experimental results are given in section 4.4.2 where they are used. By comparing 100 random areas, the produced master alloy phosphides were analysed as 64% Fe_2P and 36% Fe_3P to give an average 18.6 wt% P (a loss of

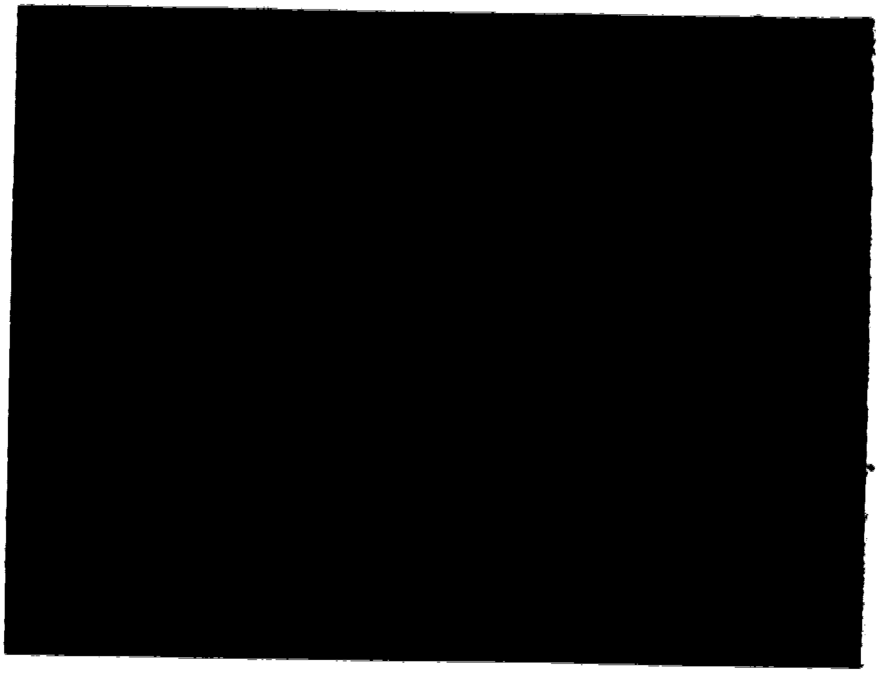

Plate 3.12 Precipitation in T500C, X480

1.4 wt% P from the nominal 20 wt% P in production). This value was used to produce the nominal 1.5 wt% P final alloys (~1.30 wt% P actually present). All final alloys were vacuum arc-melted twice to assure homogeneous distribution of P. This, plus the fact that any accidental overheating of the melt increases its vapour pressure, accounts for the loss of phosphorus.

3.4 Theoretical Techniques

The major part of this thesis, presented in chapter 4, is a theoretical analysis of intergranular segregation in iron. The equipment and techniques used are described here.

3.4.1 Equipment

All calculations were executed on a Hewlett Packard (HP) 9825A Computer using the HP Basic programing language. Most* graphs were produced on an HP 9872A Graphic Plotter. The programs used were monitored using a HP 9871A Line Printer.

3.4.2 Numerical Analysis

All analytical equations were solved directly. Generally, these functions (chemical potentials, limit of solubilities and Case I segregation equations of chapter 4) were plotted on graphs immediately as they were calculated. However, there was also the need to simultaneously solve the roots of two or more equations (e.g. Case II magnetic segregation free energies, segregation curves and boundary Curie temperatures of chapter 4). The finding of roots of equations of the form $f(x) = 0$ is one of the most frequently occurring problems in scientific work. In general, it is only possible to obtain approximate solutions, relying on some computation technique to produce the approximation.

A linear iteration method was employed for finding the roots of simultaneous equations. For a single equation, $f(x) = 0$ may be expressed as $x = g(x)$ and, geometrically, a root of $f(x) = 0$ is a number $x = z$ for which the line $y = x$ intersects the curve $y = g(x)$. The equation $x = g(x)$ is solved by a converging recursion of x. It must be noted that the condition $|g'(x)| < 1$ should be observed for convergence.

For simultaneous equations, consider the following example with 2 equations:

$$f(x,y) = 0 \text{ and } x = F(x,y)$$
$$g(x,y)= = 0 \text{ and } y = G(x,y).$$

Sufficient but not necessary conditions [36] for the convergence of the linear iteration method are:

1. F and G and their first derivatives are continuous in a neighbourhood R of the desired root.
2. The sum of the absolute values of the partial derivatives of F and G must be less than one for all points (x,y) in R.
3. The initial approximation of (x,y) is chosen in R.

Whenever possible an accelerated technique was used in place of the linear iteration method. This technique is called the Wegstein method for algebraic convergence [37] and is based on a projection technique. That is, a projection from two known points on the x = f(x) line determines a point on the y = x line. This x value is then used for f(x). The projection requires the solution of

$$x_3 = \frac{x_1y_2 - y_1x_2}{x_1 - x_2 + y_2 - y_1}$$

and x_2 and x_3 now become the new known points. This procedure is repeated until a rapid convergence is obtained. The numerical problems encountered in section 4 required the solving of at least two simultaneous equations such as:

$$x = f(x,y,T)$$
$$y = g(x,y,T)$$

This was accomplished by up to four independent iteration techniques which will be called A, B, C, and D:

A. For each constant T required, a linear iteration technique for finding x and y was used. If A failed (a certain number of recursions was exceeded), control was passed to B. This usually happened when the slope of the curve became very steep.

B. One of the curves was 'inverted' and the following equation solved:

$$T = h(x,y,T)$$
$$y = g(x,y,T)$$

For each constant x, a linear iteration technique for finding y and T was used. If B failed, control was passed to A. However, if A and B both failed, control was passed to C. A and B both failing occurred often and usually indicated an oscillation in the iteration.

C. This iteration was useful only when a special condition applied, e.g. when $x + y = 1$. For a constant x, y was set and T could be found using a Wegstein acceleration. If C could not be used, control was passed to D.

D. This technique consisted of a Wegstein accelerator inner iteration and a graphical bisection outer iteration. That is, for each step of x, an iteration similar to B found T and y. The value of x was stepped until a change in sign for the curves was noticed. Each step of x was then halved as the value of x oscillated around the root until a certain desired accuracy was reached. This technique was very slow but always produced a root. If a special condition occurred, then control would be passed to C.

The segregation and free energy curves of section 4 were produced by Program 1, Appendix 2. A flow chart of the program is also presented in Appendix 2. When an iterative method was used, up to 240 points were calculated per function to produce smooth curves. This data was stored on magnetic tape during calculation and later retrieved for plotting.

4. RESULTS AND DISCUSSION

This chapter contains a theoretical thermodynamic development, some sections of which have been previously published by the author [38]. The effects of ferromagnetism on selected properties of iron-based solid solutions are approached from a macroscopic equilibrium thermodynamic viewpoint. These properties include the solid solubility limit of a solute, the intergranular segregation of a solute, and diffusion within the solution. Although the model described is applicable to any solute in iron, phosphorus in iron is used as an example and the experimental results for the behavior of phosphorus in alpha iron are presented where convenient to support the thermodynamic development. Starting from basic definitions, the model will be built up to deal with binary and ternary solid solutions. Although all symbols used are defined at the time of their first appearance in the text, a complete compilation of symbols and their definitions is given in Appendix 1. Although use was made of the work of others, particularly Nishizawa and Guttmann, the treatment is original unless otherwise stated.

4.1 The Free Energy Function for alpha Iron

The metal under consideration is body centered cubic alpha iron. In the pure state alpha iron is stable from 0 to 1185 K. When dealing with conditions of equilibrium, it is convenient to describe the system in terms of state variables or functions. As the state of the system is changed, the change of any state function depends only on the value of the function in the initial and final states, i.e. the change in the functions is independent of the path along which the change has occurred. State variables are not necessarily independent of one another. However, once the state of a system is specified by the values of a few state functions, the values of all are fixed.

Consider the Gibbs free energy function for a pure substance. The Gibbs free energy, G, is a state function defined by

$$G = H - TS \tag{4.1}$$

Entropy, S, is a state function and enthalpy, H, is defined by

$$H = U + PV \tag{4.2}$$

where internal energy, U, pressure, P, and volume, V are state functions. For a pure substance, G depends on the chemical nature of the substance, the amount of the substance in the sample, the state (solid, liquid, gas) in which it exists, the temperature and applied pressure. The free energy of all substances decreases with increase in temperature. At 0 K the free energy is equal to the total internal energy of a solid, which is equivalent to its enthalpy. An increase in temperature increases the enthalpy.

The rate of increase of the enthalpy with temperature is the heat capacity of the substance. Similarily, as free energy decreases with increasing temperature the rate of decrease is the entropy of the substance. In general, the Gibbs free energy may be given by

$$G = {}^{o}G + RT\ell n a \tag{4.3}$$

where ${}^{o}G$ is the free energy of the substance when present in its standard state and 'a' is its activity.

Consider the total Gibbs free energy function, G^{Fe}, for alpha iron. By definition,

$$G^{Fe} = H^{Fe} - TS^{Fe} \tag{4.4}$$

However, as pointed out by Zener [39] and Weiss and Tauer [40], the total free energy function should be analysed by its component parts, i.e.

$$G^{Fe} = G^{Fe}_{magnetic} + G^{Fe}_{lattice} + G^{Fe}_{electronic} \tag{4.5}$$

This type of approach was first taken by Zener [39] who explained the abnormal form of the gamma-loop in the Fe-Cr system as being due to the magnetic transition in alpha iron. Later, Weiss and Tauer [40,41] numerically evaluated the magnetic (subscript mag) and non-magnetic (subscript nm) components of enthalpy and entropy (and hence of free energy) for alpha iron. Both the enthalpy and the entropy may be estimated from the heat capacity (or specific heat). Although below the Curie temperature the electronic heat capacity for each direction of electron spin is different and should be considered separately, the overall lattice and electronic heat capacities are similar. Therefore, the total Gibbs free energy may be given by

$$G^{Fe} = G^{Fe}_{nm} + G^{Fe}_{mag} \qquad (4.6)$$

and because G^{Fe} is an extensive function,

$$G^{Fe}_{mag} = H^{Fe}_{mag} - TS^{Fe}_{mag} \qquad (4.7)$$

The term magnetic enthalpy, as an example, refers to the magnetic component of enthalpy. There is an excellent review by Miodownik [42] which deals with non-linear magnetic components of free energy and phase stability in magnetic alloys.

The magnetic enthalpy and entropy functions used in the present work are based on the data of Weiss and Tauer [40] as shown in Table 4.1.

From this data, empirical functions of magnetic enthalpy and entropy were developed by the author as described in the following paragraphs.

Phase transitions are generally classified by order according to the presence of a discontinuity in that order of derivative of the free energy with respect to a given state variable such as temperature. First order transitions (a discontinuity is present in the first derivative) have discontinuities in entropy, volume and enthalpy at the transition temperature. Examples of first-order transitions

Table 4.1 The magnetic thermodynamic functions of alpha iron [40]

Temperature (K)	Enthalpy (J/mole)	Entropy (J/mole/K)	Free Energy (J/mole)
0	-8732	0.00	-8732
400	-8636	0.21	-8732
500	-8535	0.38	-8720
600	-8368	0.67	-8725
700	-8037	1.17	-8770
800	-7518	1.88	-8856
900	-6538	3.01	-9022
1000	-4831	4.86	-9247
1100	-2671	6.99	-9691
1200	-1842	7.70	-10360
1300	-1398	8.12	-11082
1400	-1122	8.33	-11954
1500	-925	8.46	-12784
1600	-787	8.54	-13615
1700	-716	8.58	-14451
1800	-674	8.62	-16190

are fusion, vaporization and allotropic transformations. Second-order transitions have discontinuities in the heat capacity, the compressibility and the thermal expansion coefficient. Some examples of second-order transformations are order-disorder transformations in alloys and the onset of ferromagnetism.

For materials with a paramagnetic to ferromagnetic transformation (e.g. alpha iron) the magnetic heat capacity has a very large peak (spike) at the Curie temperature T_c^{Fe} as shown in Figure 4.1. Some previous work has simulated the magnetic heat capacity Cp_{mag}^{Fe} [43] using fitting formulae such as

$$\begin{aligned} Cp_{mag} &= AR\ln([1+L^n]/[1-L^n]), \quad L < 1 \\ &= BR\ln([1+L^{-m}]/[1-L^{-m}]), \quad L > 1 \end{aligned} \tag{4.8}$$

where $L = T/T_c^{Fe}$ and $n = 3$, $m = 5$. However, in the present work these formulae were fitted to magnetic heat capacity, enthalpy and entropy data through the following:

$$\begin{aligned} H_{mag}^{Fe} &= \int Cp_{mag}^{Fe} dT \\ S_{mag}^{Fe} &= \int Cp_{mag}^{Fe} dT/T \end{aligned} \tag{4.9}$$

Since the heat capacity of iron is infinite at the Curie temperature an analytic determination of the integrals in equations (4.9) is not possible. Instead, a power series expansion for the natural logarithmic terms in equations (4.8) was used, where

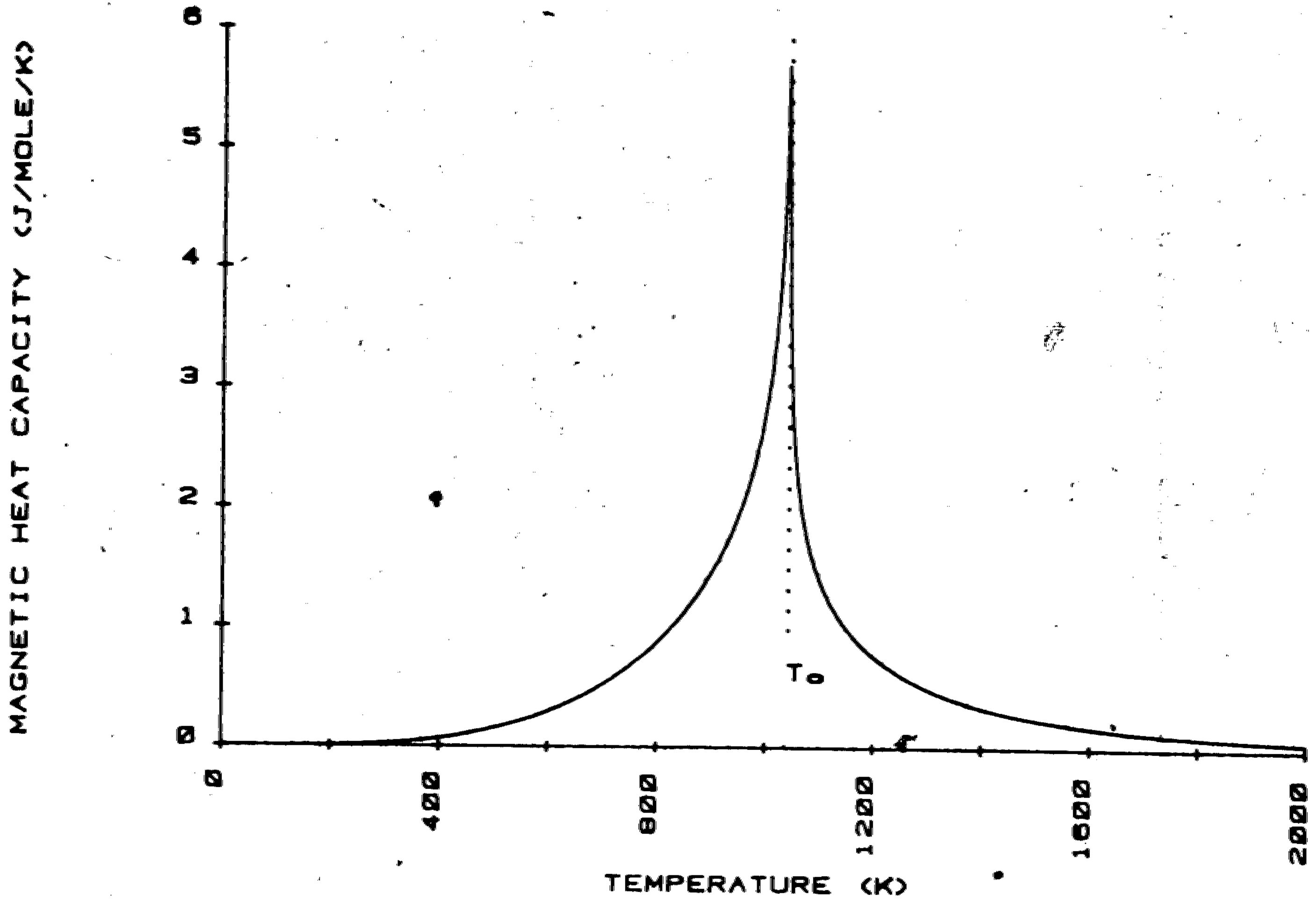

Figure 4.1
The magnetic heat capacity of alpha iron.

$$\ell n([1+X]/[1-X]) = 2[X+\frac{X^3}{3}+\frac{X^5}{5}+.....] \qquad (4.10)$$

This allowed a simple integration of equations (4.9) and a fitting of equations (4.9) to the data in Table 4.1 with the following results: for $L < 1$, $A = 1.08444$ and $n = 3.613$ and for $L > 1$, $B = 0.67423$ and $m = 4.766$. This calculated magnetic heat capacity of alpha iron is shown in Figure 4.1. The discontinuity at the Curie Temperature was avoided by arbitrarily setting a maximum for the heat capacity. Figure 4.2 shows the magnetic entropy curve while Figure 4.3 shows the magnetic enthalpy and resultant Gibbs free energy curves for alpha iron (data from Table 4.1). An assumed maximum value for magnetic heat capacity at the Curie temperature corresponds to straight line approximations immediately about the Curie temperature.

The magnetic free energy of alpha iron, $G^{Fe}_{mag}(T)$, as shown in Figure 4.3, may be divided by the Curie temperature into two regions, an uncoupled (paramagnetic) state, ${}^{u}G^{Fe}_{mag}$, and a coupled (ferromagnetic) state, ${}^{c}G^{Fe}_{mag}$, such that, in approximation:

$$\begin{aligned} G^{Fe}_{mag} &= -AT, && T > T^{Fe}_{c} \\ &= -AT^{Fe}_{c}, && T < T^{Fe}_{c} \end{aligned} \qquad (4.11)$$

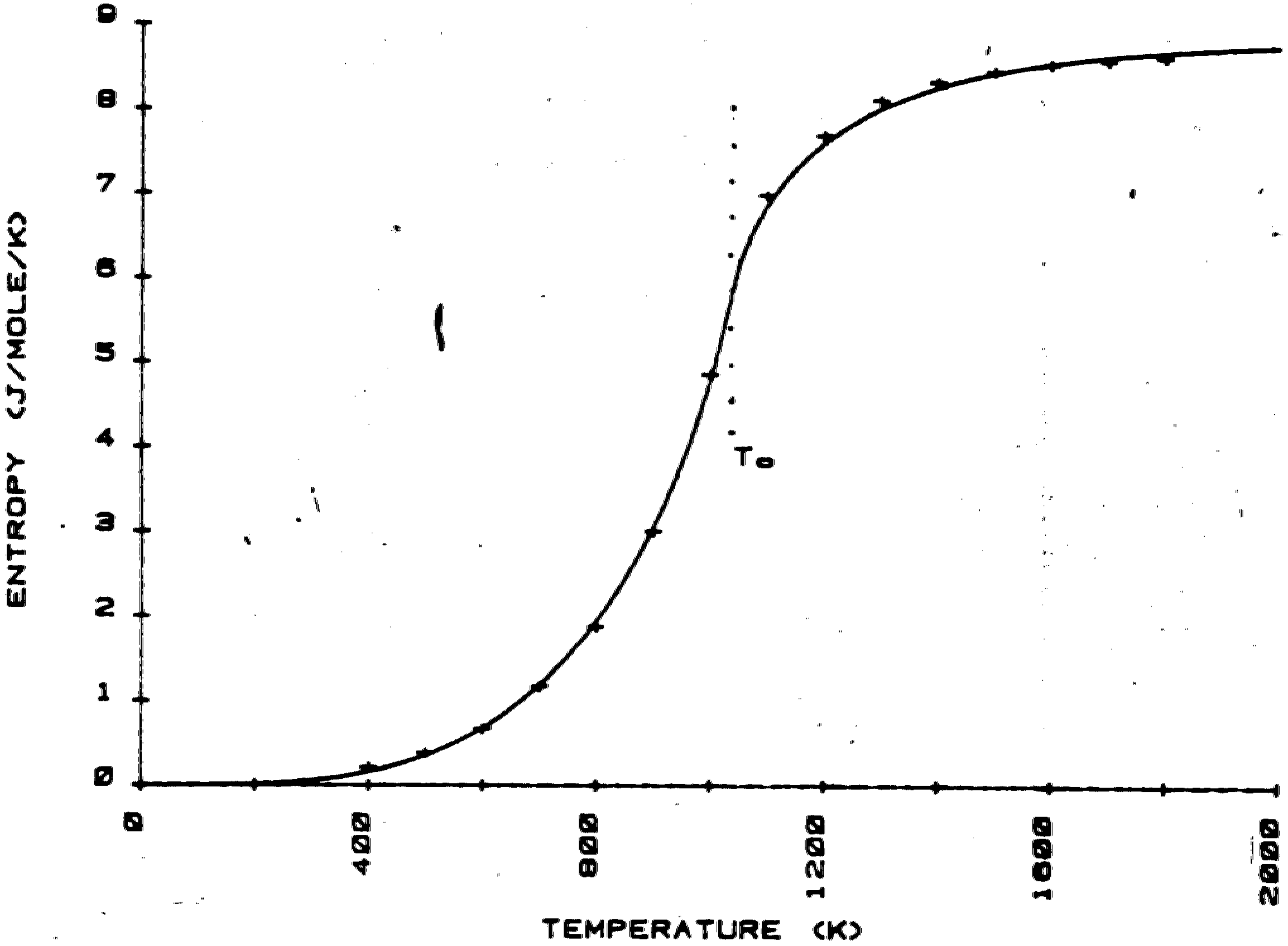

Figure 4.2
The magnetic entropy of alpha iron (+ denotes data [40])

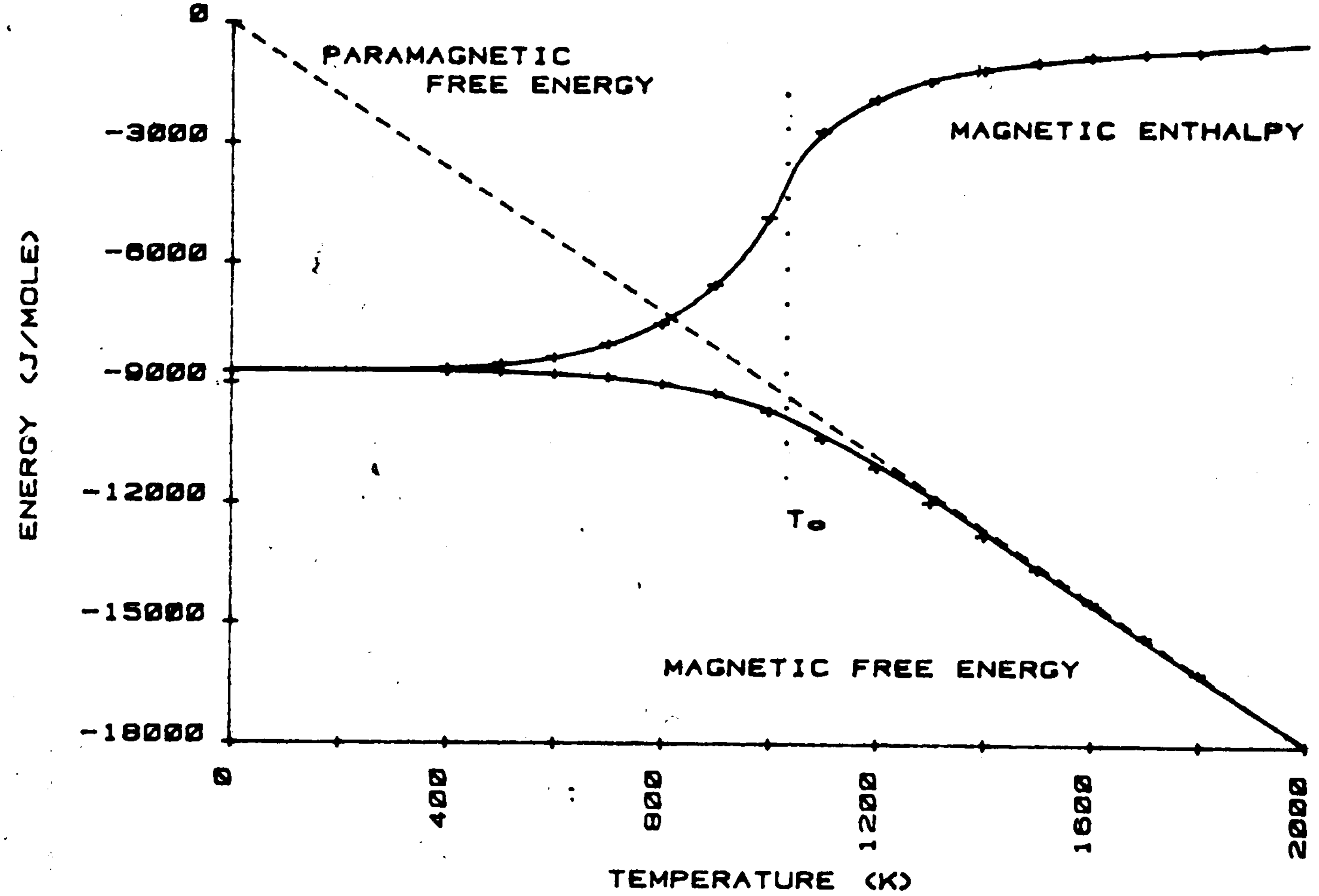

Figure 4.3
The magnetic enthalpy and Gibbs free energy of alpha'iron (+ denotes data [40]).

The constant A[6] may be evaluated by considering equation (4.7), and, differentiating with respect to T when L > 1 gives

$$\frac{\partial G^{Fe}_{mag}}{\partial T} = \frac{\partial H^{Fe}_{mag}}{\partial T} - T\frac{\partial S^{Fe}_{mag}}{\partial T} - S^{Fe}_{mag} = A \tag{4.12}$$

Evaluating the components at L > 1 shows

$$H^{Fe}_{mag} \rightarrow 0 \text{ J/mole}$$
$$S^{Fe}_{mag} \rightarrow {}^{u}S^{Fe}_{mag} = 9 \text{ J/mole/K} \tag{4.13}$$

which implies that

$$S^{Fe}_{mag}(T>>T^{Fe}_{c}) \rightarrow A\text{, a constant}$$
$${}^{u}G^{Fe}_{mag} = -T\,{}^{u}S^{Fe}_{mag}$$
$${}^{c}G^{Fe}_{mag} = -T^{Fe}_{c}\,{}^{u}S^{Fe}_{mag} \tag{4.14}$$

An alpha Fe-X solid solution will now be considered.

4.2 The alpha Fe-X Solid Solution

By analogy, the free energy of an alpha Fe-X solid solution[7], G^{α}, is assumed to have magnetic (subscript mag) and non-magnetic (subscript nm) components [39,40,44], such that

---

[6] This is not the same constant as in equation (4.9).

[7] The solution has mole fractions X and X of the components i and j.

$$G^{\alpha} = G^{\alpha}_{nm} + G^{\alpha}_{mag} \tag{4.15}$$

Consider the formation of a binary solution from the pure components in their standard state. The reaction is

$$X_i i + X_j j = (X_i, X_j) ij + \Delta G_m \tag{4.16}$$

With this reaction is associated a free energy change called the free energy of mixing, ΔG_m, such that

$$\Delta G_m = G^{\alpha} - X_i {}^{o}G^{i} - X_j {}^{o}G^{j} \tag{4.17}$$

For a solid solution

$$G^{\alpha} = \mu^{i} X_i + \mu^{j} X_j \tag{4.18}$$

where μ^i is the chemical potential of component i. Therefore, the free energy of mixing is

$$\Delta G_m = X_i[\mu^{i} - {}^{o}G^{i}] + X_j[\mu^{j} - {}^{o}G^{j}] \tag{4.19}$$

It is assumed that the non-magnetic component of the free energy of the solid solution is approximated by the regular solution model. Regular solutions are solutions formed for components for which the entropy of mixing has the value expected for an ideal solution but for which the enthalpy of mixing is not zero.* A non-zero enthalpy may be expressed by a power series of the component concentrations.

---

*The enthalpy of mixing is zero for an ideal solution.

Therefore, as expressed by Nishizawa et al., the non-magnetic component of free energy is

$$G^{\alpha}_{nm} = [1-X_X]\,{}^{o}G^{Fe}_{nm} + X_X\,{}^{o}G^{X}_{nm} + X_X[1-X_X]I^{FeX}_{nm} + RT\{[1-X_X]\ell n(1-X_X) + X_X \ell n X_X\} \qquad (4.20)$$

This free energy is expressed as an atomic fraction of solute X, X_X, where ${}^{o}G^{i}_{nm}$ is the standard free energy for non-magnetic i and I^{ij}_{nm} is the non-magnetic interaction parameter between components i and j.

Unfortunately, it is not possible to theoretically estimate the magnetic free energy in the same way; instead, descriptive modifications to the magnetic free energy of alpha iron are made [40,45], as described now.

It is well known that the addition of many species of solute to alpha iron alters its Curie temperature. This may be observed in any major compilation of binary phase diagrams such as found in the Metals Handbook [47]. The change in Curie temperature of a solution with change in solute content is often small and consequently easy to ignore. To ignore a shift in the Curie temperature is, in effect, making a zeroth approximation.

Nishizawa et al. [44] considered that the Curie temperature of iron is shifted from 1043 K by dissolving the atomic fraction X_X of solute X, such that

$$T^{\alpha}_{c} = T^{Fe}_{c} + \Delta T_X X_X \qquad (4.21)$$

The magnetic parameter for solute X, ΔT_X, represents the effectiveness of a given solute in changing the Curie temperature. This linear approximation would be valid at least for dilute solid solutions. Assuming such a concentration dependence for the Curie temperature Hillert et al. [45,46] have shown that the magnetic free energy for alpha Fe-X may be obtained by modifying the free energy of alpha iron. Figure 4.4 shows the modification where the magnetic free energy curve for alpha Fe-X is displaced along the paramagnetic free energy line, ${}^{u}G^{Fe}_{mag}$. That is, the alpha Fe-X magnetic free energy curve maintains the same position with respect to the new Curie temperature as the alpha iron free energy curve to the old Curie temperature [44].

The displacements mentioned may be described by considering for alpha iron a temperature T_1 such that

$$G^{Fe}_{mag}(T_1) = -T^{Fe}_{c} \, {}^{u}S^{Fe}_{mag} \,.$$

$$\text{where} \quad T^{Fe}_{c} - T_1 = K, \text{ a constant.} \qquad (4.22)$$

For the solid solution alpha Fe-X, there exists a temperature T_2 such that

$$G^{\alpha}_{mag}(T_2) = -T^{\alpha}_{c} \, {}^{u}S^{Fe}_{mag}$$

$$\text{where} \quad T^{\alpha}_{c} - T_2 = K \qquad (4.23)$$

This implies that

$$T^{\alpha}_{c} = T^{Fe}_{c} - T_1 + T_2$$

$$T_1 = T_2 - \Delta T_X X_X \qquad (4.24)$$

For alpha Fe-X, T_2 is the system temperature, T, but if

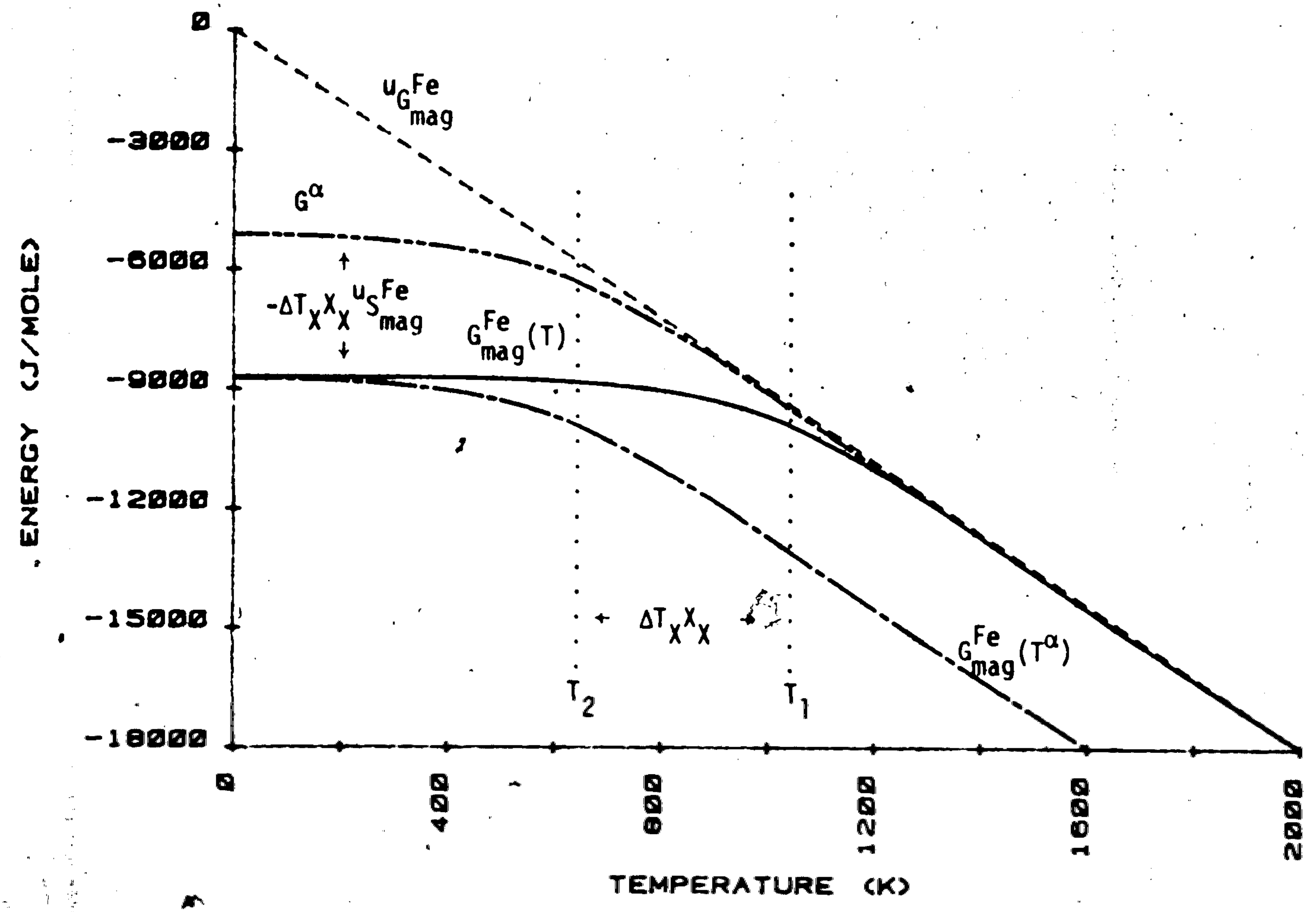

Figure 4.4
The shift in the magnetic free energy of alpha iron.

$T_1 = T^\alpha$, then (see Figure 4.4)

$$T^\alpha = T - \Delta T_X X_X$$

and

$$G^\alpha_{mag}(T) = G^{Fe}_{mag}(T^\alpha) - \Delta T_X X_X {}^u S^{Fe}_{mag} \qquad (4.25)$$

The above is true for all values of T.

Weiss and Tauer [41] pointed out the influence of the solute upon the size of the magnetic component, introducing what may be called a solute intensity factor M_X, so that in an alpha Fe-X solid solution

$$G^\alpha_{mag} = [1-M_X X_X][G^{Fe}_{mag}(T^\alpha) - \Delta T_X X_X {}^u S^{Fe}_{mag}] \qquad (4.26)$$

Therefore, the free energy of the alpha Fe-X solid solution may be expressed as

$$\begin{aligned} G^\alpha = {} & [1-X_X]{}^oG^{Fe}_{nm} + X_X {}^oG^X_{nm} + X_X[1-X_X]I^{FeX}_{nm} \\ & + RT\{[1-X_X]\ell n(1-X_X) + X_X \ \ell n X_X\} \\ & + [1-M_X X_X][G^{Fe}_{mag}(T^\alpha) - \Delta T_X X_X {}^u S^{Fe}_{mag}] \qquad (4.27) \end{aligned}$$

In recent work by Nishizawa et al. [44], the interaction term has been reformulated to include a magnetic interaction. In regard to a dilute solid, it was pointed out that:

$$I^{FeX} = I^{FeX}_{nm} + I^{FeX}_{mag}$$
$$I^{FeX}_{mag} = \Delta T_X[S^{Fe}_{mag}(T^{\alpha}) - {}^{u}S^{Fe}_{mag}]$$
$${}^{c}I^{FeX}_{mag} = I^{FeX}_{nm} - \Delta T_X {}^{u}S^{Fe}_{mag}$$
$${}^{u}I^{FeX}_{mag} = I^{FeX}_{nm} \tag{4.28}$$

The above was justified in the following manner by considering Hillert et al. [45,46]. The excess free energies or the interaction free energies, I, are very small at low alloy contents. For the magnetic term, G^{Fe}_{mag}, a small alloy addition ΔX causes the Curie temperature, T_c, to be displaced by ΔT_c. Therefore, the change in free energy of the solution at any temperature (per mole alpha iron) is

$$\Delta T_c \frac{\partial G^{Fe}_{mag}}{\partial T} \tag{4.29}$$

which, per mole alloying element, is

$$\frac{\Delta T_c}{\Delta X} \frac{\partial G^{Fe}_{mag}}{\partial T} \tag{4.30}$$

In the present case

$$\Delta X = X_X$$
$$\Delta T_c = -\Delta T_X X_X \tag{4.31}$$

and term (4.30) becomes

$$\Delta T_X S^{Fe}_{mag}(T) \tag{4.32}$$

Now, considering equation (4.26),

$$I^{FeX}_{mag} = \Delta T_X[S^{Fe}_{mag}(T^{\alpha}) - {}^{u}S^{Fe}_{mag}] \qquad (4.33)$$

which is the second of Nishizawa's equations (4.28). Therefore, the approximated alpha Fe-X free energy [44] may written as

$$G^{\alpha} = [1-X_X]{}^{o}G^{Fe}_{nm} + X_X{}^{o}G^{X}_{nm} + I^{FeX}_{nm}X_X[1-X_X]$$

$$+ RT\{[1-X_X]\ell n(1-X_X) + X_X\ell nX_X\}$$

$$+ [1-M_XX_X]\{G^{Fe}_{mag}(T) + \Delta T_XX_X[S^{Fe}_{mag}(T^{\alpha}) - {}^{u}S^{Fe}_{mag}]\} \qquad (4.34)$$

where $$G^{Fe}_{mag}(T^{\alpha}) = G^{Fe}_{mag}(T) + S^{Fe}_{mag}(T^{\alpha})\Delta T_XX_X \qquad (4.35)$$

The above free energy may be used to determine the chemical potentials of the constituents of the solid solution.

4.3 Chemical Potentials of alpha Fe-X Solid Solutions

The free energy of an alpha Fe-X solid solution may be expressed in terms of its component chemical potentials as expressed in equation (4.18). Taking the differential of equation (4.18) gives

$$\partial G^{\alpha} = \mu^{Fe}dX_{Fe} + \mu^{X}dX_X$$

where $$X_{Fe}d\mu^{Fe} + X_Xd\mu^{X} = 0 \quad \text{(Gibbs-Duhem equation)} \qquad (4.36)$$

In a binary solution $dX_{Fe} = -dX_X$ and therefore the chemical potentials are described by

$$\mu^{Fe} = G^{\alpha} - \sum_j X_j \frac{\partial G^j}{\partial X_j} = G^{\alpha} - X_X \frac{\partial G^{\alpha}}{\partial X_X}$$

$$\mu^{X} = G^{\alpha} - \sum_j X_j \frac{\partial G^j}{\partial X_j} + \frac{\partial G^{\alpha}}{\partial X_X} = \mu^{Fe} + \frac{\partial G^{\alpha}}{\partial X_X} \tag{4.37}$$

These chemical potentials may be separated into magnetic and non-magnetic components. The partial differential of the free energy of the solution with respect to the solute content is

$$\begin{aligned}\frac{\partial G^{\alpha}}{\partial X_X} = & -{}^{o}G^{Fe}_{nm} + [1-X_X]\frac{\partial\, {}^{o}G^{Fe}_{nm}}{\partial X_X} + {}^{o}G^{X}_{nm} + X_X\frac{\partial\, {}^{o}G^{X}_{nm}}{\partial X_X} \\ & + [1-2X_X]I^{Fe}_{nm} + X_X[1-X_X]\frac{\partial I^{Fe}_{nm}}{\partial X_X} + RT[\ell n X_X - \ell n(1-X_X)] \\ & - [M_X + X_X\frac{\partial M_X}{\partial X_X}][G^{Fe}_{mag}(T^{\alpha}) - \Delta T_X X_X {}^{u}S^{Fe}_{mag}] \\ & + [1-M_X X_X][\frac{\partial G^{Fe}_{mag}}{\partial X_X}(T^{\alpha}) - \Delta T_X {}^{u}S^{Fe}_{mag}]\end{aligned} \tag{4.38}$$

At this point, it is necessary to evaluate the terms present:

1. The standard non-magnetic free energy of pure alpha iron is a function of temperature only, such that,

$$\frac{\partial\, {}^{o}G^{Fe}_{nm}}{\partial X_X} = 0 \tag{4.39}$$

2. Also, the standard non-magnetic free energy of pure X is a function of temperature only, such that,

$$\frac{\partial {}^{o}G^{X}_{nm}}{\partial X_X} = 0 \tag{4.40}$$

3. The non-magnetic interaction parameter is a function of temperature only, such that

$$\frac{\partial I^{FeX}_{nm}}{\partial X_X} = 0 \tag{4.41}$$

4. The modified magnetic free energy of alpha iron is a function of temperature and the component concentrations, such that

$$\frac{\partial G^{Fe}_{mag}(T^{\alpha})}{\partial X_X} = \frac{\partial G^{Fe}_{mag}(T^{\alpha})}{\partial T^{\alpha}} \frac{\partial T^{\alpha}}{\partial X_X}$$

where $\frac{\partial T^{\alpha}}{\partial X_X} = -\Delta T_X$ (4.42)

The modified magnetic free energy is defined as a function of modified temperature by reference to equation (4.7). Differentiating equation (4.7) with respect to the modified temperature gives

$$\frac{\partial G^{Fe}_{mag}(T^{\alpha})}{\partial T^{\alpha}} = \frac{\partial H^{Fe}_{mag}(T^{\alpha})}{\partial T^{\alpha}} - S^{Fe}_{mag}(T^{\alpha}) - T^{\alpha}\frac{\partial S^{Fe}_{mag}(T^{\alpha})}{\partial T^{\alpha}} \tag{4.43}$$

As stated previously, the magnetic enthalpy and entropy were obtained from the magnetic heat capacity in such a manner that

$$\frac{\partial H^{Fe}_{mag}(T^{\alpha})}{\partial T^{\alpha}} = Cp^{Fe}_{mag}(T^{\alpha})$$

$$\frac{\partial S^{Fe}_{mag}(T^{\alpha})}{\partial T^{\alpha}} = \frac{Cp^{Fe}_{mag}(T^{\alpha})}{T^{\alpha}}$$

$$\frac{\partial G^{Fe}_{mag}(T^{\alpha})}{\partial X_X} = \Delta T_X S^{Fe}_{mag}(T^{\alpha}) \tag{4.44}$$

5. The modified magnetic entropy may be handled in a similar way, such that

$$\frac{\partial S^{Fe}_{mag}(T^{\alpha})}{\partial X_X} = \frac{-\Delta T_X Cp^{Fe}_{mag}(T^{\alpha})}{T^{\alpha}} \tag{4.45}$$

However, as noticed in figure 4.1, the modified heat capacity for alpha iron has small values even near the transition temperature. Therefore, this term has been ignored throughout.

6. The solute intensity factor may be a function of temperature and solute concentrations. In this case, M_X was chosen to be a constant, M, which depends on the magnetic properties of the solute as discussed below.

Equation (4.38) may now be written as

$$\begin{aligned}\frac{\partial G^{\alpha}}{\partial X_X} = {} & -{}^{o}G^{Fe}_{nm} + {}^{o}G^{X}_{nm} + [1-2X_X]I^{FeX}_{nm} + RT[\ell n X_X - \ell n(1-X_X)] \\ & - M[G^{Fe}_{mag}(T^{\alpha}) - \Delta T_X X_X \; {}^{u}S^{Fe}_{mag}] \\ & + [1-MX_X]\Delta T_X[S^{Fe}_{mag}(T^{\alpha}) - {}^{u}S^{Fe}_{mag}]\end{aligned} \tag{4.46}$$

The validity of the approximation in equation (4.36) may be seen from the fact that any derivative of the solution free energy remains unchanged with the approximation.

The chemical potentials of both Fe and X in the solid solution can also be separated into magnetic and non-magnetic components. Therefore, the chemical potential of Fe in alpha Fe-X is

$$\mu^{Fe} = \mu^{Fe}_{nm} + \mu^{Fe}_{mag}$$

$$\mu^{Fe}_{nm} = {}^{o}G^{Fe}_{nm} + X^2_X I^{FeX}_{nm} + RT\ell n(1-X_X) \tag{4.47}$$

$$\begin{aligned}\mu^{Fe}_{mag} = {} & G^{Fe}_{mag}(T^{\alpha}) - \Delta T_X X_X {}^{u}S^{Fe}_{mag} \\ & - X_X[1-MX_X]\Delta T_X[S^{Fe}_{mag}(T^{\alpha}) - {}^{u}S^{Fe}_{mag}]\end{aligned} \tag{4.48}$$

In the dilute approximation the magnetic chemical potential of Fe versus temperature is shown in Figure 4.5. The magnetic chemical potential of Fe is not strongly dependent on the concentration of solute X for a typical impurity concentration , such as phosphorus at 0.0001 atomic fraction,

$$\mu^{Fe}_{mag} \simeq G^{Fe}_{mag}(T), \quad \text{for small } X_X, \quad T^{\alpha} \simeq T \tag{4.49}$$

To observe equation (4.48) as a function of magnetic parameter, the solute concentration must be high, as in Figure 4.6. As may be seen, the magnetic chemical potential of Fe increases with decreasing magnetic parameter.

Likewise, the chemical potential of X in alpha Fe-X is given by

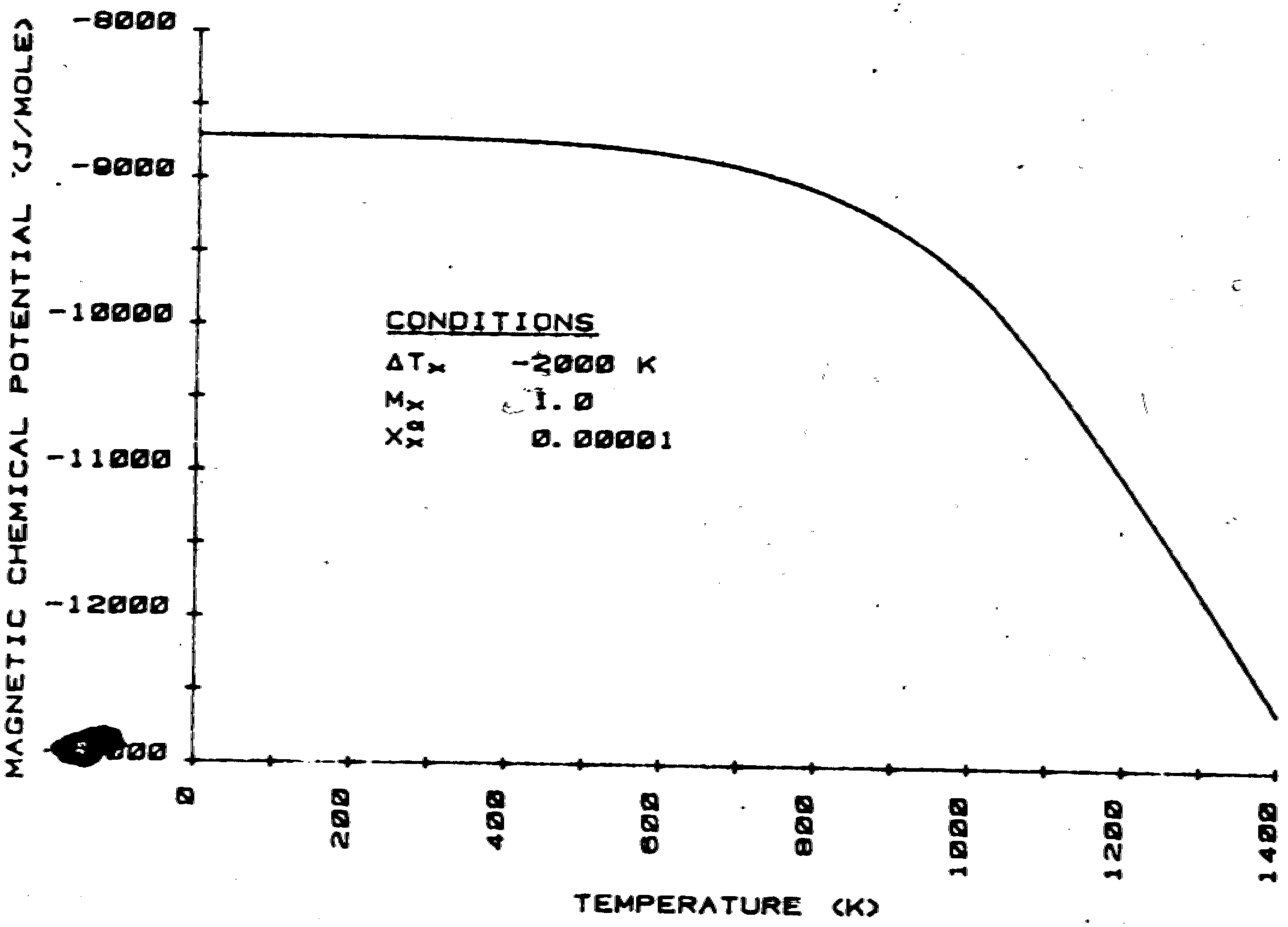

Figure 4.5
The magnetic chemical potential of Fe in alpha Fe-X.

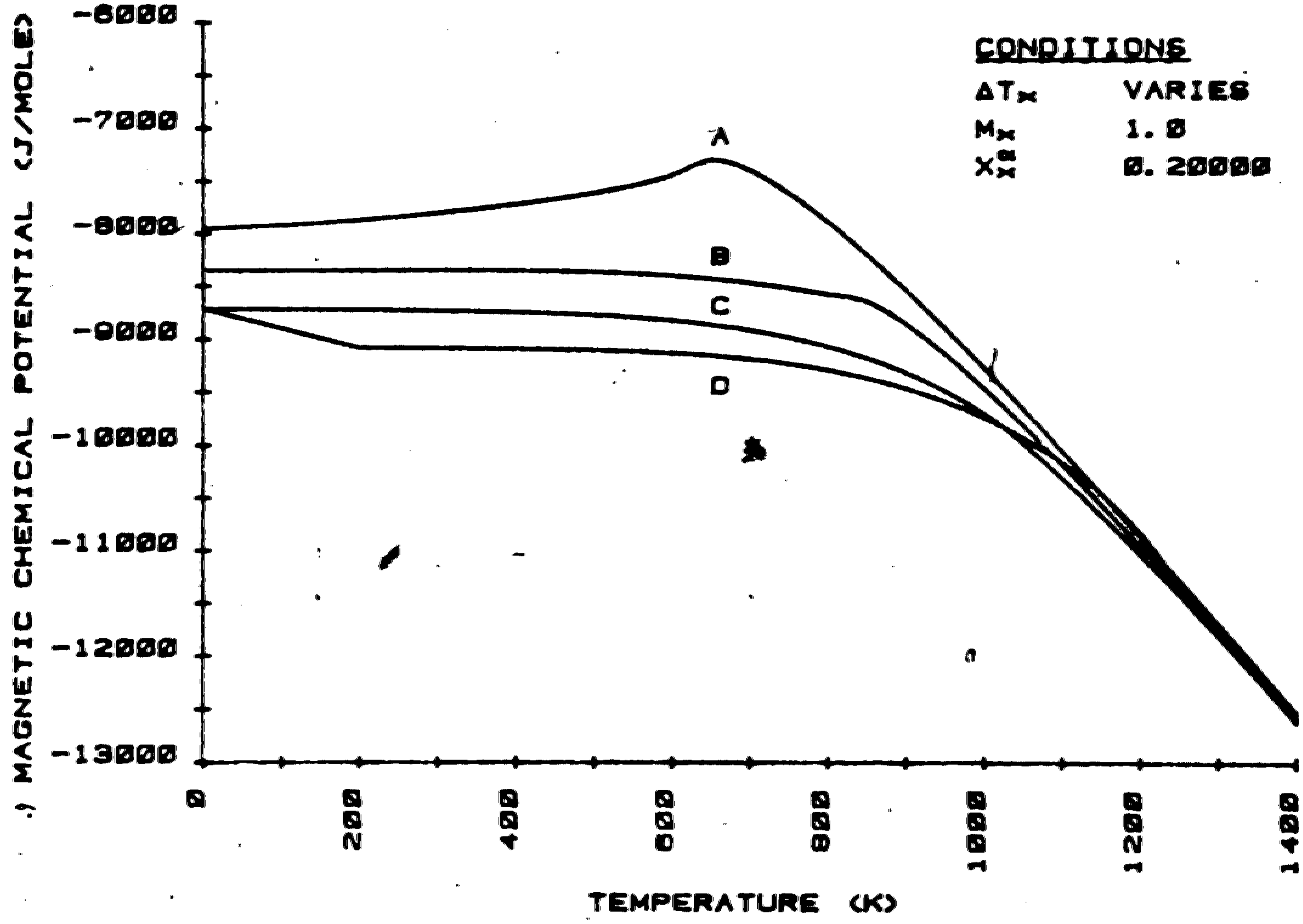

Figure 4.6
The effect of magnetic parameter on the chemical potential of Fe in alpha Fe-X (A = -2000 K, B = -1000 K, C = 0 K, D = 1000 K).

$$\mu^{X} = \mu^{X}_{nm} + \mu^{X}_{mag}$$

$$\mu^{X}_{nm} = {}^{o}G^{X}_{nm} + [1-X_{X}]^{2} I^{FeX}_{nm} + RT\ell n X_{X} \qquad (4.50)$$

$$\mu^{X}_{mag} = [1-M][G^{Fe}_{mag}(T^{\alpha}) - \Delta T_{X} X_{X} {}^{u}S^{Fe}_{mag}] + [1-X_{X}-MX_{X}+MX^{2}_{X}]\Delta T_{X}[S^{Fe}_{mag}(T^{\alpha}) - {}^{u}S^{Fe}_{mag}] \qquad (4.51)$$

The magnetic chemical potential of X versus temperature is shown in Figure 4.7 for M = 1 and varying magnetic parameter. Again, decreasing magnetic parameter increases the potential curve and, for a dilute solution,

$$\mu^{X}_{mag} \simeq \Delta T_{X}[S^{Fe}_{mag}(T) - {}^{u}S^{Fe}_{mag}] \qquad (4.52)$$

Likewise, Figure 4.8 shows the magnetic chemical potential of X for varying solute concentration.

The behavior of the chemical potential curves is as expected. A small addition of solute X to alpha iron makes little difference to the average iron atom and therefore has little effect on the chemical potential of Fe. However, each solute X atom disturbs the alpha iron lattice locally and there is a tendency for rejection of X from the lattice. This increases the chemical potential of X.

Nishizawa et al. [44], have conjectured that M = 0 may be used for magnetic solute such as cobalt and M = 1 may be used for non-magnetic solute such as phosphorus. However, M may be temperature and concentration dependent. For M = 1,

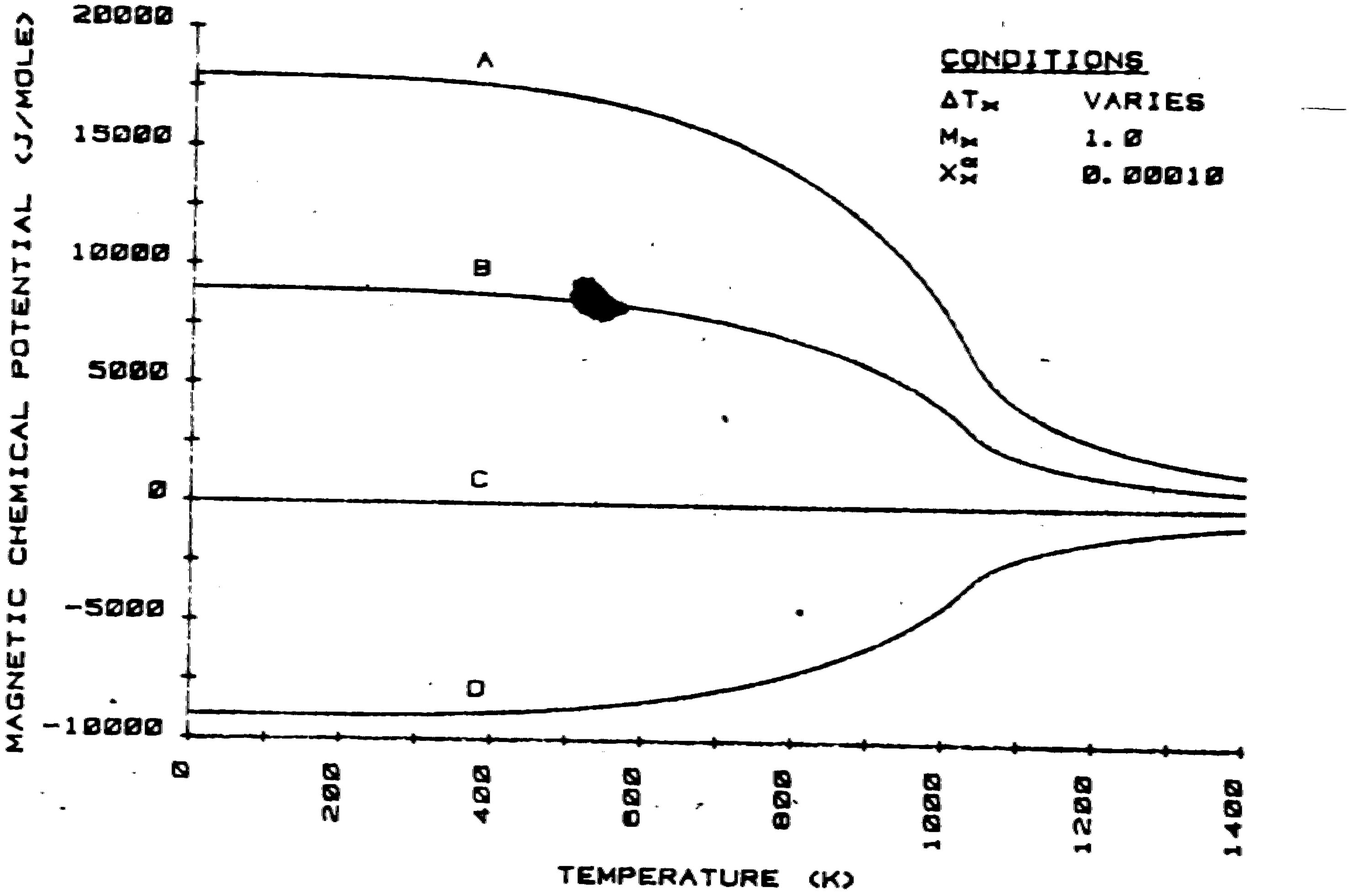

Figure 4.7
The effect of the magnetic parameter on the chemical potential of X in alpha Fe-X (A = -2000 K, B = -1000 K, C = 0 K, D = 1000 K).

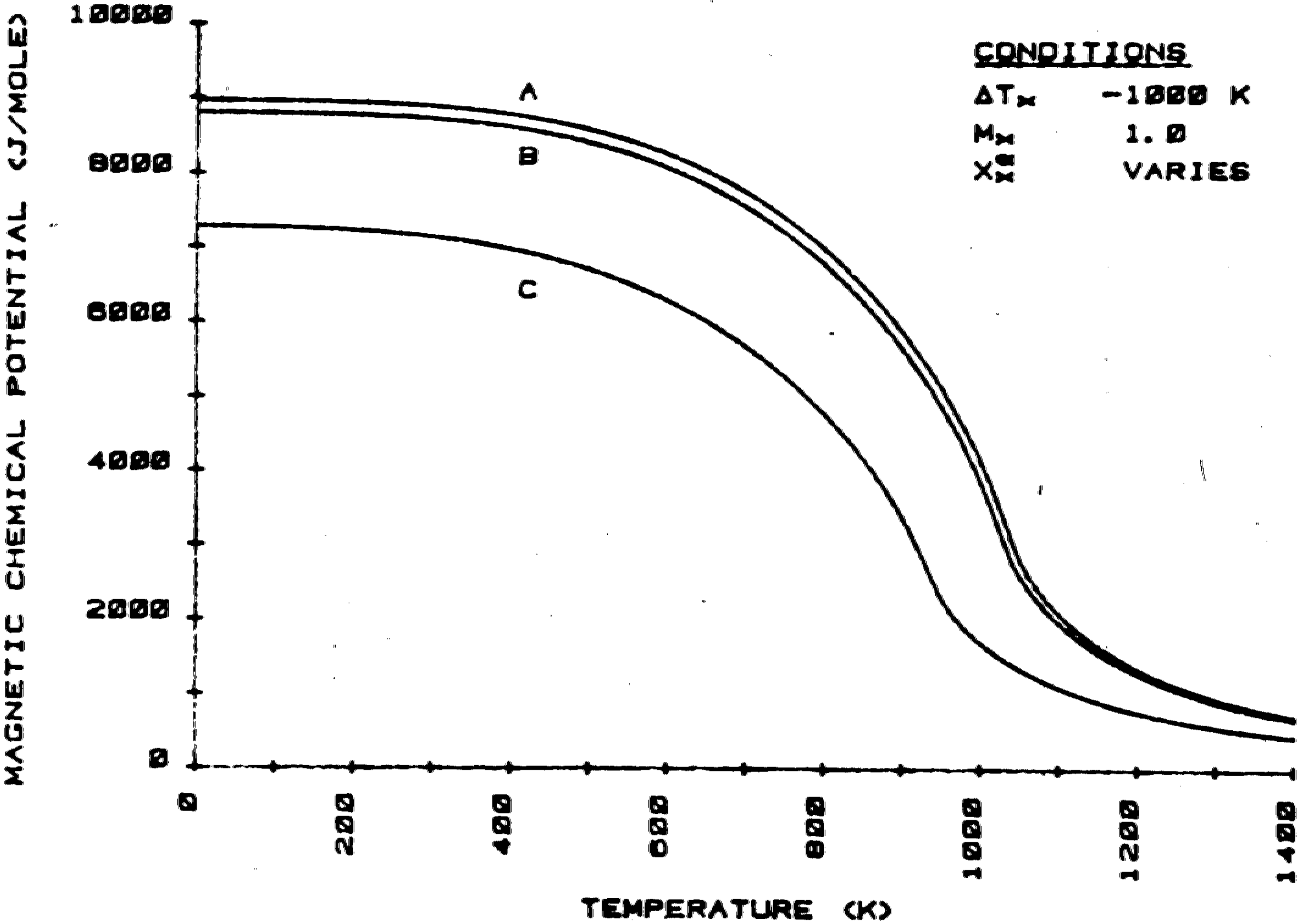

Figure 4.8
The effect of bulk solute concentration on the chemical potential of X in alpha Fe-X (A = 0.001, B = 0.01, C = 0.1).

the chemical potentials are summarized below:

$$
\begin{aligned}
&1.\quad \mu^{Fe}_{nm} = {}^{o}G^{Fe}_{nm} + X^{2}_{X} I^{FeX}_{nm} + RT\ell n(1-X_X)\\
&2.\quad \mu^{Fe}_{mag} = G^{Fe}_{mag}(T^{\alpha}) - \Delta T_X X_X \, {}^{u}S^{Fe}_{mag}\\
&\qquad\qquad - X_X[1-X_X]\Delta T_X[S^{Fe}_{mag}(T^{\alpha}) - {}^{u}S^{Fe}_{mag}]\\
&3.\quad \mu^{X}_{nm} = {}^{o}G^{X}_{nm} + [1-X_X]^{2} I^{FeX}_{nm} + RT\ell n X_X\\
&4.\quad \mu^{X}_{nm} = [1-X_X]^{2}\Delta T_X[S^{Fe}_{mag}(T^{\alpha}) - {}^{u}S^{Fe}_{mag}]
\end{aligned}
\qquad (4.53)
$$

4.4 Limit of Solubility for X in alpha Fe-X Solid Solution

A change in the chemical potentials due to the onset of ferromagnetism must affect the limit of solubility of a solute in alpha iron. The general case is considered first.

4.4.1 Alpha Fe-X Solid Solutions

The limit of solubility for a solute X in alpha Fe-X occurs when a second phase, Fe_aX_b (denoted θ), is in equilibrium with the alpha Fe-X solid solution. The a and b are defined as fractions such that a + b = 1.

Figure 4.9 shows a schematic of free energy versus concentration for two phases in equilibrium at a particular temperature. The dashed line represents a 'tie' line that determines the concentration of solute in each phase. If X_X is the concentration of X in the alpha phase, then

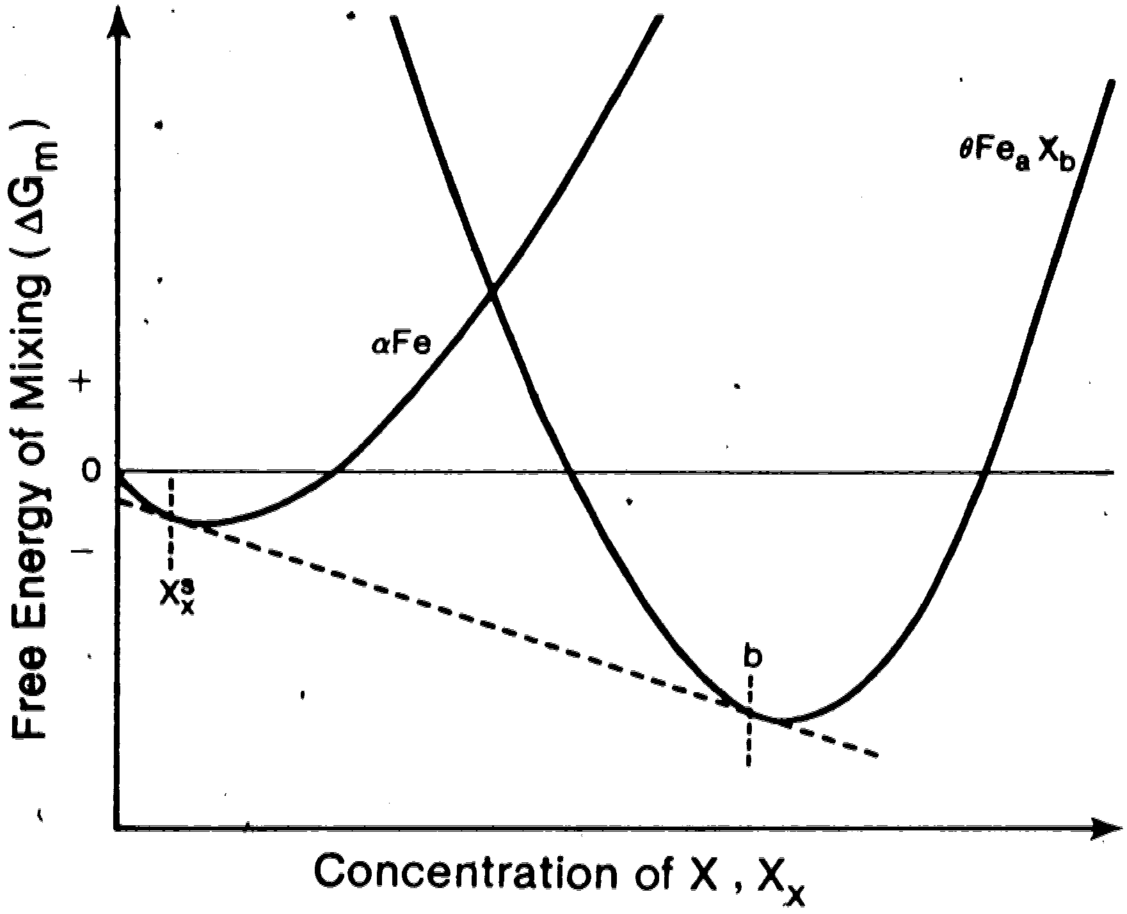

Figure 4.9 A schematic of free energy for two phases in equilibrium.

$$G^{\alpha} = X_X\mu^X + [1-X_X]\mu^{Fe} \qquad (4.54)$$

and when equations (4.34) and (4.35) give the free energy of the solution, the 'tie' line is given by

$$G^{\alpha} = [\mu^X - \mu^{Fe}]X_X + \mu^{Fe} \qquad (4.55)$$

Therefore, assuming the second phase is stoichiometric, i.e. the atomic fraction of X in the second phase is b,

$$G^{\theta} = (\mu^X - \mu^{Fe})b + \mu^{Fe} \qquad (4.56)$$

and the condition for equilibrium of 1 mole of θ is given by

$$a\mu^{Fe} + b\mu^X = G^{\theta} \qquad (4.57)$$

where G^{θ} is the molar free energy of the second phase.

The following formalism was developed by Ko and Nishizawa [29] for alpha iron.[9] For a dilute solid solution, where $X_X << 1$, a dilute approximation may be applied,

$$\mu^{Fe} \simeq {}^{o}G^{Fe}_{nm} + G^{Fe}_{mag}(T)$$

$$\mu^X \simeq {}^{o}G^{X}_{nm} + I^{FeX}_{nm} + RT\ell n X_X + \Delta T_X[S^{Fe}_{mag}(T) - {}^{u}S^{Fe}_{mag}] \qquad (4.58)$$

and equation (4.57) may be written as

---

[9] Recently, solubility in alpha cobalt has also been thermodynamically analysed [48].

$$\begin{aligned} G^{\theta} = {} & a[{}^{o}G_{nm}^{Fe} + G_{mag}^{Fe}(T)] \\ & + b\{{}^{o}G_{nm}^{X} + I_{nm}^{FeX} + RT\ell n X_{X}^{S} + [1-M]G_{mag}^{Fe}(T) \\ & + \Delta T_{X}[S_{mag}^{Fe}(T) - {}^{u}S_{mag}^{Fe}]\} \end{aligned} \tag{4.59}$$

Rearranging this equation gives the limit of solid solubility, X_{X}^{S}, as

$$\begin{aligned} X_{X}^{S} &= \exp(-[Q_{nm}+Q_{mag}]/bRT) \\ Q_{nm} &= a^{o}G_{nm}^{Fe} + b[{}^{o}G_{nm}^{X} + I_{nm}^{FeX}] - G^{\theta} = C + DT \\ Q_{mag} &= [1-bM]G_{mag}^{Fe}(T) + b\Delta T_{X}[S_{mag}^{Fe}(T) - {}^{u}S_{mag}^{Fe}] \end{aligned} \tag{4.60}$$

The behavior of the magnetic free energy of solution, Q versus temperature, is shown in Figure 4.10 for M = 1, b = 0.5 and varying magnetic parameter. The magnetic free energy of solution is approximately linear with temperature above the Curie temperature as would be expected for a non-magnetic situation. However, this is not true near and below the Curie temperature; there is a wide variation of the magnetic free energy of solution with magnetic parameter. A decrease in the magnetic parameter increases the magnetic free energy of solution. As the free energy of solution increases, the limit of solubility for the solute will have to decrease.

Table 4.2 shows calculated magnetic parameters for various elements when added to Fe [44]. Figure 4.11 shows the corresponding Curie temperature for selected alpha Fe-X binaries.

Table 4.2 Magnetic parameters of solute in alpha iron calculated from solubility data [44]

Element	Magnetic Parameter (K)
Be	-1800
Mn	-1300
P	-1200
Cu	-1000
Cr	-800
Zn	-630
Ni	-400
Mo	-300
Ti, Sn, Sb, W	0
Co	+1020

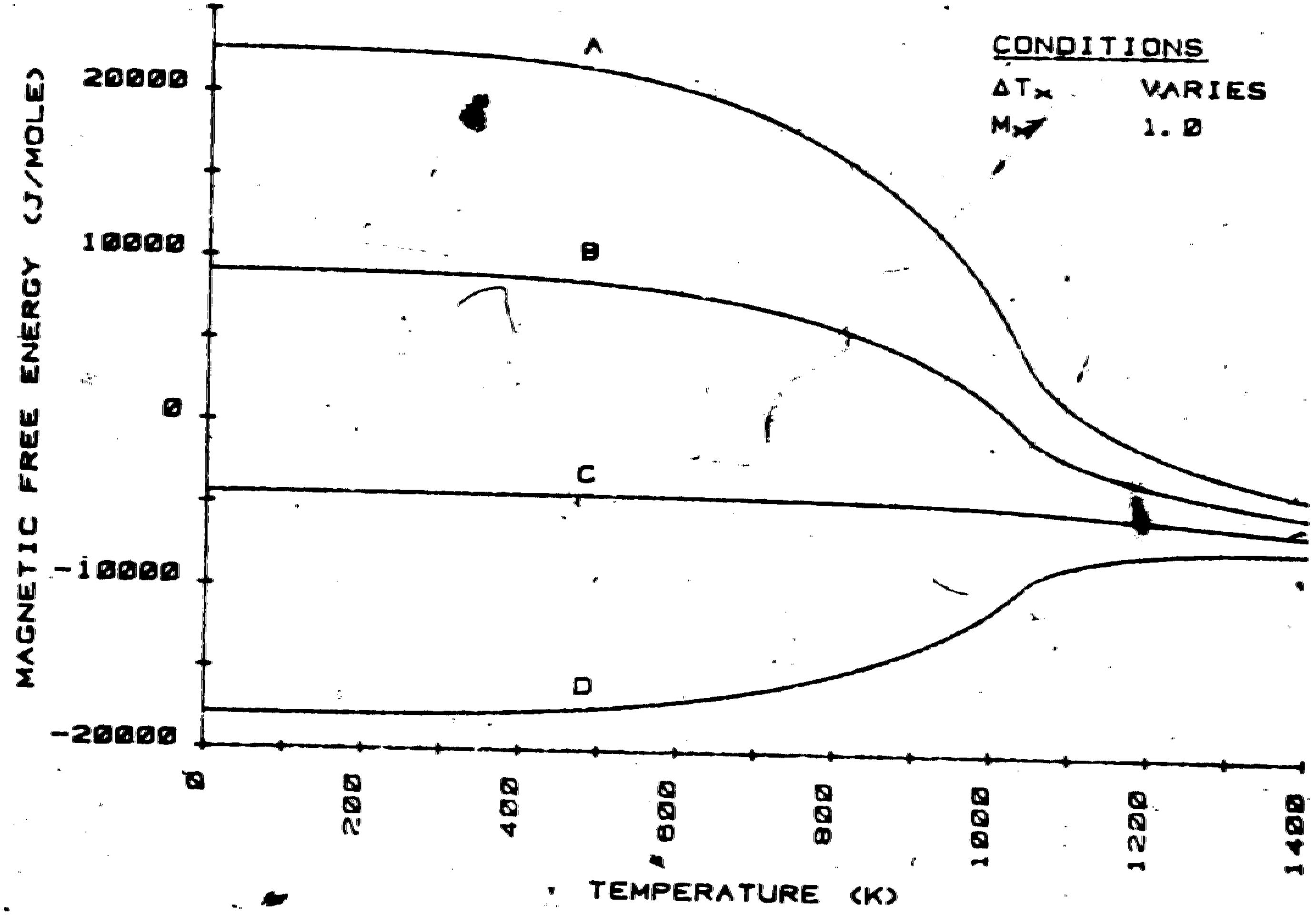

Figure 4.10
The effect of the magnetic parameter on the free energy of solution (A = -2000 K, B = -1000 K, C = 0 K, D = 1000 K).

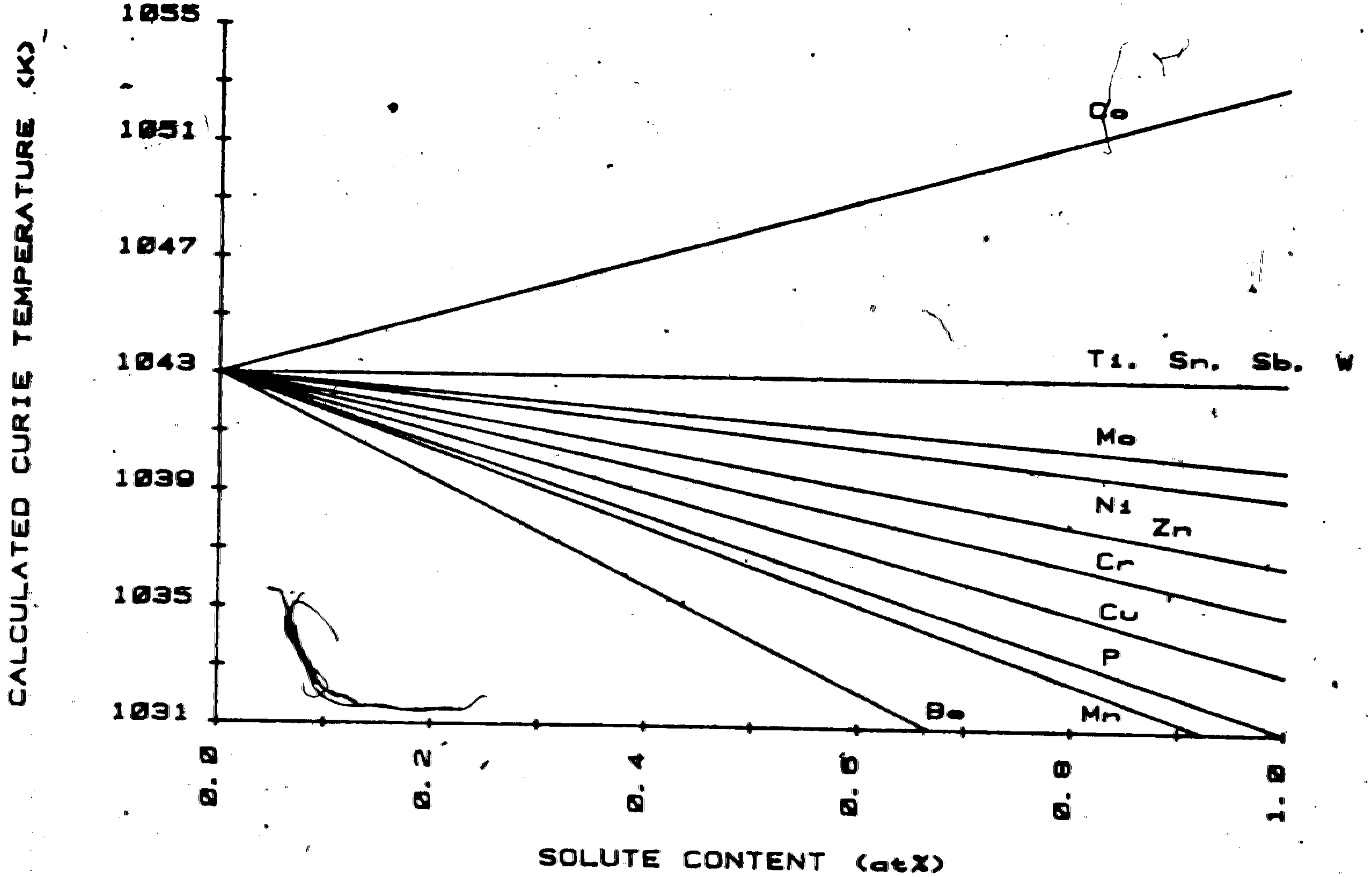

Figure 4.11
Calculated Curie temperatures for various alpha Fe-X binaries.

The behavior of $ln(X^S_X)$ versus inverse temperature, related to Figure 4.10, is shown in Figure 4.12. As expected, the solubility decreases with increasing magnetic parameter, especially below the Curie temperature of the binary alloy. That is, solutes that strongly decrease the Curie temperature (large negative magnetic parameter) also strongly decrease the limit of solubility. The dashed line represents the paramagnetic solubility line for all magnetic parameters. This is a situation where magnetic free energy is linear with temperature and magnetic entropy is constant. Therefore, the paramagnetic behavior is the same as the traditional 'non-magnetic' formulation. Solubility data above the Curie temperature approximates the paramagnetic limit of solubility but it must be remembered that short range magnetic interactions still exist and cause some deviation from paramagnetic behavior.

The experimental determination of solid solubility at low temperatures (below 800 C) requires a sophisticated investigation technique with a small spatial resolution. Furthermore, to approach a state of equilibrium, very long ageing at temperature is needed. However the advent of quantitative Electron Microprobe Analysis (EPMA) has resulted in a substantial amount of experimental data over the last decade. Some of this data is shown in Figure 4.13. As is evident, the solubilities of many solutes in alpha iron follow the form shown in Figure 4.12.

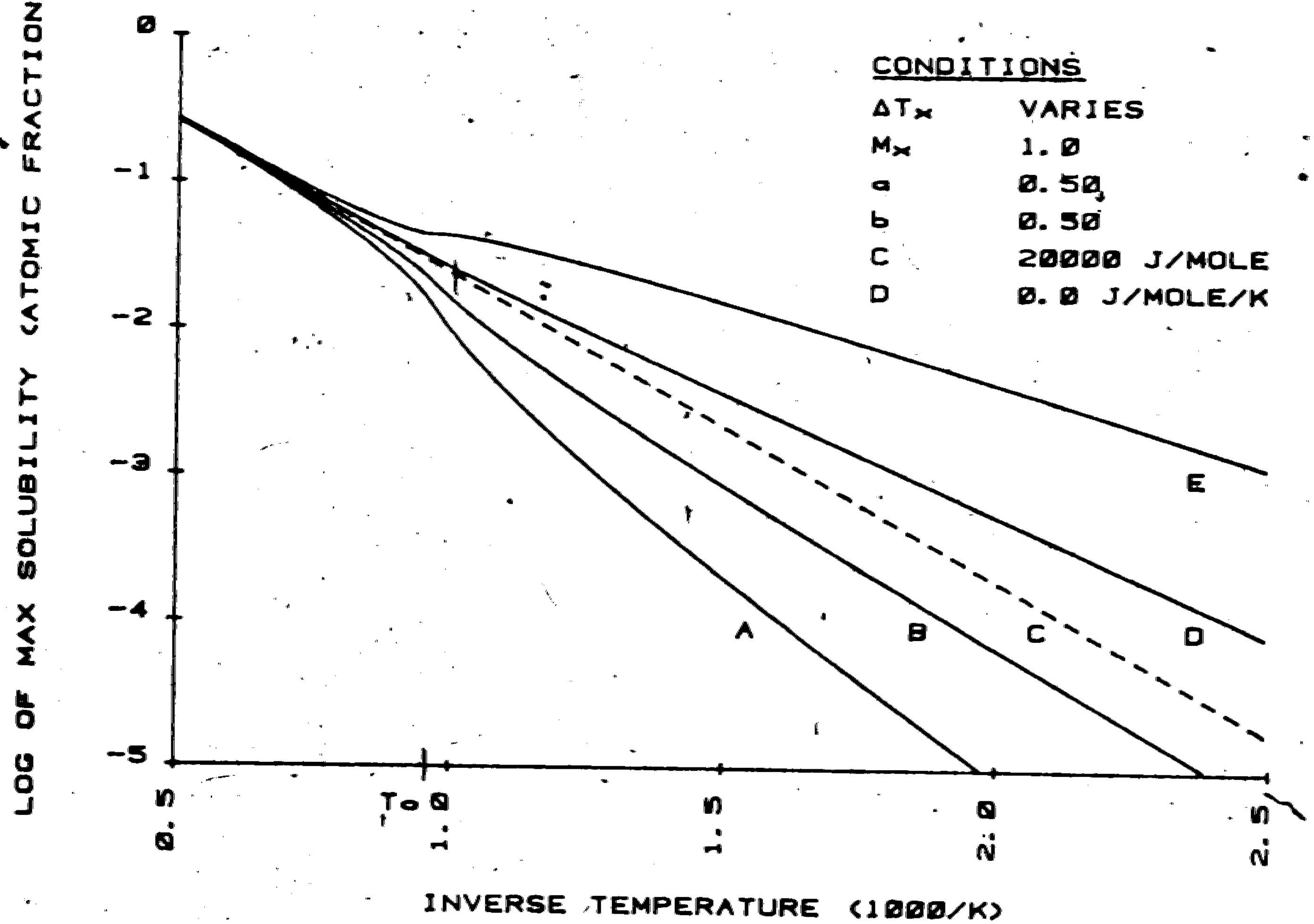

Figure 4.12
The effect of magnetic parameter on predicted solid solubility in Fe (A = -2000 K, B = -1000 K, C = paramagnetic, D = 0 K, E = 1000 K).

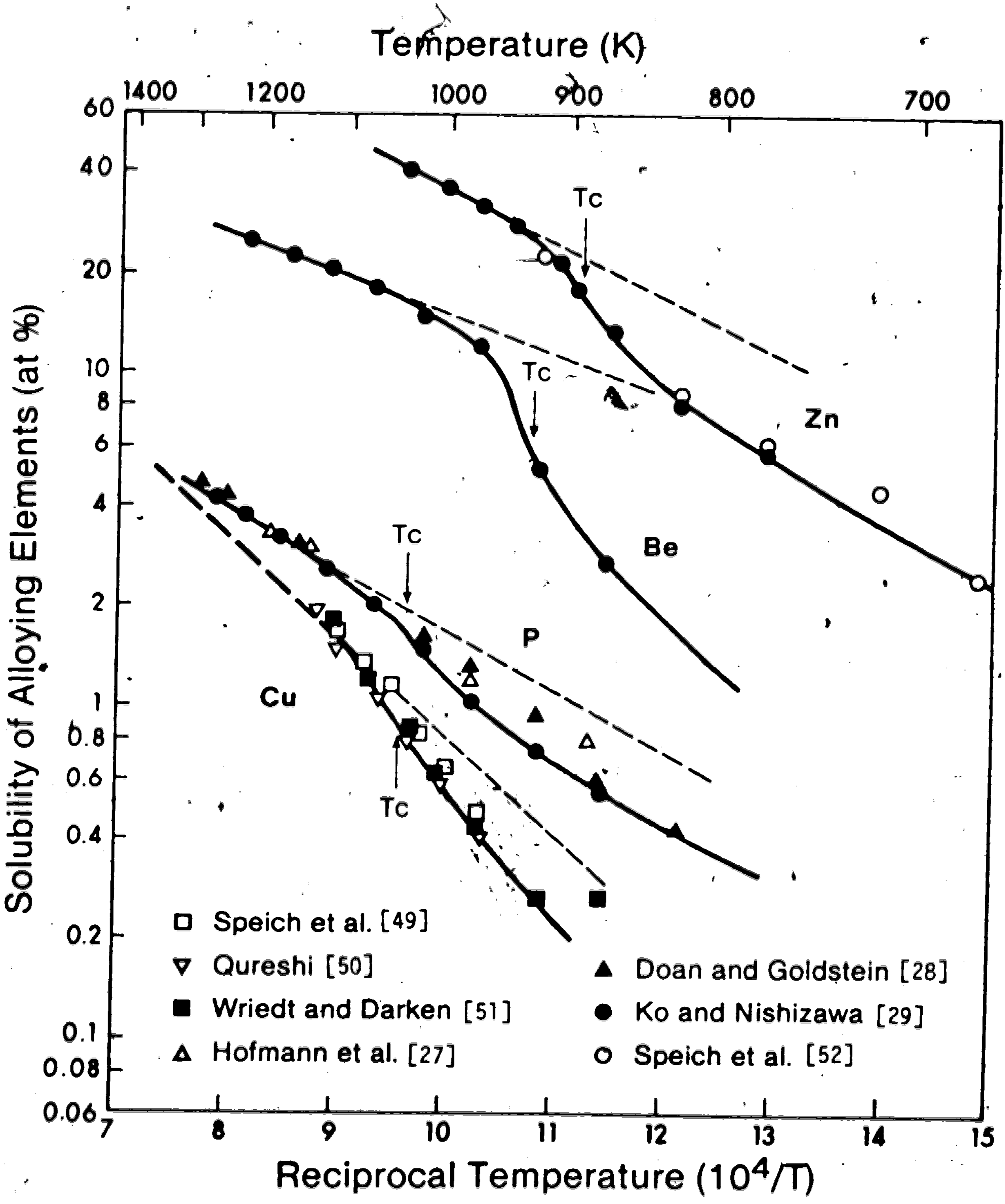

Figure 4.13
Examples of solid solubility for X in alpha Fe.

4.4.2 The Limit of Solubility For P in alpha Fe-P

The experimental results for the solubility of phosphorus in alpha iron from the present work are shown in Table 4.3.

These results were obtained from concentration profiles near second phase precipitates. The growth of an iron phosphide precipitate requires a concentration gradient from the surface of the particle into the bulk. If it is assumed that the region immediately near the particle surface is in quasi-equilibrium, then the solute concentration of the bulk in this region is the real limit of solubility for that temperature. This is especially true at lower temperatures as the time to reach true equilibrium may be prohibitively long and the concentration gradient becomes very steep near the precipitate surface. An example of such a concentration profile is shown in Figure 4.14.

The experimental limit of solubility for P in alpha Fe (denoted by □) is shown in an Arrhenius plot in Figure 4.15. Also shown is the calculated limit of solubility (solid line) and the paramagnetic limit of solubility (dashed line). This latter has been approximated from the data of Kaneko et al. [23] who proposed the following solubility equation (in at%)

$$X_P^S = \exp(4.97 - 4490/T) \qquad (4.61)$$

This gives a non-magnetic free energy of solution of

Table 4.3 Experimental results of bulk phosphorus content

Alloy	phosphorus (at%)
T800C	1.97
T750C	1.50
T700C	0.95
T65[illegible]C	0.72
T600C	0.56
T550C	0.43
T500C	no result
Master 1	32.60
Master 2	24.62

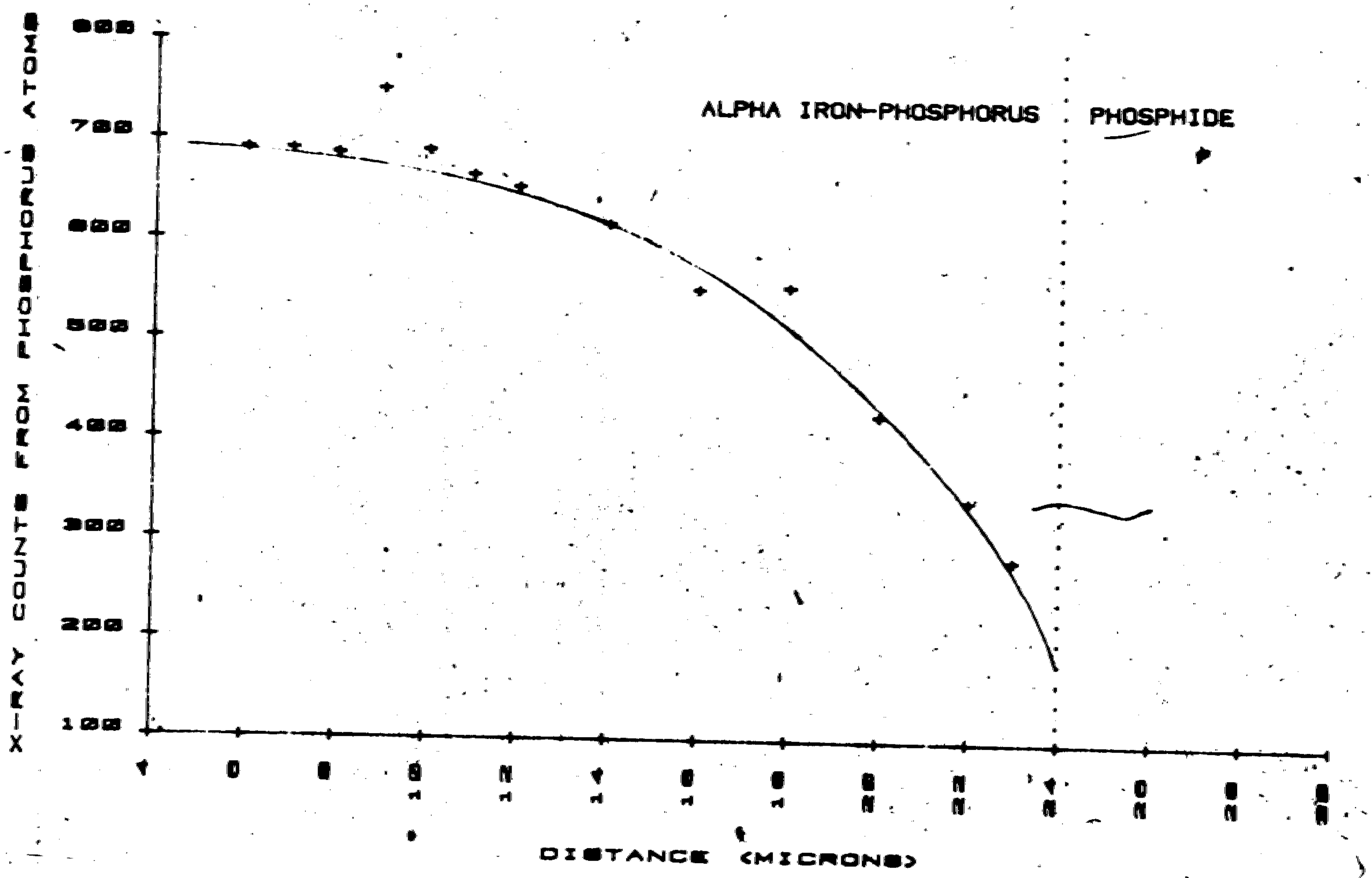

Figure 4.14
An example concentration profile from T550.

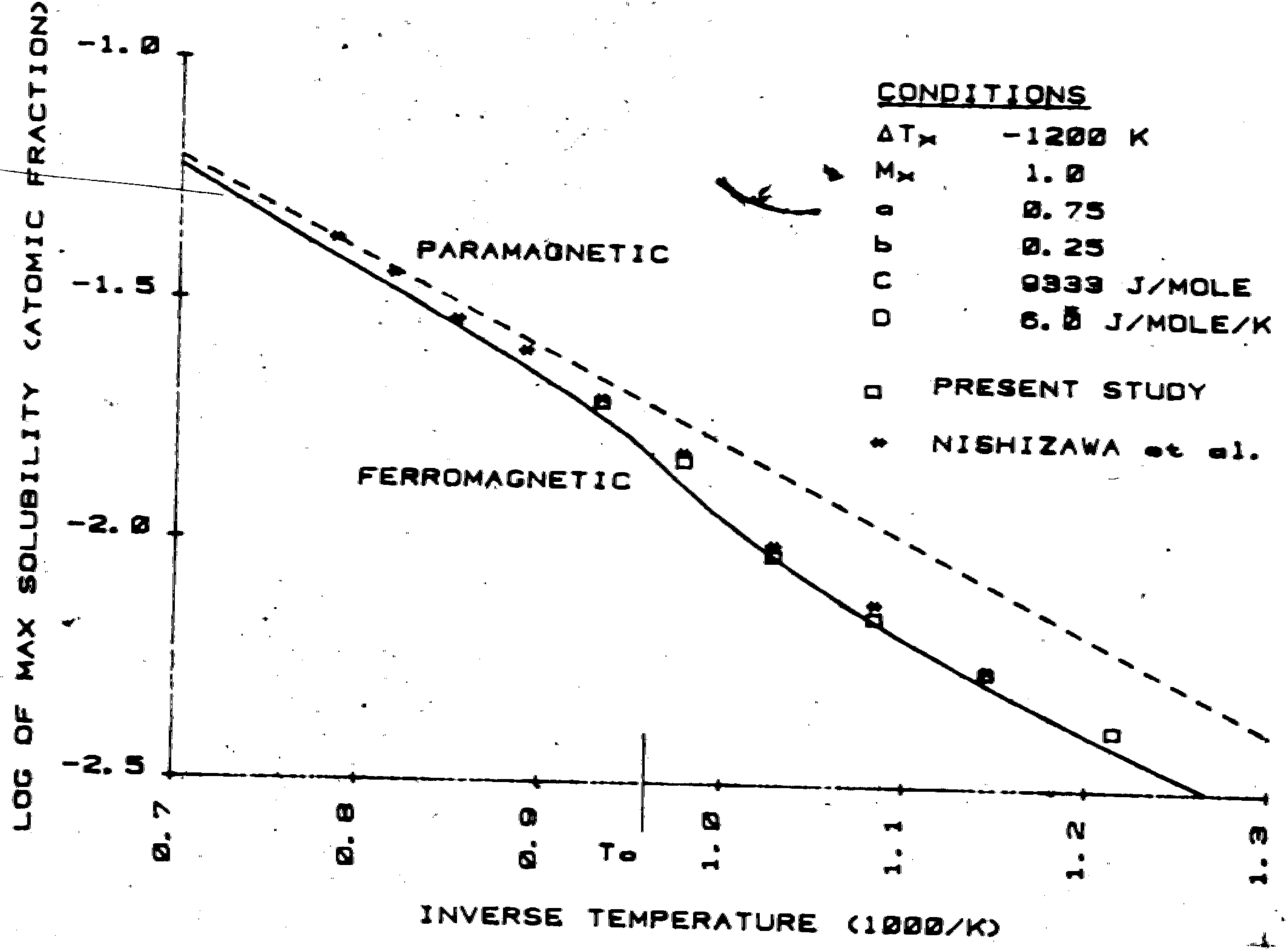

Figure 4.15
The experimental limit of solubility for P in alpha Fe (□ denotes data).

$$Q_{nm} = 9333 + 6.0T \text{ J/mole} \tag{4.62}$$

From data obtained using EPMA, Nishizawa et al. [44] proposed

$$Q_{nm} = 9500 + 5.9T \text{ J/mole} \tag{4.63}$$

and the values b = 0.25 and ΔT_p = -1200 K. The present investigation gave slightly lower concentrations than that of Nishizawa et al. This may be due to the fact that Nishizawa et al. used a proportional constant to derive concentration from the raw data of X-ray counts. This method is not as accurate as making iterative ZAF corrections of the raw data as performed by the EDATA2 program.

The calculated solubility in Figure 4.15 makes use of -1200 K for the magnetic parameter. The experimental data fits well below the Curie temperature but approaches the paramagnetic limit too quickly. There are several possible reasons for this slight discrepancy. The magnetic parameter was determined by a least squares fit of

$$RT\ell n X_p^S + [\frac{1-bM}{b}]G_{mag}^{Fe}(T) = -\frac{Q_{nm}}{b} - \Delta T_X[S_{mag}^{Fe}(T) - {}^uS_{mag}^{Fe}] \tag{4.64}$$

over the entire solubility region. The shape of the magnetic heat capacity curve (which determines the magnetic entropy and enthalpy curves) is different above and below the Curie temperature. It may be that the heat capacity curve decreases much more rapidly above the Curie temperature. Alternatively the magnetic parameter may be temperature and concentration dependent (a non-linear variation of Curie temperature). Furthermore, very little is known about the behavior of the solute intensity factor, M.

In general, this approach using empirical excess magnetic free energies seems justified. The thermodynamic formalism fits the experimental data quite well. The magnetic thermodynamic functions are then valid approximations of reality and it is now possible to apply this information to other properties of iron-based alloys.

4.5 Vacancy Concentrations in alpha Iron

Previous developments by the author and others as described above are now extended to the case of vacancies in alpha iron.

4.5.1 A Hypothetical Iron Solution

Consider an alpha iron crystal at absolute zero. This solid state contains no vacancies. Now assume there exists a hypothetical alpha iron, denoted A, with no vacancies at any temperature. Let the free energy of this material be

$$G^A = G^A_{nm} + G^A_{mag} \tag{4.65}$$

Assume that vacancies may be treated like solute atoms. Therefore, one has an alpha Fe-v binary solid solution. By analogy with an alpha Fe-X regular solid solution, the free energy of alpha Fe-v may be written as

$$G^{Fe} = X_A\,{}^{o}G^{A}_{nm} + X_v\,{}^{o}G^{v}_{nm} + X_A X_v I^{Av} + RT[X_A \ell n X_A + X_v \ell n X_v]$$
$$+ [1-M_v X_v][G^{A}_{mag}(T^{a}) - \Delta T_v X_v\,{}^{u}S^{Fe}_{mag}]$$

where $T^{a} = T - \Delta T_v X_v$ (4.66)

It is well known there are relatively few vacancies present at lower temperatures; therefore, in dilute approximation, X_v is very small and the free energy of pure iron approximates the free energy of the hypothetical iron. At a temperature T, there is a vacancy content such that the system free energy is a minimum. This occurs when the derivative of free energy with respect to the vacancy concentration is zero. In the dilute approximation, vacancy concentration is small and

$$\frac{\partial G^{Fe}}{\partial X_v} = -{}^{o}G^{Fe}_{nm} + RT\ell n X_v$$
$$- G^{Fe}_{mag}(T) + \Delta T_X[S^{Fe}_{mag}(T) - {}^{u}S^{Fe}_{mag}]$$

where ${}^{o}G^{Fe}_{nm} = {}^{o}G^{A}_{nm} + I^{Av}_{nm}$, ${}^{o}G^{v}_{nm} = 0$

$G^{A}_{mag}(T^{a}) \neq G^{Fe}_{mag}(T)$ (4.67)

This gives the equilibrium vacancy concentration as

$$X_v = \exp(-[Q_{nm} + Q_{mag}]/RT)$$
$$Q_{mag} = - G^{Fe}_{mag}(T) + \Delta T_X[S^{Fe}_{mag}(T) - {}^{u}S^{Fe}_{mag}] \quad (4.68)$$

The energies of vacancy formation are normally measured at high temperatures and therefore may be considered as the paramagnetic energies of vacancy formation, i.e. when

$$S^{Fe}_{mag}(T) \approx {}^{u}S^{Fe}_{mag}$$
$$G^{Fe}_{mag}(T) \approx -{}^{u}S^{Fe}_{mag}T \qquad (4.69)$$

The equilibrium concentration of vacancies in alpha iron varies with temperature in a manner similar to the variation of the limit of solubility for a solute. It is expected that the magnetic parameter for vacancies is large and negative, since the formation of a vacancy distorts the iron lattice and there are no electrons available for coupling.

4.5.2 Predicted Vacancy Concentrations from alpha Iron Self-Diffusion Data

It is well known that self-diffusion in a pure element depends strongly on the vacancy concentration present.[10] If the vacancy concentration is affected by ferromagnetism, then self-diffusion must be affected. The anomaly should show up in the self-diffusion coefficient. In fact the self-diffusion coefficient for alpha iron has been experimentally determined by various workers [53-56]. Figure 4.16 shows an Arrhenius plot of the self-diffusion coefficient for alpha iron taken from Hettich et al. [56].

The similarity between this figure and the solubility limits in Figure 4.12 is striking. Indeed, experimental

---

[10] The motion of an atom is equivalent to the motion of a vacancy in substitutional solutions.

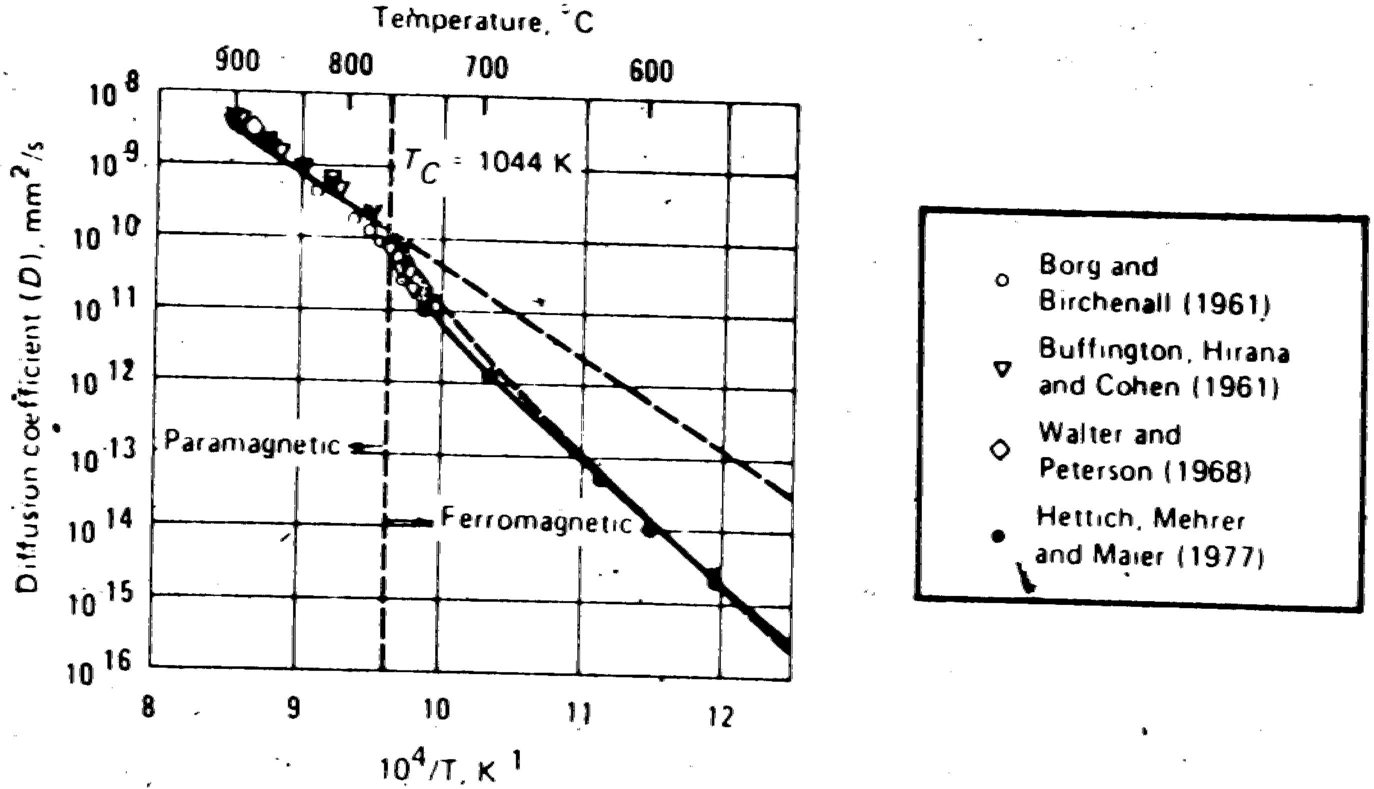

Figure 4.16
Experimental self-diffusion data for alpha Fe [53-56, respectively].

values of the self-diffusion coefficient for alpha iron may be used to determine a magnetic parameter ΔT_v for vacancies in alpha iron.

Consider the paramagnetic self-diffusion coefficient for alpha iron, D_{Fe}, as measured by Hettich et al. [56]

$$D_{Fe} = D_p \exp(-Q_p/RT)$$
$$D_p = 0.98 \text{ cm}^2/\text{sec}$$
$$Q_p = 236400 \text{ J/mole} \tag{4.70}$$

Similarly, a paramagnetic diffusion coefficient for vacancies in alpha iron has been determined [57]

$$D_v = 0.5 \exp(-88770/RT) \text{ cm}^2/\text{sec} \tag{4.71}$$

The self-diffusion coefficient may be given [57] in terms of the diffusion coefficient of vacancies and the free energy of formation of vacancies, ΔG_F^v.

$$D_{Fe} = KD_v \exp(-\Delta G_F^v/RT) \tag{4.72}$$

where K = 0.72, a correlation factor. This allows the paramagnetic free energy of vacancy formation to be determined as 147600 - 8.33T J/mole. The non-magnetic version would be 147600 - 17.33T J/mole. Note that equation (4.71) also shows that the free energy of vacancy migration in alpha iron is approximately 0.4 times the free energy of formation (i.e. the activation free energy for vacancy diffusion is approximately 1.4 times the free energy of formation).

Therefore a magnetic parameter for vacancies was determined by a least squares fit similar to that carried out for equation (4.64), and, keeping in mind that this value is 1.4 times too large, the magnetic parameter for vacancies in alpha iron is found to be approximately -2400 K, a large negative value as expected. Figure 4.17 shows the magnetic free energy of vacancy formation. Vacancy formation becomes much more difficult in the ferromagnetic region. Figure 4.18 is the corresponding equilibrium vacancy concentration curve.

Therefore the individual vacancy affects the magnetic properties of iron as significantly as any solute. However, there are generally few vacancies present so that the total effect is small.

4.6 The Thermodynamics of Equilibrium Grain Boundary Segregation

It is first necessary to understand the thermodynamics of interfaces (in this case grain boundaries) and of equilibrium segregation. Guttmann's thermodynamic treatment of multi-component segregation [5,17,58] is based on the formalism initiated by Defay and Prigogine [59]. The basic hypothesis is that an interface, ϕ, can be considered as a two dimensional (2-d) phase in which all the thermodynamic functions can be defined as in the bulk, α. The following define the necessary variables and functions:

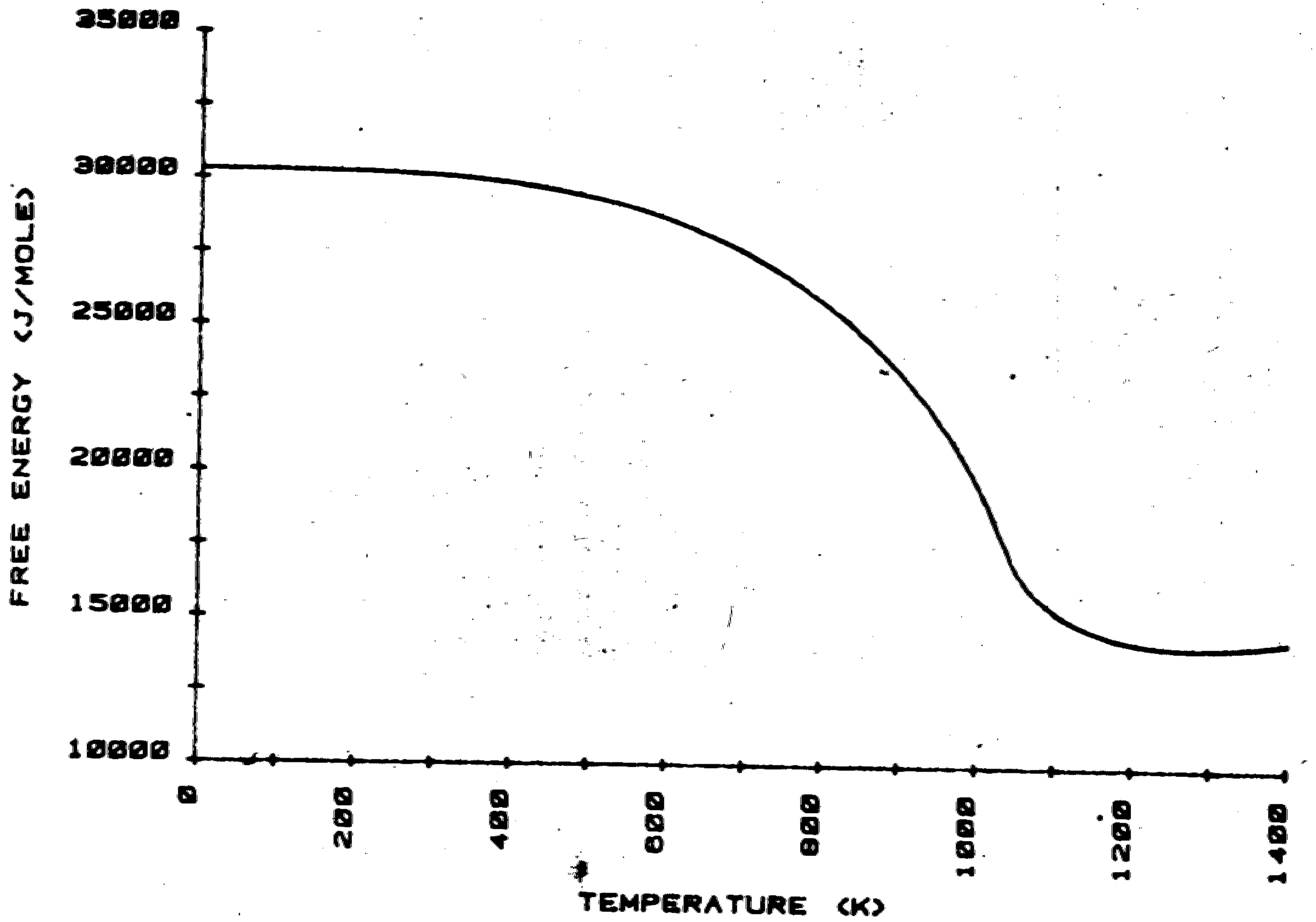

Figure 4.17
Predicted magnetic free energy of vacancy formation in alpha Fe.

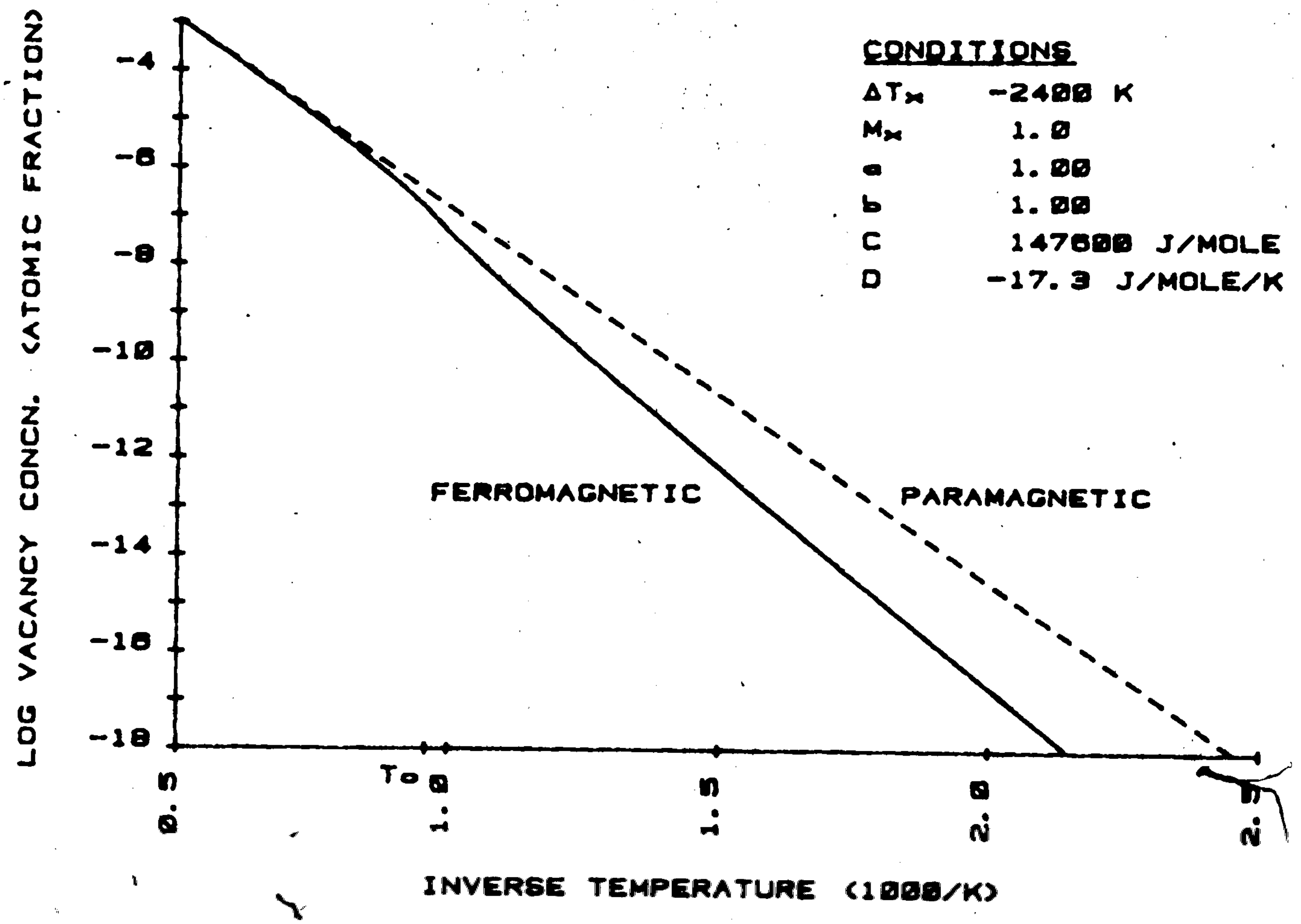

Figure 4.18
Predicted equilibrium vacancy concentration in alpha Fe.

N_i^ϕ = number of i atoms in ϕ

N_i^α = number of i atoms in alpha (bulk)

σ = surface tension of ϕ

Ω = area of ϕ

$G^\phi = G\,(P,T,\sigma,N_i^\phi,N_i^\alpha)$ = Gibbs free energy at ϕ

$G^\alpha = G\,(P,T,N_i^\alpha)$

$F^\phi = F\,(V,T,\sigma,N_i^\phi,N_i^\alpha)$ = Helmoltz free energy at ϕ

$F^\alpha = F\,(V,T,N_i^\alpha)$

The Helmoltz and Gibbs free energies are related by:

$$G^\phi = F^\phi - \sigma\Omega$$

$$G^\alpha = F^\alpha + PV^\alpha \tag{4.73}$$

The only difference between a 2-d and a 3-d phase is the surface tension of the 2-d phase. The surface tension of ϕ is associated with essentially zero thickness and the extensivity of ϕ is described only by the boundary area, Ω. This is equivalent to ignoring the volume of ϕ and thus the PV terms in the free energy of ϕ. Also, the ϕ is assumed incompressible in the thickness direction, the mechanical contributions to G^ϕ arising only from the 2-d term $+\sigma\Omega$. The free energy of ϕ is a function of the intensive variable which means that the entropy at ϕ and the chemical potential of i at ϕ have to be calculated at constant surface tension.

A simple form of the boundary chemical potentials may be assumed by analogy with bulk functions:

$$\mu^{\alpha i} = {}^{o}\mu^{\alpha i}(P,T) + RT\ell n a_i^{\alpha}$$

$$\mu^{\phi i} = {}^{o}\mu^{\phi i}(P,T,\sigma) + RT\ell n a_i^{\phi} \qquad (4.74)$$

Also by analogy

$$F^{\phi} = \sum_i N_i^{\phi} \zeta^{\phi i} \qquad (4.75)$$

where ξ^i is the Helmholtz equivalent of chemical potential for i. The partial molar area of i is defined as:

$$\omega_i = (\partial\Omega/\partial N_i^{\phi})_{P,T,\sigma,N_{j\neq i}^{\phi}} \qquad (4.76)$$

and, since the total boundary area obeys Euler's theorem for extensive quantities:

$$\Omega = \sum_i N_i^{\phi}\omega_i \qquad (4.77)$$

Likewise, Gibbs free energy may be given by:

$$G^{\phi} = \sum_i N_i^{\phi}\mu^{\phi i}$$

$$= F^{\phi} - \sigma\Omega$$

which allows $\mu^{\phi} = \zeta^{\phi i} - \sigma\omega_i$ (4.78)

Consider a system with grain boundaries, ϕ. The equilibrium segregation and surface tension are given by:

$$X_i^{\phi} = f(P,T,X_1^{\alpha},X_2^{\alpha},\ldots\ldots,X_n^{\alpha})$$

$$\sigma = g(P,T,X_1^{\alpha},X_2^{\alpha},\ldots\ldots,X_n^{\alpha}) \qquad (4.79)$$

The conditions for equilibrium between a two- and a three-dimensional phase, for all i, are

$$\mu^{\phi i} = \mu^{\alpha i} \tag{4.80}$$

For an ideal solution the activities are the concentrations, and

$$\mu^{\phi i} = {}^{o}\zeta^{\phi i} - \sigma\omega_i + RT\ell n X_i^{\phi} = {}^{o}\mu^{\alpha i} + RT\ell n X_i^{\alpha} \tag{4.81}$$

However, for non-ideal solutions, partial excess free energies, ${}^{E}\bar{G}_i^{\phi}$, may be introduced so that:

$${}^{o}\zeta^{\phi i} + {}^{E}\bar{G}_i^{\phi} - \sigma\omega_i + RT\ell n X_i^{\phi} = {}^{o}\mu^{\alpha i} + {}^{E}\bar{G}_i^{\alpha} + RT\ell n X_i^{\alpha} \tag{4.82}$$

for i = 1,2,...,n-1. The solvent is given by i = n, so that:

$${}^{o}\zeta^{\phi n} + {}^{E}\bar{G}_n^{\phi} - \sigma\omega_n + RT\ell n X_n^{\phi} = {}^{o}\mu^{\alpha n} + {}^{E}\bar{G}_n^{\alpha} + RT\ell n X_n^{\alpha} \tag{4.83}$$

Multiplying equation (4.83) by ω_i/ω_n and subtracting it from equation (4.82) to eliminate σ gives:

$$\begin{aligned} RT\ell n([X_n^{\alpha}/X_n^{\phi}]^{\omega_i/\omega_n} X_i^{\phi}/X_i^{\alpha}) &= \Delta G^{i} \\ &= \frac{\omega_i}{\omega_n}[{}^{o}\zeta^{\phi n} - {}^{o}\mu^{\alpha n} + {}^{E}\bar{G}_n^{\phi} - {}^{E}\bar{G}_n^{\alpha}] \\ &\quad - [{}^{o}\zeta^{\phi i} - {}^{o}\mu^{\alpha i} + {}^{E}\bar{G}_i^{\phi} - {}^{E}\bar{G}_i^{\alpha}] \end{aligned} \tag{4.84}$$

Where ΔG^{i} is the segregation binding energy for atoms i at the boundary.

Guttmann and McLean [58] have shown that for the case of regular behavior with solute site competition[11], the segregation is given by:

$$X_i^\phi = \frac{X_i^\alpha \exp(\Delta G^i/RT)}{1 + \sum_{j=1}^{n-1} [\exp(\Delta G^j/RT) - 1]X_j^\alpha} \qquad (4.85)$$

For a non-competitive case, each solute species takes up a different set of sites in the boundary. If Y_i^ϕ is the fraction of sites filled by solute i, then, in dilute bulk approximation,

$$Y_i^\phi = \frac{Y_i^\alpha \exp(\Delta G^i/RT)}{1 + Y_i^\alpha \exp(\Delta G^i/RT)} \qquad (4.86)$$

Any or all of the solute species present may saturate ($Y_i^\phi = 1$) the boundary under the appropriate conditions. The segregation behavior of any solute is independent of the segregation of any other solute except through the free energy of segregation. Examples of segregation curves are given in Figure 4.19. These curves were generated using the computer program developed in the present work without magnetic effects (setting magnetic terms to zero). It should be noted that in a non-competitive ternary system, the segregation curves of both solutes will be similar to the binary behavior described in section 4.7. It has been suggested by Guttmann [60] that similar atoms are competitive (e.g. metalloid atoms such as P,As) and unlike atoms are non-competitive. However, the evidence is not

---

[11] All atoms at the boundary compete for one set of boundary sites.

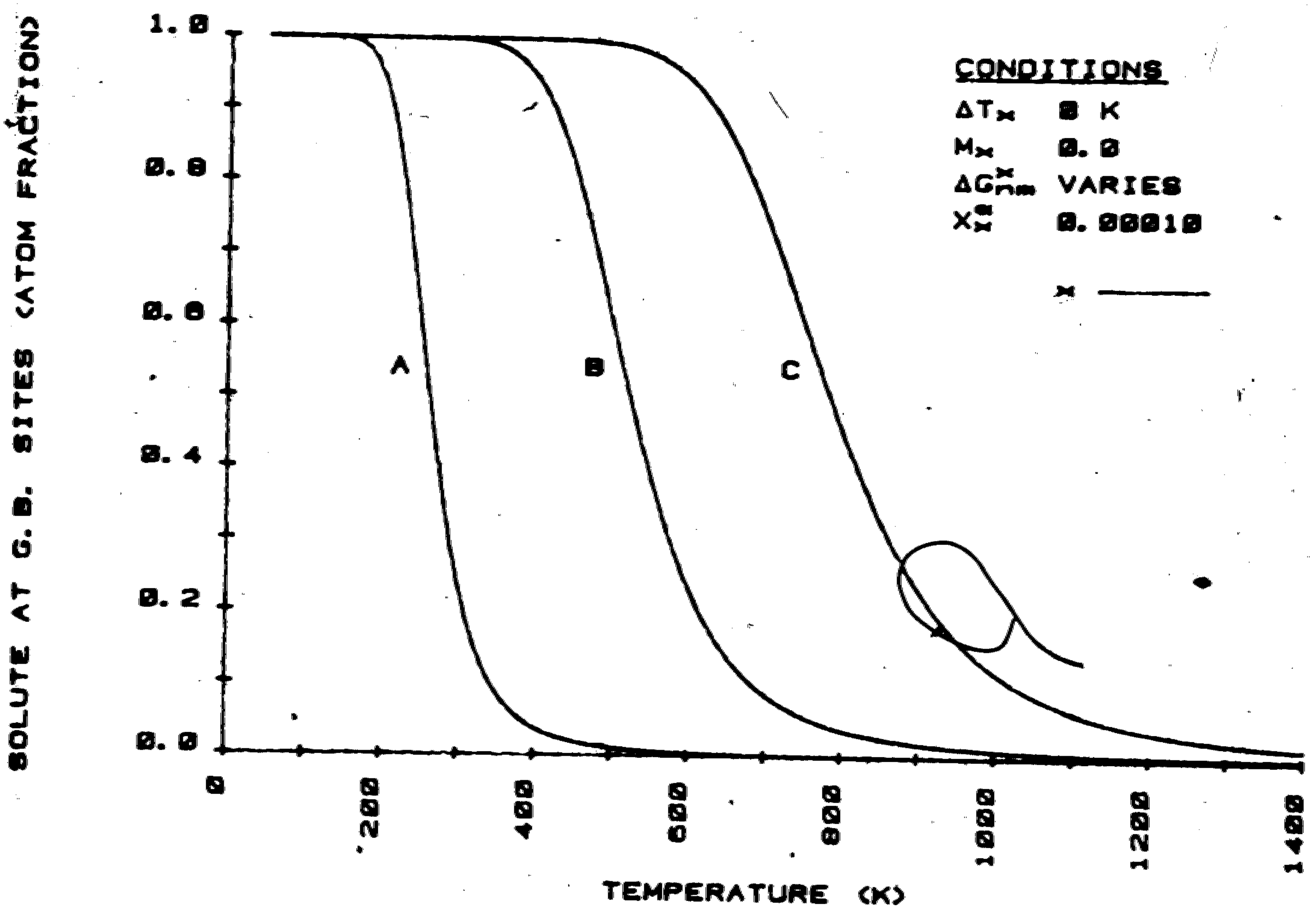

Figure 4.19
Typical McLean segregation curves.

conclusive.

4.7 Grain Boundary Segregation in Binary alpha Fe-X Solid Solutions

Guttmann's analysis is now applied to binary alpha Fe-X solid solutions using the chemical potentials obtained in section 4.3 and found in equations (4.44) to (4.48). For convenience of presentation the following simplifications will now be applied (excess energy terms are assumed to be non-magnetic)

$$ {}^{o}\mu_{nm}^{\phi i} = {}^{o}\zeta^{\phi i} + {}^{E}\bar{G}_{i}^{\phi} \tag{4.87} $$

4.7.1 Case I: Grain Boundary Free Energy Without Magnetic Terms

As a first approximation, the grain boundaries will be considered non-magnetic. That is, the atoms in the boundaries cannot take part in any magnetic interactions and there are no magnetic terms possible when describing the boundary free energies. As the magnetic free energy terms would be directly dependent on the boundary solute concentrations, this simplified case allows direct analytic solutions which, despite their limitations, do indicate trends.

To obtain an equilibrium segregation equation, the following conditions are applied for some temperature, T:

$$\mu^{\phi X} = \mu^{\alpha X}$$
$$\mu^{\phi Fe} = \mu^{\alpha Fe} \qquad (4.88)$$

Concentrations of solute X in the bulk and boundary are X^{α}_{X} and X^{ϕ}_{X} respectively, and, as with equations (4.82) and (4.83)

$$\begin{aligned} \mu^{\phi X} &= {}^{o}\mu^{\phi X}_{nm} + RT\ell n X^{\phi}_{X} - \sigma\omega_{X} \\ &= {}^{o}\mu^{\alpha X}_{nm} + RT\ell n X^{\alpha}_{X} + \mu^{\alpha X}_{mag} \\ &= \mu^{\alpha X} \end{aligned} \qquad (4.89)$$

$$\begin{aligned} \mu^{\phi Fe} &= {}^{o}\mu^{\phi Fe}_{nm} + RT\ell n(1-X^{\phi}_{X}) - \sigma\omega_{Fe} \\ &= {}^{o}\mu^{\alpha Fe}_{nm} + RT\ell n(1-X^{\alpha}_{X}) + \mu^{\alpha Fe}_{mag} \\ &= \mu^{\alpha Fe} \end{aligned} \qquad (4.90)$$

The excess free energy terms are taken to be non-magnetic. Multiplying equation (4.90) by ω_{X}/ω_{Fe} and subtracting from equation (4.89) results in

$$RT\ell n(\{[1-X^{\alpha}_{X}]/[1-X^{\phi}_{X}]\}^{\omega_{X}/\omega_{Fe}} X^{\phi}_{X}/X^{\alpha}_{X}) = {}^{I}\Delta G^{X} = \Delta G^{X}_{nm} + {}^{I}\Delta G^{X}_{mag} \qquad (4.91)$$

$$\Delta G^{X}_{nm} = \frac{\omega_{X}}{\omega_{Fe}} [{}^{o}\mu^{\phi Fe}_{nm} - {}^{o}\mu^{\alpha Fe}_{nm}] - [{}^{o}\mu^{\phi X}_{nm} - {}^{o}\mu^{\alpha X}_{nm}]$$
$${}^{I}\Delta G^{X}_{mag} = \mu^{\alpha X}_{mag} - \frac{\omega_{X}}{\omega_{Fe}} \mu^{\alpha Fe}_{mag} \qquad (4.92)$$

The superscript I in the segregation free energies refers to Case I. Superscript II will refer to Case II (section 4.7.2).

At this point, it is assumed that the atomic structure of the grain boundary is not altered throughout the segregation process. In other words, substitution is perfect with both species occupying the same area in ϕ, that is:

$$\omega_{Fe} = \omega_{X} \qquad (4.93)$$

Equation (4.92) then becomes (applying the approximation in equation (4.35)):

$$^{I}\Delta G^{X}_{mag} = -MG^{Fe}_{mag}(T) + [1-2\dot{M}X^{\alpha}_{X}]\Delta\dot{T}_{X}[S^{Fe}_{mag}(T^{\alpha}) - {}^{u}S^{Fe}_{mag}] \qquad (4.94)$$

The behavior of this magnetic free energy of segregation may be evaluated by considering a dilute bulk approximation, where $X_X \ll 1$, and

$$^{I}\Delta G^{X}_{mag}(X_X \rightarrow 0) = -MG^{Fe}_{mag}(T) + \Delta T_{X}[S^{Fe}_{mag}(T) - {}^{u}S^{Fe}_{mag}] \qquad (4.95)$$

Figure 4.20 shows the behavior of equation (4.94) with temperature, using the previously established equations for thermodynamic functions.

It is immediately evident that the magnetic segregation free energy has a large value at low temperatures. With increasing temperature, there is first a gradual decline, then an increasing rapid decline near the bulk Curie temperature culminating in a minimum just above the Curie temperature. Above this point, the curve approaches a linear

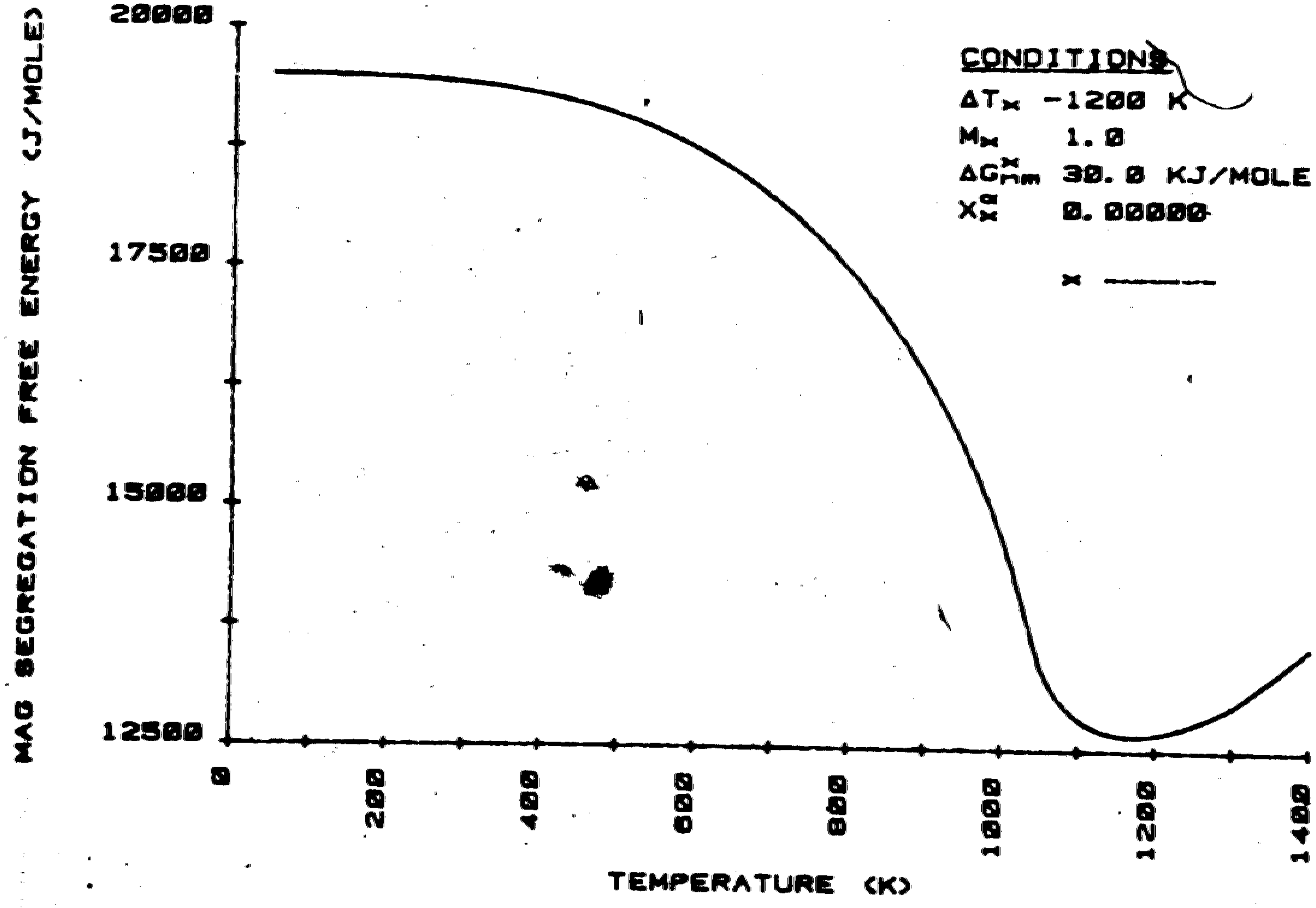

Figure 4.20
Free energy of segregation for P in alpha Fe (dilute bulk approximation).

increase with temperature. This may be seen from equation (4.94) by considering that

$$S^{Fe}_{mag}(T>>T^{Fe}_{c}) = {}^{u}S^{Fe}_{mag}$$

$$G^{Fe}_{mag}(T>>T^{Fe}_{c}) = -T\,{}^{u}S^{Fe}_{mag}$$

$${}^{I}\Delta G^{X}_{mag}(T>>T^{Fe}_{c}) = +MT\,{}^{u}S^{Fe}_{mag} \qquad (4.96)$$

Increasing the bulk solute concentration decreases or slightly flattens the curve below the Curie temperature.

In order to appreciate the effect of the segregation free energy on equilibrium grain boundary segregation, consider the segregation equation (4.84). For constant temperature, as the free energy of segregation increases, the boundary solute content also increases. This is equivalent to displacing the segregation curve to the right as shown in Figure 4.21. To evaluate his equilibrium segregation equations, Guttmann set a constant standard free energy of segregation. That is, there is only one type of site for segregated solute atoms at the grain boundary. Likewise, in evaluating the magnetic contribution to segregation in the present work, the non-magnetic components of segregation free energy are set to a constant value.

These assumptions, that all partial molar boundary areas are equal and that the non-magnetic segregation free energy is a constant, are quite restrictive. In reality, there is a 'spectrum' of available grain boundary sites for solute segregation. Each 'type' of site will lower (or raise) the energy of the system a particular amount when it

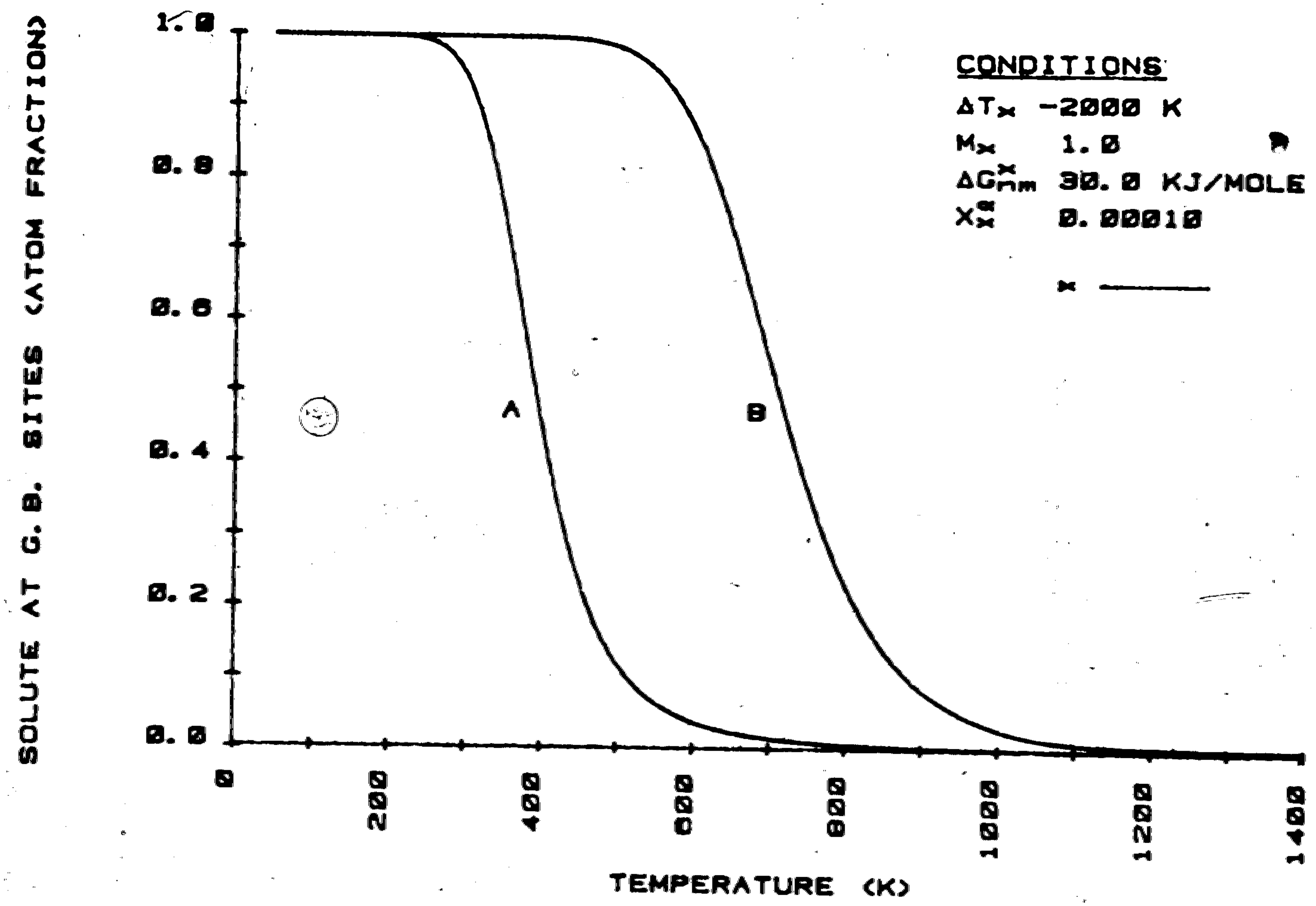

Figure 4.21
The effect of the segregation free energy on intergranular solute concentration (A = non-magnetic, B = magnetic).

is occupied by a particular species of atom. This is known as the 'spectrum of binding energies' approach [61]. Unfortunately, the spectrum of binding energies cannot be theoretically calculated and there is a paucity of available experimental data [62]. Furthermore, competition for grain boundary sites may occur if the binding energies for different solute species are similar. The coverage of solute will also vary from grain boundary to grain boundary as the sites available in the boundary will change with the structure of the boundary [63] which changes with boundary misorientation, etc.

As an example, consider the alpha Fe-P system. Figure 4.22 shows a grain boundary concentration versus temperature plot for an alpha Fe - 0.1 at% P solid solution. Three curves are presented for non-magnetic, paramagnetic, and ferromagnetic situations for the same alloy. It is clear that the effect of the magnetic contribution is to increase segregation and its temperature dependence over a commercially important range of temperatures (700 to 1000 K). The effect of increasing bulk solute concentration is to raise the segregation curve and shift it to the right. If the dilute bulk approximation is not made, so that terms with powers of X_X^α must be included in the chemical potentials, the effect is to shift the segregation curve to slightly lower temperatures.

The magnetic component of segregation free energy as a function of temperature for several values of magnetic

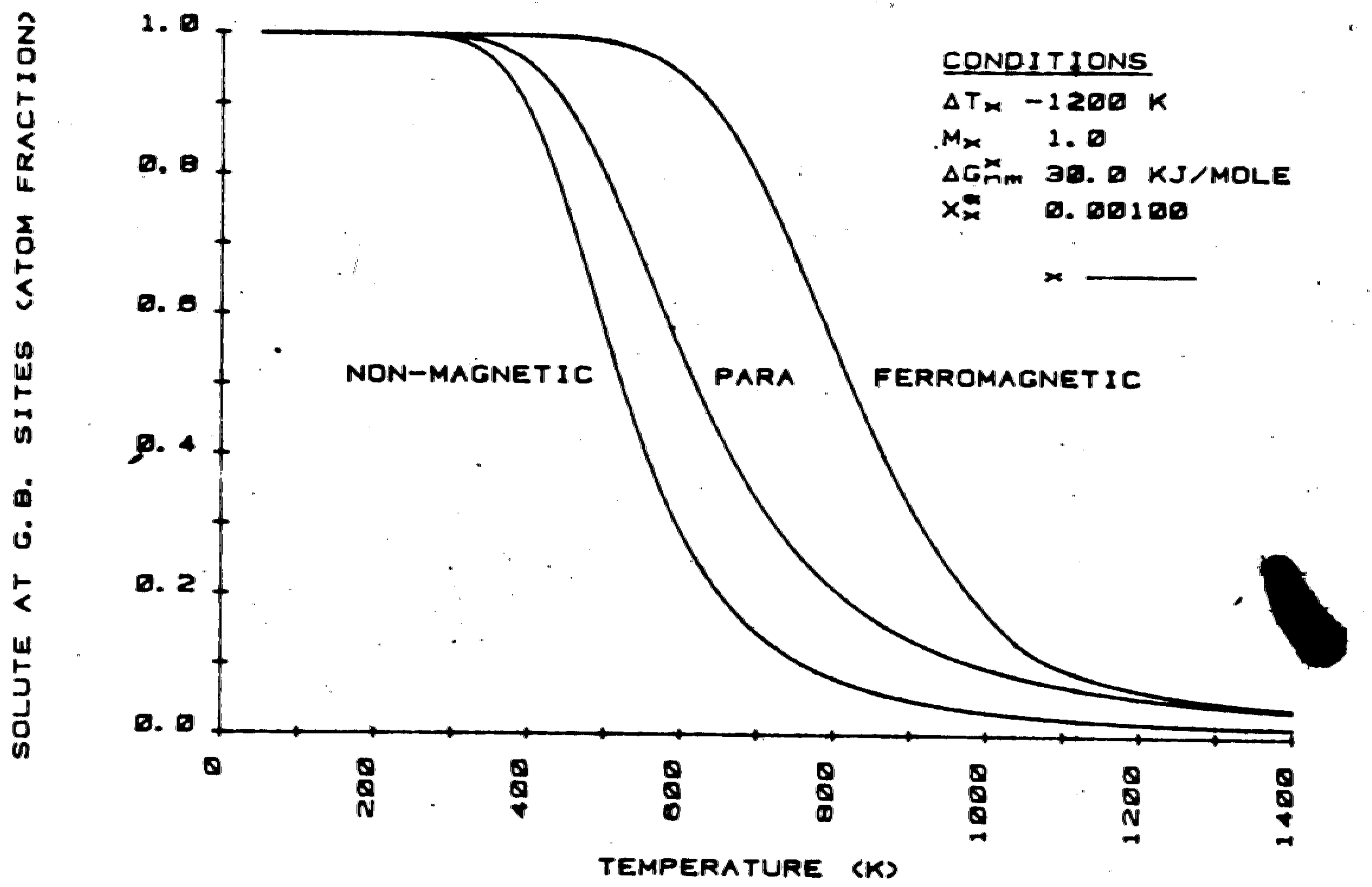

Figure 4.22
Predicted grain boundary solute concentrations for the alpha Fe-P system according to case I.

parameter is shown in Figure 4.23. The corresponding boundary segregation curves are shown in Figure 4.24. for an arbitrary but reasonable value of ΔG_{nm}^{i} = 30 KJ/ mole. It is clear that solutes which depress the Curie temperature (negative magnetic parameters) shift the segregation curve to higher temperatures. Likewise, solutes which increase the Curie temperature (positive magnetic parameters) shift the segregation curve to lower temperatures. The shift, as indicated, may be hundreds of degrees. The grain boundary segregation curves for several bulk solute concentrations is shown in Figure 4.25 using the appropriate magnetic parameter for phosphorus. This figure also displays the effect of the solubility of P in alpha Fe as shown by the solid segment of curve D. For the dashed lines the solubility is ignored. The boundary solute content is proportional to the bulk solute content and the exponential of the segregation free energy (see equation (4.85)). At high temperatures the exponential term is small which allows solubility effects (changing the bulk solute content term) to be apparent. At low temperatures the exponential term completely dominates the bulk term and solubility effects are not apparent. Therefore, changes in the bulk solute concentration or the free energy of segregation terms have similar effects on the segregation curve. All these facts are completely consistent with the changes in the limit of solid solubility as determined by the magnetic parameter.

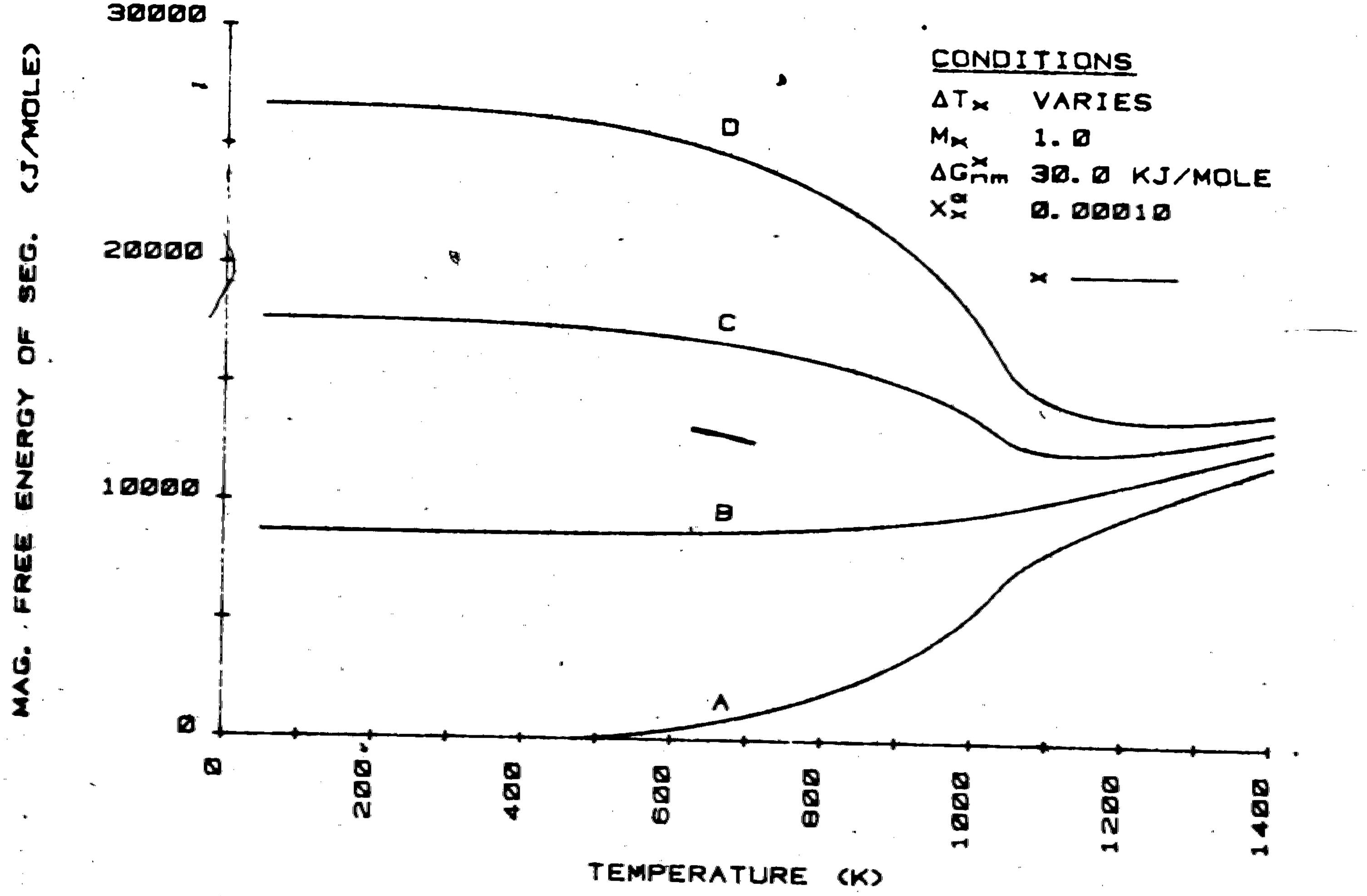

Figure 4.23.
The magnetic component of the segregation free energy according to Case I (A = 1000 K., B = 0 K, C = -1000 K, D = -2000 K).

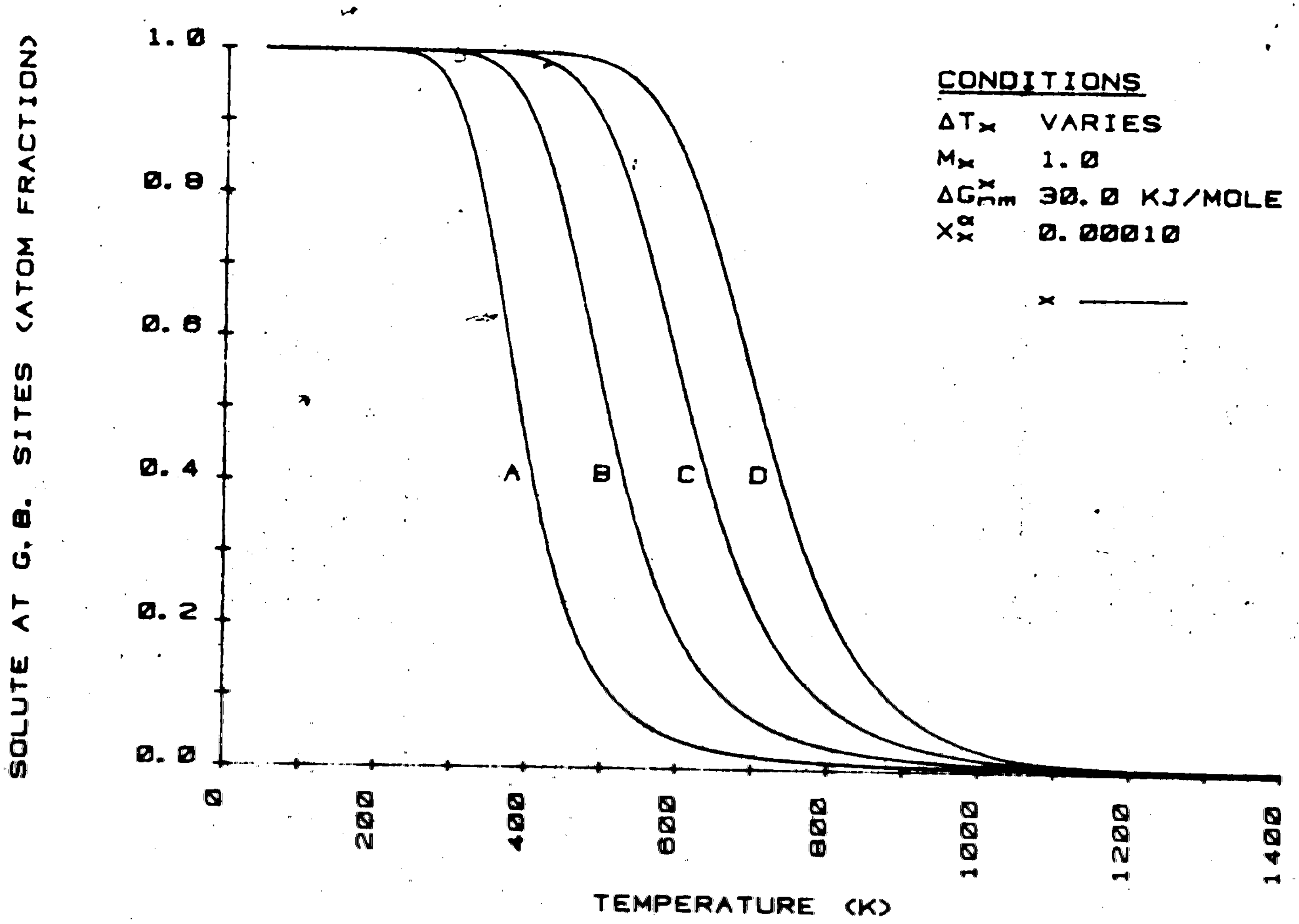

Figure 4.24
Predicted grain boundary solute concentration according to Case I (A = 1000 K, B = 0 K, C = -1000 K, D = -2000 K).

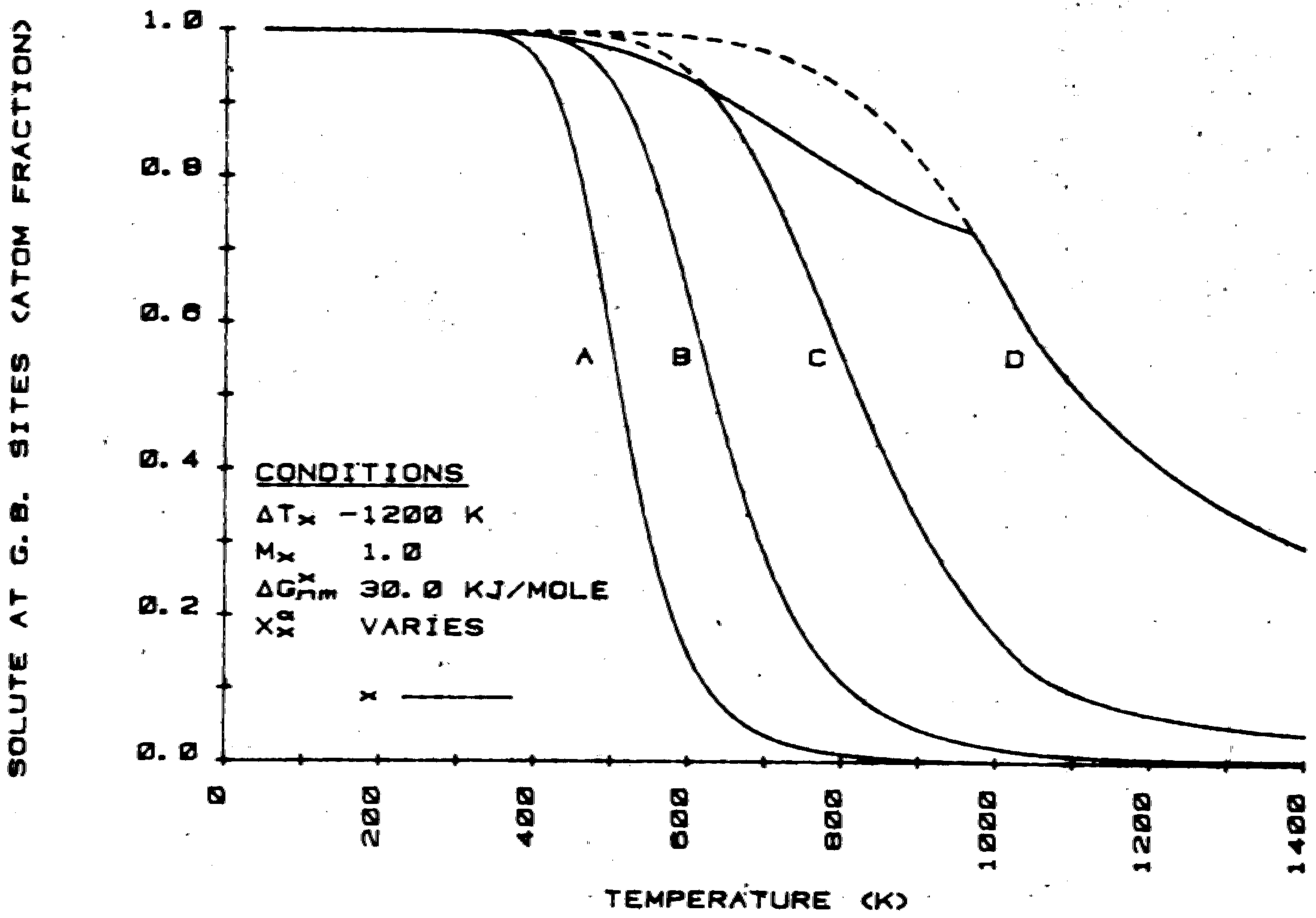

Figure 4.25
The effect of bulk solute content on predicted grain boundary solute concentration according to Case I (A = 0.00001, B = 0.0001, C = 0.001, D = 0.01).

As is evident, Case I immediately points out the general trends of the effect of ferromagnetism on segregation, however, some inconsistencies are present. The $\Delta T_X = 0$ K condition should represent no magnetic effect, i.e., zero variance of the Curie temperature, and the magnetic contribution to the segregation free energy should be zero. It may be seen that Figure 4.23 shows a non-zero magnetic segregation free energy for the condition $\Delta T_X = 0$ K. Also, above the Curie temperature the free energy slowly increases for any magnetic parameter, a situation which is clearly not reasonable. Therefore, Case II will now be considered.

4.7.2 Case II: Segregation when Grain boundaries may be Ferromagnetic

The assumption that the only difference between a 2-d and a 3-d phase is the 2-d surface tension, σ, realistically demands that the grain boundary of a ferromagnetic 3-d phase may itself be ferromagnetic. Thus, the chemical potentials of the grain boundary species would have magnetic components (which they do not have in equations (4.87) and (4.88)). Hence, one may write

$$\begin{aligned} \mu^{\phi i} &= \mu^{\phi i}_{nm} + \mu^{\phi i}_{mag} \\ &= {}^{o}\mu^{\phi i}_{nm} + RT\ln X^{\phi}_{i} - \sigma\omega_i + \mu^{\phi i}_{mag} \qquad (4.97) \end{aligned}$$

where $\mu^{\phi i}$ is a magnetic free energy component of the boundary. It is assumed that the magnetic chemical potential in ϕ may be described as in the bulk, i.e.

$$\mu^{\phi Fe}_{mag} = G^{Fe}_{mag}(T^{\phi}) - \Delta T_X X^{\phi}_X {}^{u}S^{Fe}_{mag} - X^{\phi}_X[1-MX^{\phi}_X]\Delta T_X[S^{Fe}_{mag}(T^{\phi}) - {}^{u}S^{Fe}_{mag}] \qquad (4.98)$$

$$\mu^{\phi X}_{mag} = [1-MX^{\phi}_X][G^{Fe}_{mag}(T^{\phi}) - \Delta T_X X^{\phi}_X {}^{u}S^{Fe}_{mag}] + [1-X^{\phi}_X-MX^{\phi}_X+MX^{\phi^2}_X]\Delta T_X[S^{Fe}_{mag}(T^{\phi}) - {}^{u}S^{Fe}_{mag}] \qquad (4.99)$$

where $T^{\phi} = T - \Delta T_X X^{\phi}_X$. As in Case I, the Guttmann analysis is applied to obtain an equilibrium segregation equation, i.e. for some temperature, T,

$$\begin{aligned}
\mu^{\phi X} &= {}^{o}\mu^{\phi X}_{nm} + RT\ln X^{\phi}_X - \sigma\omega_X + \mu^{\phi X}_{mag} \\
&= {}^{o}\mu^{X}_{nm} + RT\ln X^{\alpha}_X + \mu^{\alpha X}_{mag} \\
&= \mu^{\alpha X} \\
\mu^{\phi Fe} &= {}^{o}\mu^{\phi Fe}_{nm} + RT\ln(1-X^{\phi}_X) - \sigma\omega_{Fe} + \mu^{\phi Fe}_{mag} \\
&= {}^{o}\mu^{\alpha Fe}_{nm} + RT\ln(1-X^{\alpha}_X) + \mu^{\alpha Fe}_{mag} \\
&= \mu^{\alpha Fe}
\end{aligned} \qquad (4.100)$$

After treatment as in Case I and again assuming $\omega_{Fe} = \omega_X$, a segregation equation results:

$$RT\ln(X_X^{\phi}[1-X_X^{\alpha}]/X_X^{\alpha}[1-X_X^{\phi}]) = {}^{II}\Delta G^X$$

$$= \Delta G_{nm}^X + {}^{II}\Delta G_{mag}^X$$

$$\begin{aligned} {}^{II}\Delta G_{mag}^X = {} & M[G_{mag}^{Fe}(T^{\phi}) - G_{mag}^{Fe}(T^{\alpha}) - [X_X^{\phi}-X_X^{\alpha}]\Delta T_X {}^{u}S_{mag}^{Fe}] \\ & - [1-MX_X^{\phi}]\Delta T_X[S_{mag}^{Fe}(T^{\phi}) - {}^{u}S_{mag}^{Fe}] \\ & + [1-MX_X^{\alpha}]\Delta T_X[S_{mag}^{Fe}(T^{\alpha}) - {}^{u}S_{mag}^{Fe}] \end{aligned} \tag{4.101}$$

No technique was found to evaluate this equation directly, but by considering equation (4.85), then

$$X_X^{\phi} = \frac{X_X^{\alpha}\exp(\Delta G^X/RT)}{1 + X_X^{\alpha}[\exp(\Delta G^X/RT) - 1]} \tag{4.102}$$

is solved for roots of X_X^{ϕ}. This may be done, for example, by the graphical bisection method or an iterative substitution of X_X^{ϕ} and/or T. The computer programs and techniques developed for these numerical solutions can be found in Appendix II. To better understand the expression for the magnetic free energy of segregation consider the two bounding ranges, high temperatures ($T \gg T_c^{Fe}$) and low temperatures ($T \ll T_c^{Fe}$). At higher temperatures, above the Curie temperature, the boundary and bulk solute concentrations are similar ($X_X^{\phi} \sim X_X^{\alpha}$) and since the magnetic segregation free energy is the difference between magnetic components of the grain boundary and the bulk segregation free energies, ${}^{\Pi}\Delta G_{mag}^X(T > T_c^{\alpha})$ will tend to zero (the magnetic effects are effectively zero above the Curie temperature). As the grain boundary becomes saturated with solute (X_X^ϕ approaches 1) at lower temperatures, the shift in T^α (i.e. $T - \Delta T_X X_X$) reaches a maximum. For typical values of $\Delta T = -1000$ K, this implies

$$\begin{aligned} G^{Fe}_{mag}(T^\phi) &< G^{Fe}_{mag}(T^\alpha) \\ S^{Fe}_{mag}(T^\alpha) &< S^{Fe}_{mag}(T^\phi) = {}^{u}S^{Fe}_{mag} \end{aligned} \qquad (4.103)$$

Also, as X approaches saturation, the boundary solute concentration is much greater than in the bulk ($X_X^\phi >> X_X^\alpha$, thus the terms containing X_X^α and $S^{Fe}_{mag}(T^\alpha)$ may be neglected. The overall effect is that at low temperatures

$$\begin{aligned} \Delta G^X_{mag}(X_X \to 1) &= M[G^{Fe}_{mag}(T^\phi) - G^{Fe}_{mag}(T^\alpha)] \\ &\quad - \Delta T_X\, {}^{u}S^{Fe}_{mag}[1+M] \end{aligned} \qquad (4.104)$$

The first term is negative and proportional to ${}^{u}S^{Fe}_{mag}$, however the second term has a much greater positive value. This leads to an increase in segregation free energy and hence in equilibrium segregation, the reverse being true for positive magnetic parameters.

Figure 4.26 shows the magnetic contribution to the segregation free energy as a function of temperature for various values of magnetic parameter. The non-magnetic component of segregation free energy was chosen as 40 KJ/mole. This value is higher than that used in Case I because of the constant positive (background) magnetic segregation free energy of approximately 10 KJ/mole found in Case I (see Figure 4.23). Again, a large negative magnetic parameter leads to a larger segregation free energy. For the

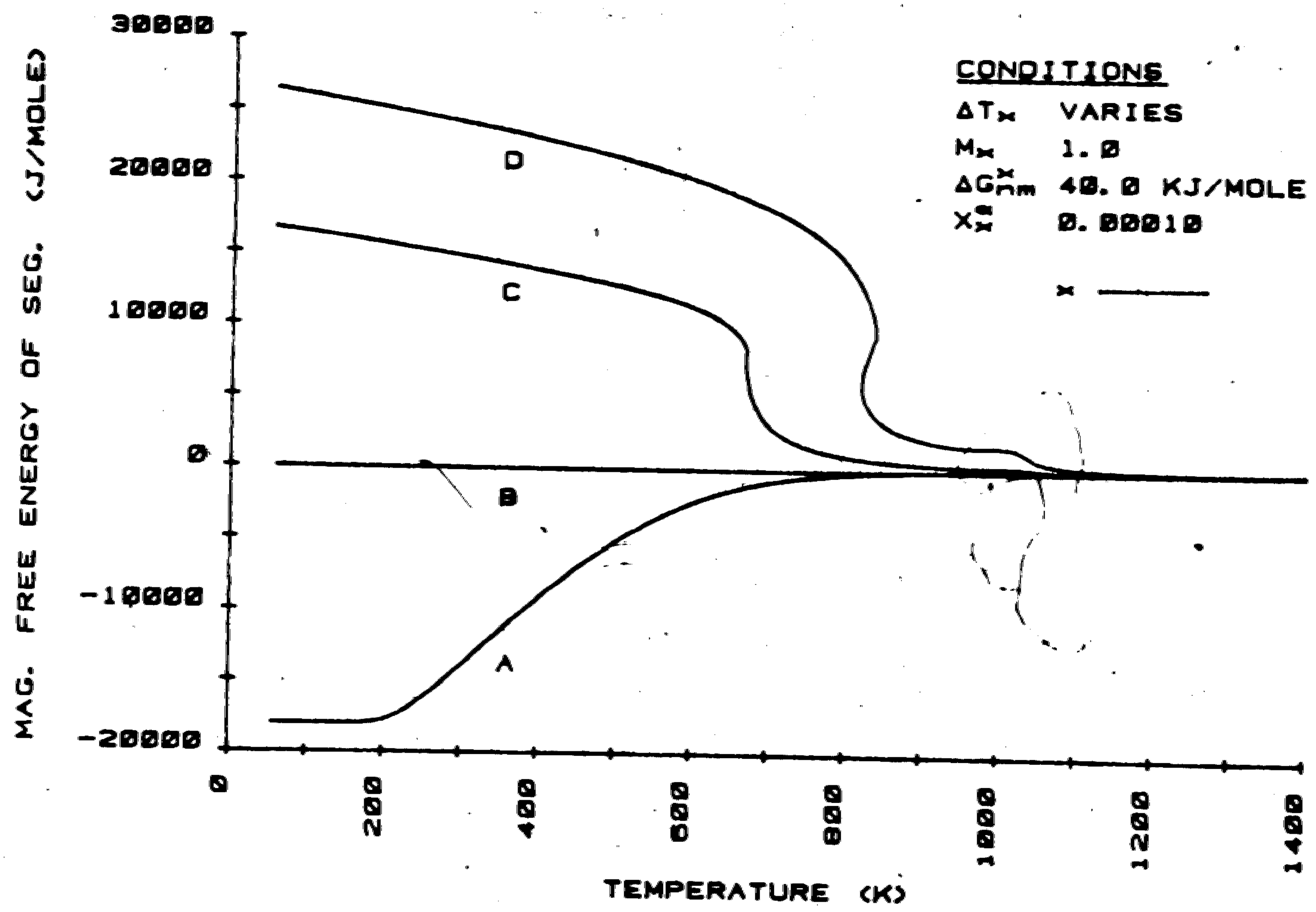

Figure 4.26
The magnetic component of segregation free energy according to Case II (A = 1000 K, B = 0 K, C = -1000 K, D = -2000 K).

ΔT_X = 0 K condition, the magnetic free energy is indeed zero for all temperatures and, above the bulk Curie temperature, all magnetic free energies tend to zero. Case II, then, is more realistic than Case I. The corresponding amounts of grain boundary segregation for Figure 4.26 are shown in Figure 4.27. It is clear that decreasing values of magnetic parameter cause the segregation curves to shift to higher temperatures and they can also develop a sharp step below the bulk Curie temperature. Similar steps appear in the segregation curves of ternary alloys [58] where increases in segregation free energy are caused by solute-solute interaction. For magnetic parameters large and negative, the magnetic free energy of segregation curves may be divided into 3 regions:

1. at temperatures above the Curie temperature, the free energy is very small;
2. at some temperature usually below the Curie temperature there is a rapid increase in the free energy; and
3. at lower temperatures the free energy increases with decreasing temperature in a roughly linear manner.

The effect of bulk solute concentration on the magnetic segregation free energy is shown in Figure 4.28, and the corresponding grain boundary concentration curves in Figure 4.29. Interestingly, the shape of the magnetic segregation free energy curves is reminiscent of a magnetization curve, having large values at low temperatures and dropping rapidly to very small values near the

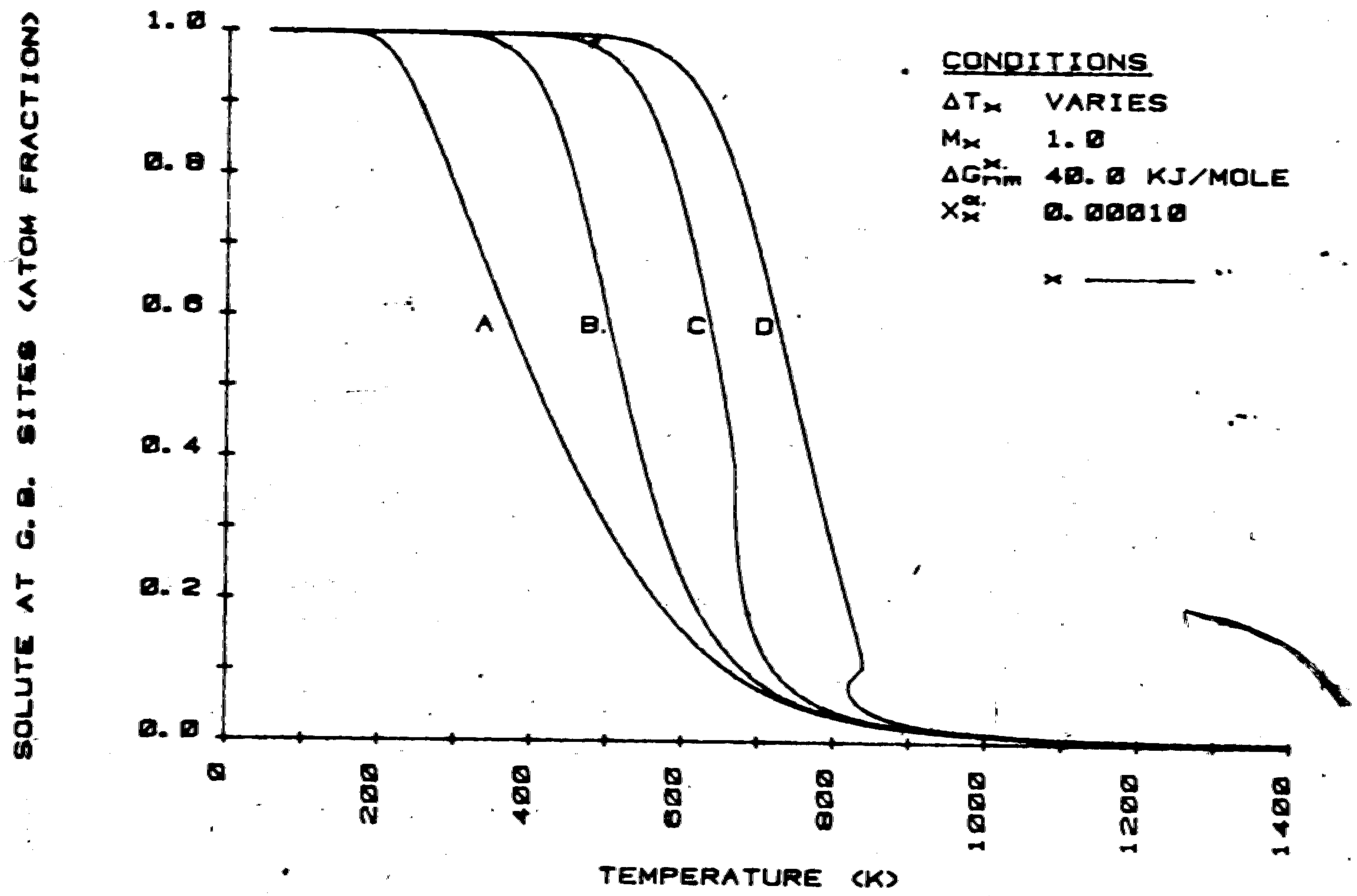

Figure 4.27
Predicted grain boundary solute concentrations according to Case II (A = 1000 K, B = 0 K, C = -1000 K, D = -2000 K).

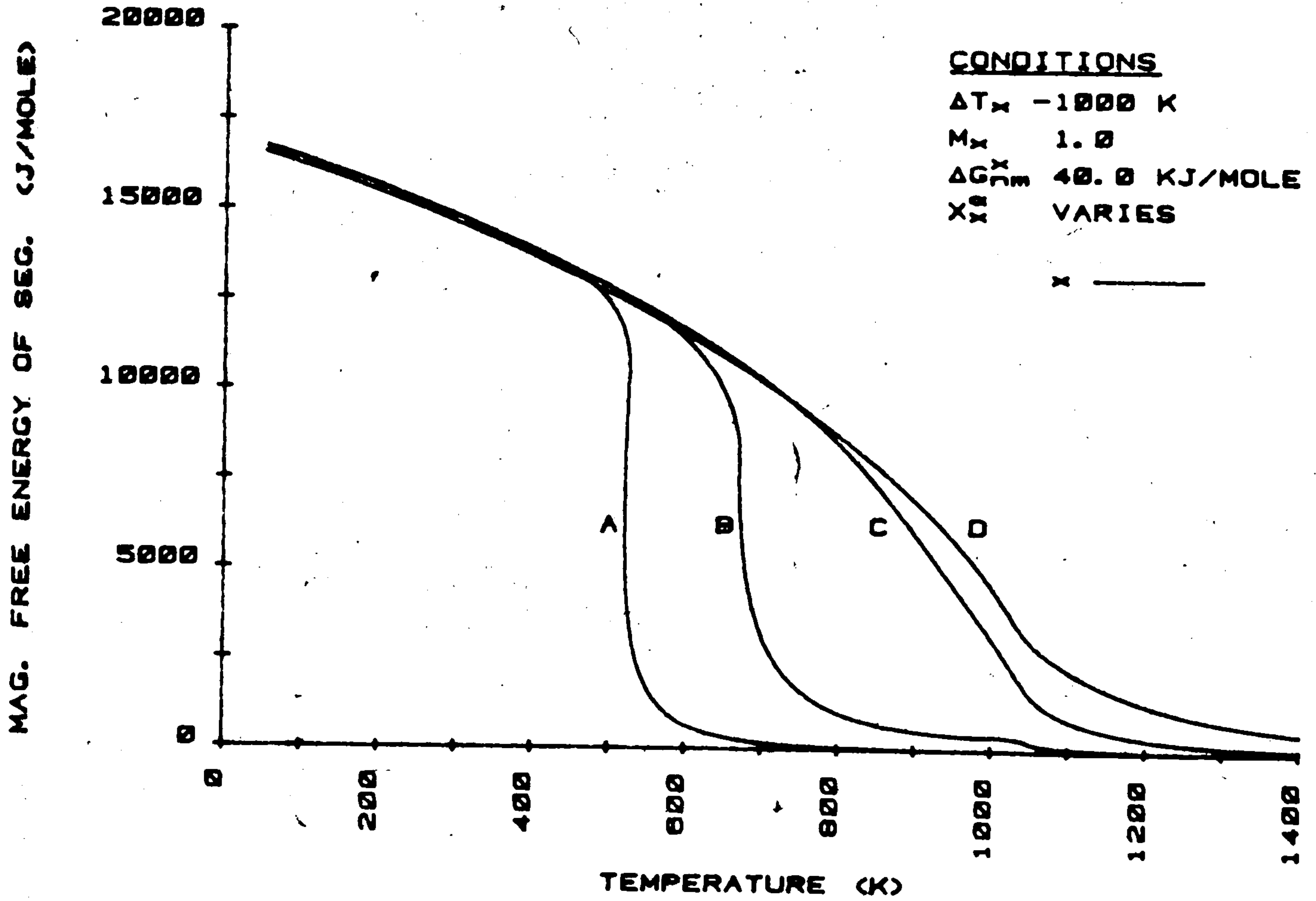

Figure 4.28
The effect of bulk solute content on the magnetic segregation free energy according to Case II (A = 0.00001, B = 0.0001, C = 0.001, D = 0.01).

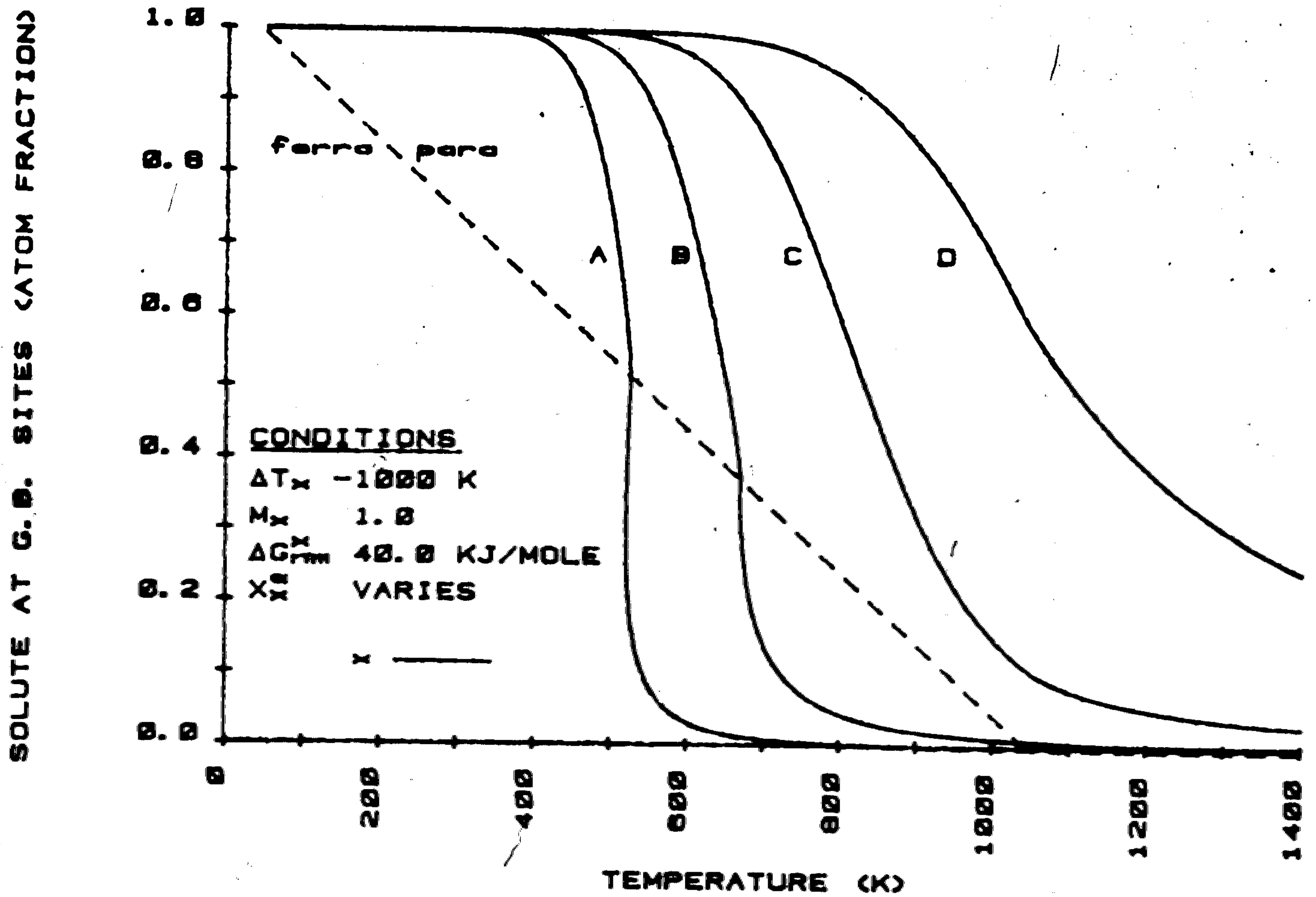

Figure 4.29
The effect of bulk solute content on predicted grain boundary solute concentrations according to Case II (A = 0.00001, B = 0.0001, C = 0.001, D = 0.01).

order-disorder transition temperature (Curie temperature). The effect of decreasing bulk solute is to 'chop off' a right hand portion of the magnetic segregation free energy curve by introducing steps at decreasing temperatures, thus, shifting the region of rapid segregation increase to lower temperatures. Again, consider the segregation equation (4.85). It is obvious that the changes in the bulk solute concentration and the exponential term should have similar effects.

The effect of non-magnetic segregation free energy on the magnetic segregation free energy is shown in Figure 4.30. and the corresponding segregation curves in Figure 4.31. These figures are very similar to Figures 4.28 and 4.29 for magnetic segregation free energy.

The present analysis predicts that small amounts of solute with large negative magnetic parameters have a large effect on the equilibrium segregation behavior. Thus grain boundary segregation behavior in iron-based alloys is different than segregation in non-magnetic alloys. In general, as many important impurities in iron-based alloys are non-magnetic with large negative magnetic parameters (see Table 4.2), the temperature range over which the grain boundaries are saturated extends to higher temperatures than would be expected from purely non-magnetic considerations. At these higher temperatures, impurity diffusion is easier and equilibrium segregation is achieved more rapidly. As intergranular embrittlement of many materials has been

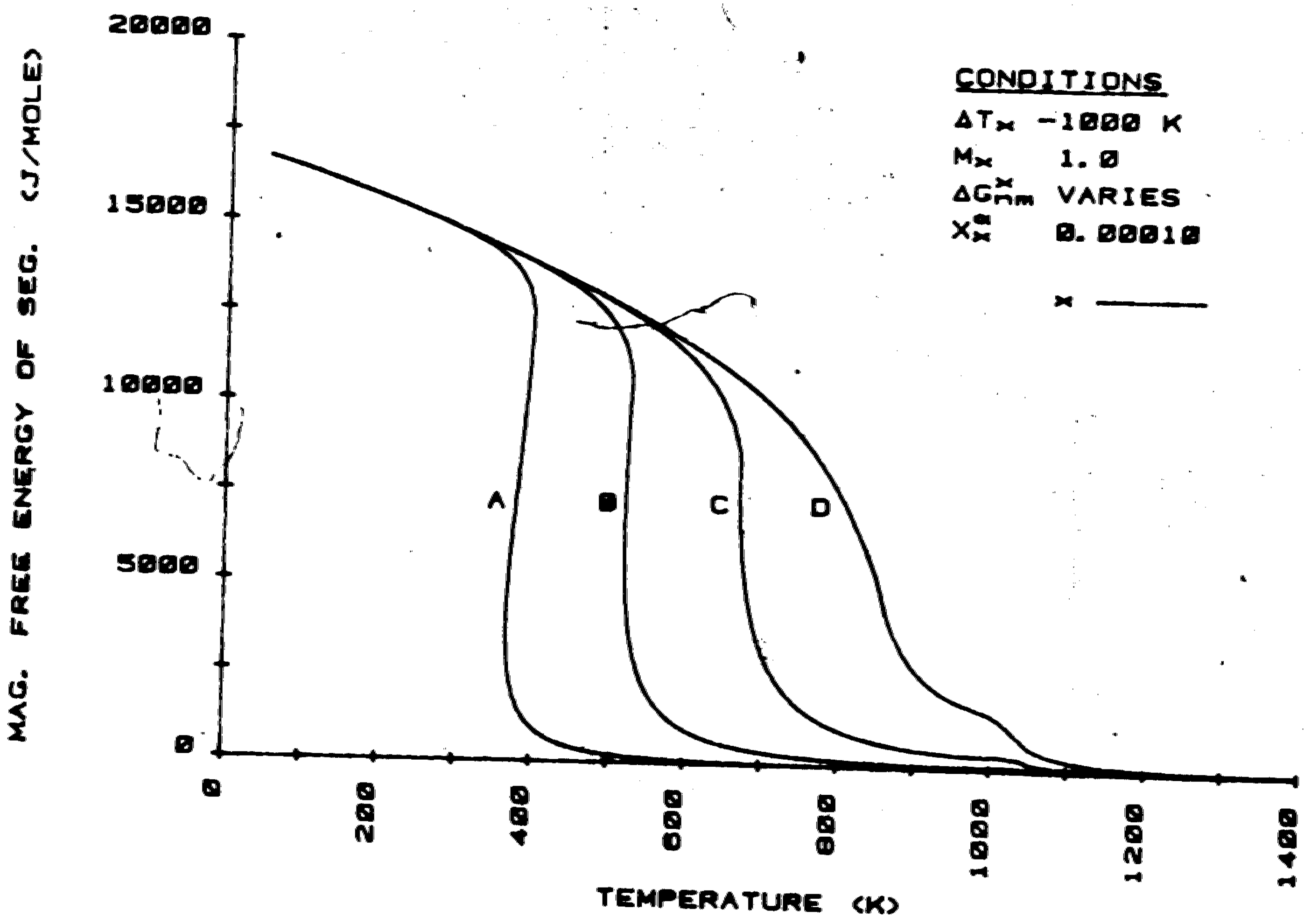

Figure 4.30
The effect of the non-magnetic segregation free energy on the magnetic segregation free energy according to Case II (A = 20 KJ/mole, B = 30 KJ/mole, C = 40 KJ/mole, D = 50 KJ/mole).

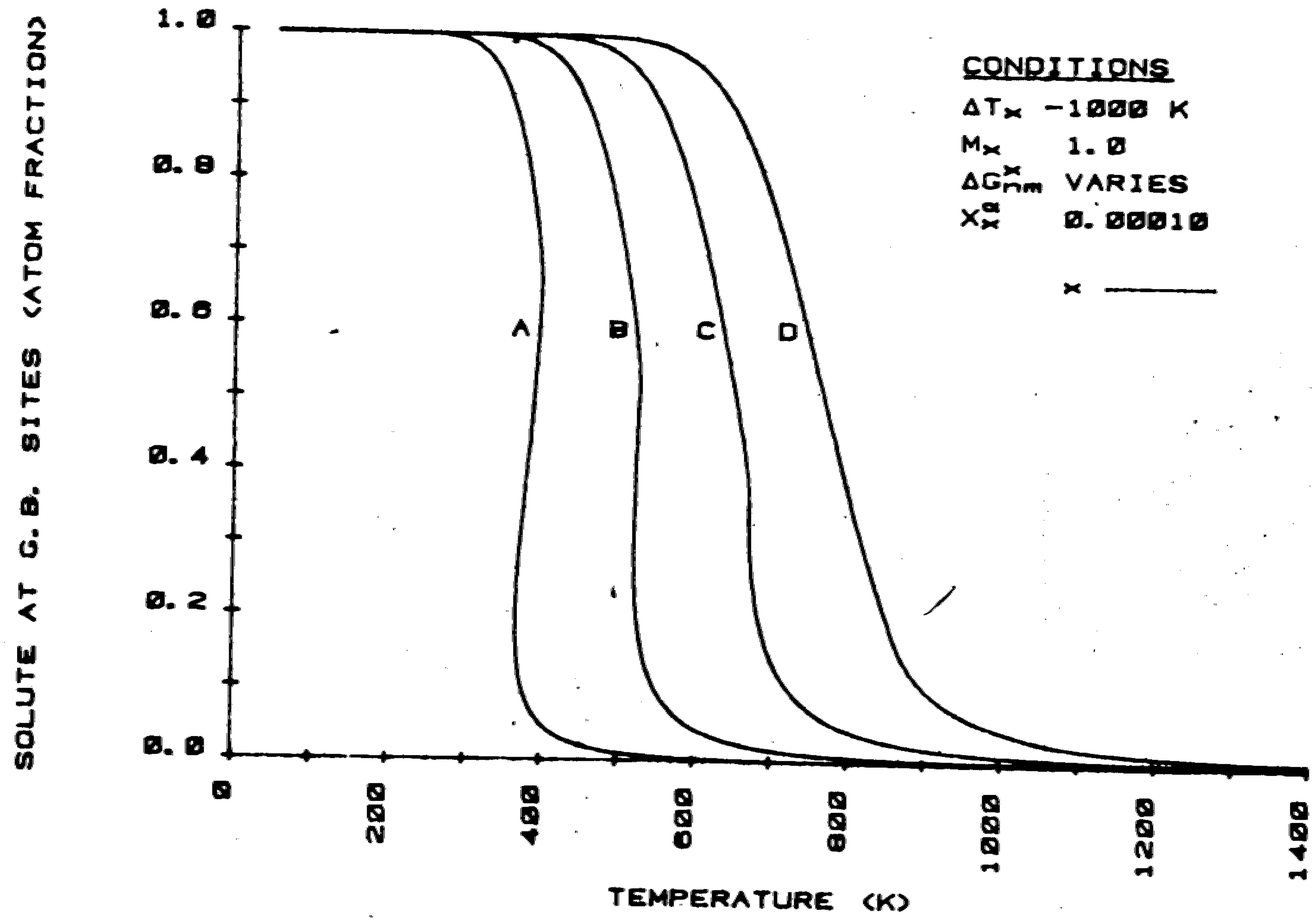

Figure 4.31
The effect of the non-magnetic segregation free energy on the grain boundary solute concentration according to Case II (A = 20 KJ/mole, B = 30 KJ/mole, C = 40 KJ/mole, D = 50 KJ/mole).

linked to grain boundary impurity segregation, the present analysis indicates magnetic materials are likely to be more susceptible at higher temperatures to embrittlement than equivalent non-magnetic materials.

Approximations of Case I and Case II for the alpha Fe-P system are shown in Figure 4.32. This figure emphasizes the major differences between Case I and Case II, that is, Case II may have a step in the curve and the Case I curve is displaced to higher temperatures. The displacement is due to the fact that, for Case I, the magnetic segregation free energy has an unrealistic positive component present as seen in Figure 4.23. The step in the Case II curve is believed due to a magnetic transition which will now be discussed.

4.8 The Magnetic State of the Boundary Phase

An interesting outcome of the above analysis arises from the solute dependence of the Curie temperature. Boundaries rich in solute (with a large negative magnetic parameter) can achieve transition to the paramagnetic state as the Curie temperature of the boundary falls below the system temperature. Thus situations can arise such that as the temperature falls, the boundary phase transforms from paramagnetic to ferromagnetic near the bulk Curie temperature then at a lower temperature segregation causes the boundary Curie temperature to fall low enough that the boundary phase again becomes paramagnetic.

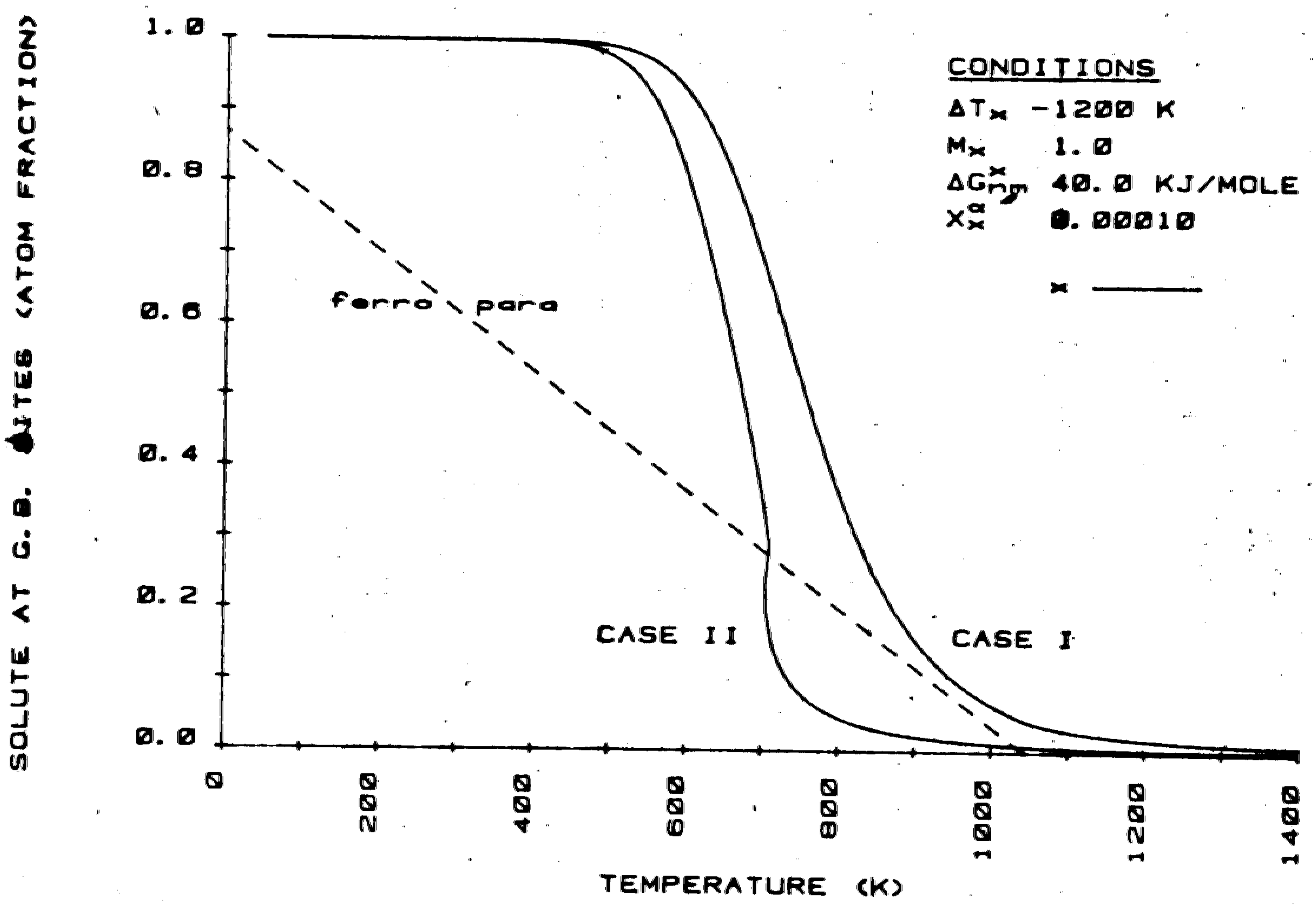

Figure 4.32
Case I and Case II segregation curves for the alpha Fe-P system.

The grain boundary Curie temperature is

$$T_c^{\phi} = T_c^{Fe} + \Delta T_X X_X^{\phi} \tag{4.105}$$

where T_c^{Fe} is the Curie temperature of iron (1043 K). Thus at a temperature T, the grain boundary will be ferromagnetic if

$$X_X^{\phi} \leq \frac{[T - T_c^{Fe}]}{\Delta T_X}, \qquad \Delta T_X \text{ negative}$$

$$X_X^{\phi} \geq \frac{[T - T_c^{Fe}]}{\Delta T_X}, \qquad \Delta T_X \text{ positive} \tag{4.106}$$

At any temperature a maximum solute content $X_X^{\phi *}$ (or critical solute content) exists beyond which the grain boundary phase will be paramagnetic. A line representing $X_X^{\phi *}$ versus temperature is shown for the Fe-P system in Figure 4.32. Shown in Figure 4.29 is a more general case at several bulk solute contents. It can be seen that in this case, for $X_X^{\alpha} = 0.001$, the boundary is always paramagnetic whereas for $X_X^{\alpha} = 0.0001$ the double transformation occurs. It is noted that a step in the segregation curve exists only when the $X_X^{\phi *}$ line crosses the segregation curve, that is, when a second magnetic transition takes place. However, a second magnetic transition may occur without a step occurring in the segregation curve for small negative magnetic parameter. The segregation curves seem to indicate that the $X_X^{\phi *}$ line crosses at or near an inflection point in the segregation curve. Increasing the bulk content has the effect of decreasing the temperature range for which the grain boundary may be ferromagnetic.

The information in figure 4.28 may be displayed in a different manner which will be more useful in subsequent sections. Figure 4.33 shows equilibrium grain boundary Curie temperatures versus the system temperature. The conditions for a ferromagnetic boundary would be

$$T_c^{\phi} \geq T \tag{4.107}$$

The dashed line separates the ferromagnetic and paramagnetic regions.

4.9 The Thermodynamics of Dilute alpha Fe-M-X Solid Solutions

The theories and formalisms previously applied to alpha Fe-X binary solutions are now used to describe alpha Fe-M-X ternary solutions. Although Nishizawa et al. have empirically calculated the free energy and solid solubility specifically for Fe-Co-X, the author now presents a general formalism for alpha Fe-M-X systems.

The total Gibbs free energy function, G^{α}, for an alpha Fe-M-X solid solution will be, by definition,

$$G^{\alpha}(T) = H^{\alpha}(T) - TS^{\alpha}(T) \tag{4.108}$$

As with binary solutions, the total free energy functions of ternary solutions may also be analysed by their component parts. That is, it is assumed, by analogy, that

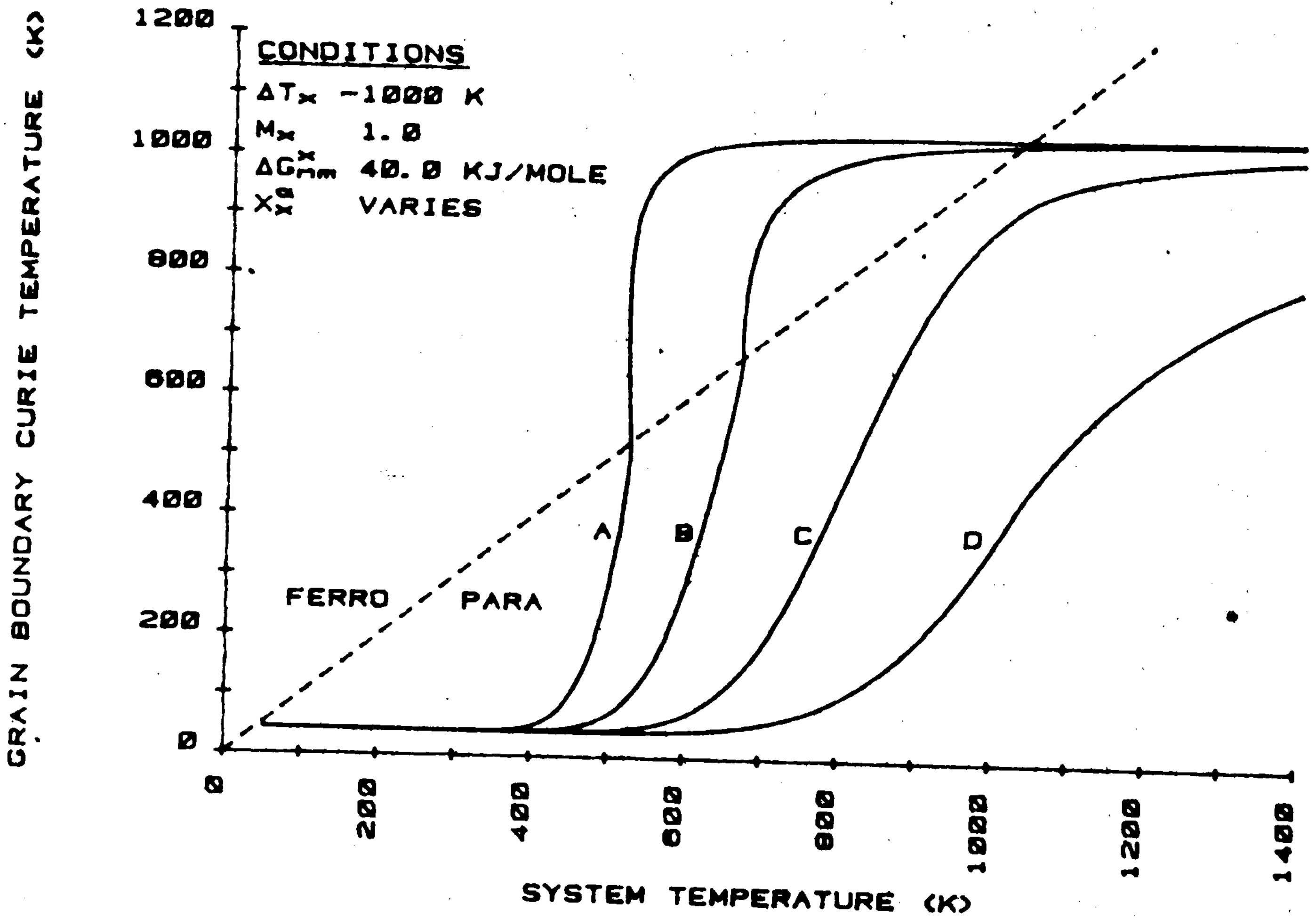

Figure 4.33
The effect of bulk solute content on the boundary Curie temperature.

$$G^{\alpha}(T) = G^{\alpha}_{nm}(T) + G^{\alpha}_{mag}(T) \tag{4.109}$$

The non-magnetic component, G^{α}_{nm}, may be theoretically described by way of the ordinary regular solution approximation (the quasi-binary approximation). The regular solution approximation gives the following:

$$\begin{aligned} G^{\alpha}_{nm} &= X_{Fe}\,{}^{o}G^{Fe}_{nm} + X_{M}\,{}^{o}G^{M}_{nm} + X_{X}\,{}^{o}G^{X}_{nm} \\ &+ X_{M}[1-X_{M}]I^{FeM}_{nm} + X_{X}[1-X_{X}]I^{FeX}_{nm} + X_{M}X_{X}I^{MX}_{nm} \\ &+ RT[X_{Fe}\ln X_{Fe} + X_{M}\ln X_{M} + X_{X}\ln X_{X}] \end{aligned} \tag{4.110}$$

where

${}^{o}G^{i}_{nm}$ is the non-magnetic standard free energy for i,

I^{ij}_{nm} is the non-magnetic interaction coefficient between i and j,

X_i denotes the concentration of impurity i, and

X_M denotes the concentration of a transition metal M.

A descriptive modification of the magnetic free energy for the ternary solution is based upon the modification used for the binary solution. As in the binary analysis, the Curie temperature of a solid solution is assumed to vary linearly with solute concentration. Therefore, by dissolving atomic fractions X^{α}_{X} and X^{α}_{M} of solute,

$$T^{\alpha}_{c} = T^{Fe}_{c} + \Delta T_{X}X_{X} + \Delta T_{M}X_{M} \tag{4.111}$$

where ΔT_M is the magnetic parameter for M.

The magnetic free energy of alpha Fe-M-X may be obtained by modifying the free energy of alpha Fe (or alpha Fe-X) in such a manner that the alpha Fe-M-X magnetic free energy curve maintains the same position with respect to a new Curie temperature as the alpha Fe (alpha Fe-X) free energy curve maintains to the old Curie temperature. The displacements may be obtained in the manner described by equations 4.22 to 4.25, such that

$$T^{\alpha} = T - [\Delta T_X X_X + \Delta T_M X_M] \tag{4.112}$$

$$G^{\alpha}_{mag}(T) = G^{Fe}_{mag}(T^{\alpha}) - [\Delta T_X X_X + \Delta T_M X_M]\,{}^{u}S^{Fe}_{mag} \tag{4.113}$$

The influence of the solutes upon the size of the magnetic component [41] introduces two constant solute intensity factors M_X, M_M, so that

$$G^{\alpha}_{mag} = [1-M_M X_M][1-M_X X_X][G^{Fe}_{mag}(T^{\alpha}) - [\Delta T_X X_X + \Delta T_M X_M]\,{}^{u}S^{Fe}_{mag}] \tag{4.114}$$

If $\Delta T_C = (\Delta T_X X_X + \Delta T_M X_M)$, equation 4.114 is the form for the magnetic free energy of dilute ternary solid solutions implicit in the work of Nishizawa et al.[44]. Species X and M are considered non-magnetic and are assumed not to interact magnetically. The magnetic interaction terms may be defined as in equations (4.28) to (4.33) to give the interaction per unit mole of solute.

$$[\Delta T_X + \Delta T_M][S^{Fe}_{mag}(T^{\alpha}) - {}^{u}S^{Fe}_{mag}] \qquad (4.115)$$

This gives the alpha Fe-M-X total free energy as

$$\begin{aligned} G^{\alpha}(T) = {} & X_{Fe}{}^{o}G^{Fe}_{nm} + X_M{}^{o}G^{M}_{nm} + X_X{}^{o}G^{X}_{nm} \\ & + X_M[1-X_M]I^{FeM}_{nm} + X_X[1-X_X]I^{FeX}_{nm} + X_MX_XI^{MX}_{nm} \\ & + RT[X_{Fe}\ell nX_{Fe} + X_M\ell nX_M + X_X\ell nX_X] \\ & + [1-M_MX_M][1-M_XX_X][G^{Fe}_{mag}(T^{\alpha})-[\Delta T_XX_X+\Delta T_MX_M]{}^{u}S^{Fe}_{mag}] \end{aligned}$$

(4.116)

4.10 Chemical Potentials For Alpha Fe-M-X

The chemical potential, μ^i, of species i, in alpha Fe-M-X is described in the normal manner, with magnetic and non-magnetic components, so that,

$$\begin{aligned} \mu^{Fe} &= G^{\alpha} - X_X\frac{\partial G^{\alpha}}{\partial X_X} - X_M\frac{\partial G^{\alpha}}{\partial X_M} \\ \mu^{X} &= \mu^{Fe} + \frac{\partial G^{\alpha}}{\partial X_X} \\ \mu^{M} &= \mu^{Fe} + \frac{\partial G^{\alpha}}{\partial X_M} \end{aligned} \qquad (4.117)$$

As for the binary case in section 4.3 various terms must be evaluated to obtain a useful chemical potential:

1. $$\frac{\partial\, {}^{o}G^{i}_{nm}}{\partial X_j} = 0$$

2. $$\frac{\partial I^{ij}_{nm}}{\partial X_k} = 0$$

3. $$\frac{\partial X_{Fe}}{\partial X_{i \neq Fe}} = -1$$

4. $$\frac{\partial X_{i \neq Fe}}{\partial X_j} = 0$$

5. $$\frac{\partial G^{Fe}_{mag}(T^{\alpha})}{\partial X_i} = \Delta T_i S^{Fe}_{mag}(T^{\alpha})$$

6. $$M_i(X_i, T) = \text{constant} \tag{4.118}$$

The partial differential of the total free energy of alpha Fe-M-X with respect to the bulk concentration of X is

$$\frac{\partial G^{\alpha}_{nm}}{\partial X_X} = -{}^{o}G^{Fe}_{nm} + {}^{o}G^{X}_{nm} + [1-2X_X]I^{FeX}_{nm} + X_M I^{MX}_{nm} + RT[\ell n X_X - \ell n X_{Fe}] \tag{4.119}$$

$$\frac{\partial G^{\alpha}_{mag}}{\partial X_X} = - M_X[1-M_M X_M][G^{Fe}_{mag}(T^{\alpha})-[\Delta T_X X_X+\Delta T_M X_M]\,{}^{u}S^{Fe}_{mag}] + [1-M_M X_M][1-M_X X_X][S^{Fe}_{mag}(T^{\alpha})-{}^{u}S^{Fe}_{mag}]\Delta T_X \tag{4.120}$$

The partial differential of the total free energy of alpha with respect to bulk concentration of M is

$$\frac{\partial G^{\alpha}_{nm}}{\partial X_M} = -{}^{o}G^{Fe}_{nm} + {}^{o}G^{M}_{nm} + [1-2X_M]I^{FeM}_{nm} + X_X I^{MX}_{nm} + RT[\ell n X_M - \ell n X_{Fe}] \tag{4.121}$$

$$\frac{\partial G^{\alpha}_{mag}}{\partial X_M} = -M_M[1-M_X X_X][G^{Fe}_{mag}(T^{\alpha})-[\Delta T_X X_X+\Delta T_M X_M]{}^{u}S^{Fe}_{mag}] + [1-M_M X_M][1-M_X X_X][S^{Fe}_{mag}(T^{\alpha})-{}^{u}S^{Fe}_{mag}]\Delta T_M \tag{4.122}$$

The chemical potential of Fe is

$$\mu^{Fe}_{nm} = {}^{o}G^{Fe}_{nm} + X_X^2 I^{Fe}_{nm} + X_M^2 I^{Fe}_{nm} - X_M X_X I^{MX}_{nm} + RT\ell n X_{Fe} \tag{4.123}$$

$$\mu^{Fe}_{mag} = [1-M_M M_X X_M X_X][G^{Fe}_{mag}(T^{\alpha})-[\Delta T_X X_X+\Delta T_M X_M]{}^{u}S^{Fe}_{mag}] - [1-M_M X_M][1-M_X X_X][\Delta T_X X_X+\Delta T_M X_M][S^{Fe}_{mag}(T^{\alpha})-{}^{u}S^{Fe}_{mag}] \tag{4.124}$$

The chemical potential of X is

$$\mu^{X}_{nm} = {}^{o}G^{X}_{nm} + [1-X_X]^2 I^{FeX}_{nm} - X_M[1-X_X]I^{FeM}_{nm} + X_M[1-X_X]I^{MX}_{nm} + RT\ell n X_{Fe} \tag{4.125}$$

$$\mu^{X}_{mag} = [1-M_X+M_M M_X X_M-M_M M_X X_M X_X][G^{Fe}_{mag}(T^{\alpha})-[\Delta T_X X_X+\Delta T_M X_M]{}^{u}S^{Fe}_{mag}] + [1-M_M X_M][1-M_X X_X][\Delta T_X[1-X_X]-\Delta T_M X_M][S^{Fe}_{mag}(T^{\alpha})-{}^{u}S^{Fe}_{mag}] \tag{4.126}$$

The chemical potential of M is

$$\mu^{M}_{nm} = {}^{o}G^{M}_{nm} - X_X[1-X_M]I^{FeX}_{nm} + [1-X_M]^2 I^{FeM}_{nm} + X_X[1-X_M]I^{MX}_{nm} + RT\ln X_M \tag{4.127}$$

$$\mu^{M}_{mag} = [1-M_M+M_M M_X X_X - M_M M_X X_M X_X][G^{Fe}_{mag}(T^{\alpha}) - [\Delta T_X X_X + \Delta T_M X_M]\,{}^{u}S^{Fe}_{mag}] + [1-M_M X_M][1-M_X X_X][\Delta T_M[1-X_M] - \Delta T_X X_X][S^{Fe}_{mag}(T^{\alpha}) - {}^{u}S^{Fe}_{mag}] \tag{4.128}$$

For a dilute solution, the magnetic chemical potential of Fe versus temperature is essentially the same as shown in Figure 4.5. The magnetic chemical potential of X in a ternary has essentially the same behavior with respect to its magnetic parameter as in a binary solution (see Figure 4.7). The effect of the magnetic parameter of M depends largely on the concentration of M but as seen in Figure 4.34, decreasing magnetic parameter increases the chemical potential. The effect of the concentration of solute M on the chemical potential of X is shown in Figure 4.35. Increasing solute content decreases this potential.

4.11 The Solid solubility of X in Alpha Fe-M-X Solid Solutions

The limit of solid solubility of solute X in alpha Fe-M-X occurs when Fe_aX_b or M_aX_b phases are in equilibrium with the alpha Fe-M-X solid solution. Solute M will be

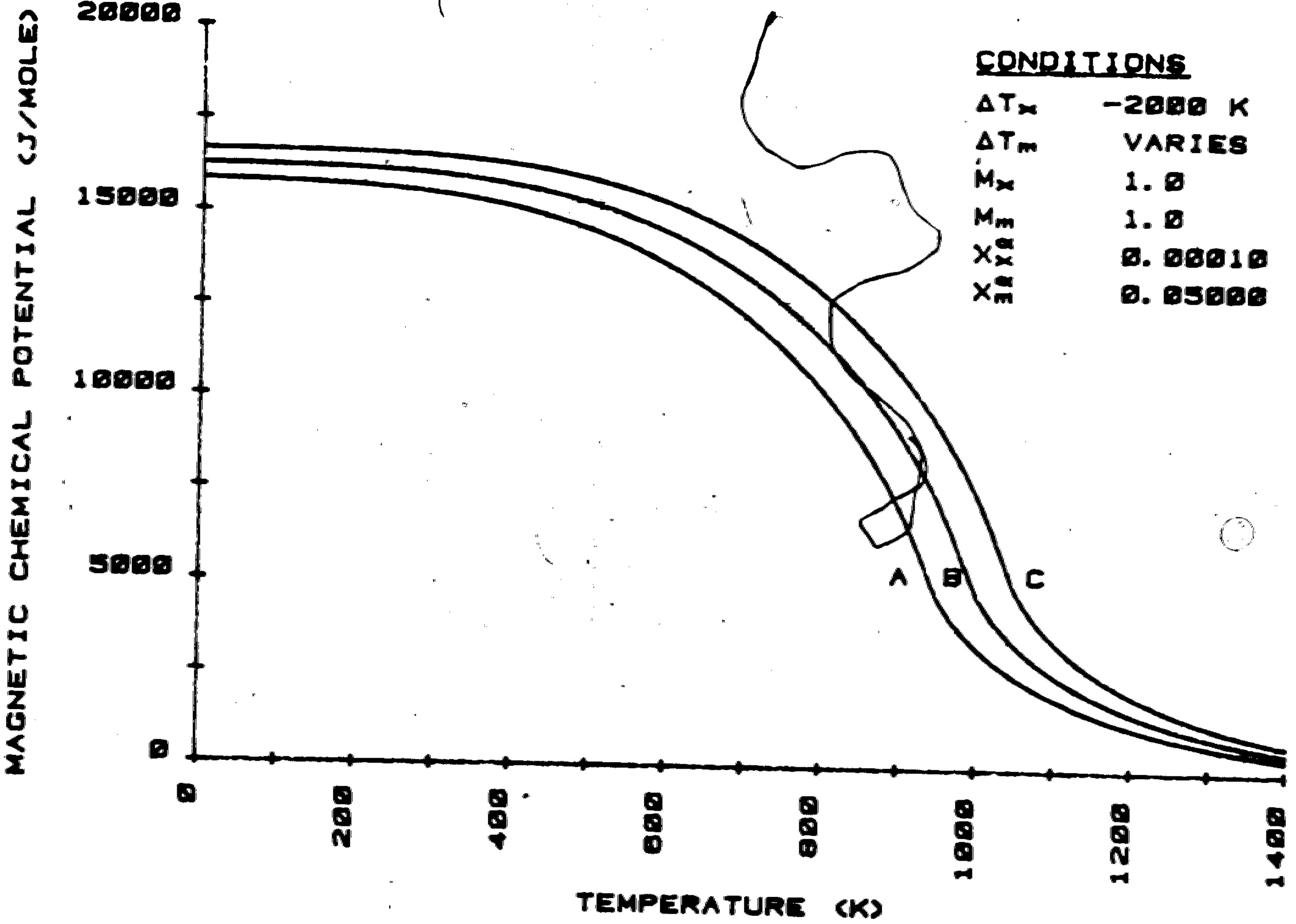

Figure 4.34
The effect of the magnetic parameter of M on the magnetic chemical potential of X (A = -1000 K, B = 0 K,C = 1000 K).

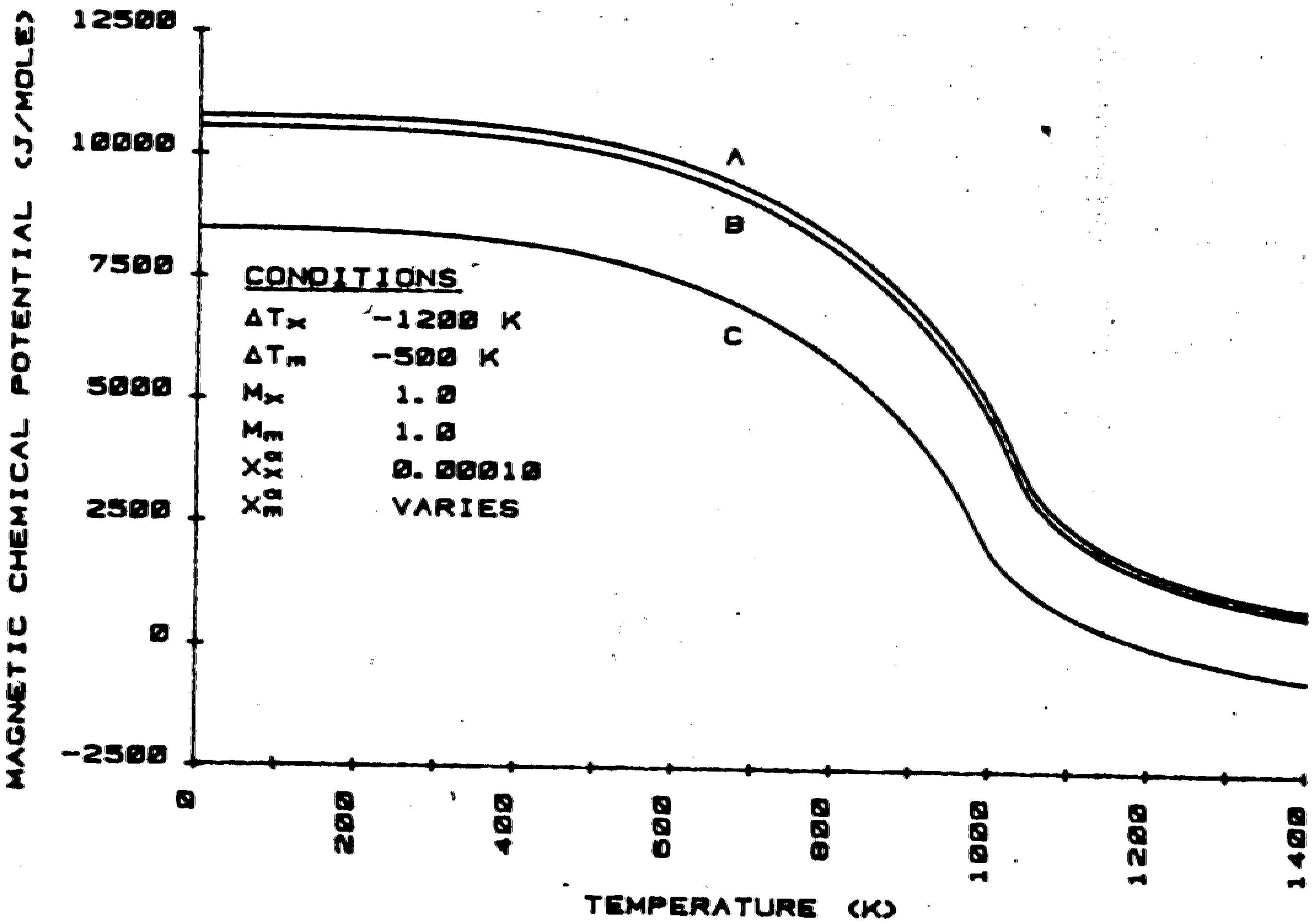

Figure 4.35
The effect of the content of M on the magnetic chemical potential of X (A = 0.001, B = 0.01, C = 0.1).

considered a transition metal element such as Mn, Cr, Mo, and V. Solute X will be considered an impurity element such as P, Sb, and As. When dealing with systems exhibiting temper embrittlement it has been noticed [64] that the intermetallic compounds Fe_aX_b and M_aX_b have the same crystal structure and that complete miscibility exists between them. Therefore the compound beta $(Fe_yM_{1-y})_aX_b$ (where a + b = 1) is in equilibrium with the alpha Fe-M-X solid solution. As shown by Hillert [65] and by Guttmann [64], the conditions of equilibrium between the solid solution alpha and the compound beta are obtained by treating beta as a regular solution of the two binary compounds Fe_aX_b (denoted $\theta 1$) and M_aX_b (denoted $\theta 2$) with concentrations y and 1-y, that is

$$\begin{aligned} G^{\theta 1} &= {}^{o}G^{\theta 1} + aRT\ell n y \\ G^{\theta 2} &= {}^{o}G^{\theta 2} + aRT\ell n(1-y) \end{aligned} \qquad (4.129)$$

At equilibrium, the condition set out in equation (4.57) must be applied such that

$$\begin{aligned} a\mu^{Fe} + b\mu^{X} &= G^{\theta 1} \\ a\mu^{M} + b\mu^{X} &= G^{\theta 2} \\ \text{where} \quad \mu^{i} &= {}^{o}\mu^{i} + RT\ell n X_i \end{aligned} \qquad (4.130)$$

Equations 4.129 and 4.130 are combined to give the system of equations

$$a^{o}\mu^{Fe} + aRT\ell n X_{Fe} + b^{o}\mu^{X} + bRT\ell n X_{X} = {}^{o}G^{\theta 1} + aRT\ell n y$$

$$a^{o}\mu^{M} + aRT\ell n X_{M} + b^{o}\mu^{X} + bRT\ell n X_{X} = {}^{o}G^{\theta 2} + aRT\ell n(1-y) \tag{4.131}$$

$$\Delta G^{\theta 1} = {}^{o}G^{\theta 1} - a^{o}\mu^{Fe} - b^{o}\mu^{X}$$

$$\Delta G^{\theta 2} = {}^{o}G^{\theta 2} - a^{o}\mu^{M} - b^{o}\mu^{X} \tag{4.132}$$

To solve these equations for the solubility, X_X^S, it is necessary to eliminate y and assume a dilute solution. The exponentials of equations (4.131) are taken and y separated out to give

$$y = X_{Fe}X_X^{b/a}\exp(-\Delta G^{\theta 1}/aRT)$$

$$1-y = X_M X_X^{b/a}\exp(-\Delta G^{\theta 2}/aRT) \tag{4.133}$$

Eliminating y gives

$$1 = X_X^{b/a}[X_{Fe}\exp(-\Delta G^{\theta 1}/aRT)+X_M\exp(-\Delta G^{\theta 2}/aRT)] \tag{4.134}$$

Applying the dilute bulk approximation, where the concentration of X is small, gives

$$X_X^S = \frac{\exp(\Delta G^{\theta 1}/bRT)}{[1-X_M+X_M\exp(-\Delta G'/aRT)]^{a/b}} \tag{4.135}$$

$$\Delta G' = \Delta G^{\theta 2} - \Delta G^{\theta 1} \tag{4.136}$$

The numerator of equation (4.135) denotes the solubility limit of X in alpha Fe in the absence of M and is exactly equivalent to equation (4.60). It is immediately obvious that both $\Delta G^{\theta 1}$ and $\Delta G'$ have terms of excess free energy that are magnetic in nature such that:

$$\Delta G^{\theta 1} = {}^{o}G^{\theta 1} - [a\mu_{nm}^{Fe} + b\mu_{nm}^{X}] - [a\mu_{mag}^{Fe} + b\mu_{mag}^{X}] \qquad (4.137)$$

$$\Delta G' = {}^{o}G^{\theta 2} - {}^{o}G^{\theta 1} - a[\mu_{nm}^{M} - \mu_{nm}^{Fe} + \mu_{mag}^{M} - \mu_{mag}^{Fe}]$$

$$(4.138)$$

Applying the dilute bulk regular solution approximation, the magnetic componeht of equation (4.137) becomes

$$-\Delta G_{mag}^{\theta 1} = [1 - bM_X + bM_M M_X X_M][G_{mag}^{Fe}(T^{\alpha}) - \Delta T_M X_M {}^{u}S_{mag}^{Fe}]$$

$$- [1 - M_M X_M][b\Delta T_X - \Delta T_M][S_{mag}^{Fe}(T^{\alpha}) - {}^{u}S_{mag}^{Fe}] \qquad (4.139)$$

Likewise, the magnetic component of equation (4.138) is

$$\Delta G'_{mag} = -a \frac{\partial G_{mag}^{\alpha}}{\partial X_M} \qquad (4.140)$$

Which is equivalent to a constant times equation (4.122) and

$$\Delta G'_{mag} = aM_M[G_{mag}^{Fe}(T^{\alpha}) - \Delta T_M X_M {}^{u}S_{mag}^{Fe}]$$

$$- a[1 - M_M X_M \underline{]\Delta T_M[} S_{mag}^{Fe}(T^{\alpha}) - {}^{u}S_{mag}^{Fe}] \qquad (4.141)$$

where $T^{\alpha} = T - \Delta T_M X_M$. Under these circumstances the limit of solid solubility for X may be obtained from equation (4.135) analytically.

The effect of the magnetic parameter of the transition metal alloying element, ΔT_M, on phosphorus solid solubility in alpha Fe-0.01M-P is shown in Figure 4.36. As can be noticed, the general shape of the binary solubility curve (see Figure 4.12) is retained. However, a large negative magnetic parameter of M further decreases the solubility below the Curie temperature significantly. An increase in the amount of transition metal, M, present also significantly decreases solubility of P in alpha Fe-M-P as is shown in Figure 4.37.

The two previous figures are concerned with magnetic interactions. It is of interest to also consider chemical interaction among the elements as in the work of Guttmann [58]. He defined a preferential interaction coefficient between M and X, I', such that, in the paramagnetic limit,

$$-\Delta G' = abI' \qquad (4.142)$$

A large positive I' denotes a strong attraction between M and X atoms.[12] The effect of I' on P solubility in alpha Fe-0.01M-P is shown in Figure 4.38. As expected, large positive I' drastically reduces the maximum amount of P in solution. In other words, M atoms 'scavenge' P atoms and form some type of complex. The definition of ΔG' allows for its calculation from experimental data. Guttmann determined I' for various transition metal- phosphorus combinations as shown in Table 4.4

by making use of the experimental solubility data of Kaneko [23], Figure 4.39. Table 4.4 also contains magnetic

---

[12] I' will be more fully explained in section 4.13.

Table 4.4 Interaction parameters for M-P calculated from solubility data [64]

M element	Interaction parameter I' (KJ/mole)	Magnetic Parameter (K)
Ni	30.1	-400
Mn	66.9	-1300
Cr	100.3	-800
V	143.8	1000
W	170.7	-
Mo	184.0	-300
Ti	221.0	-
Zr	256.4	-

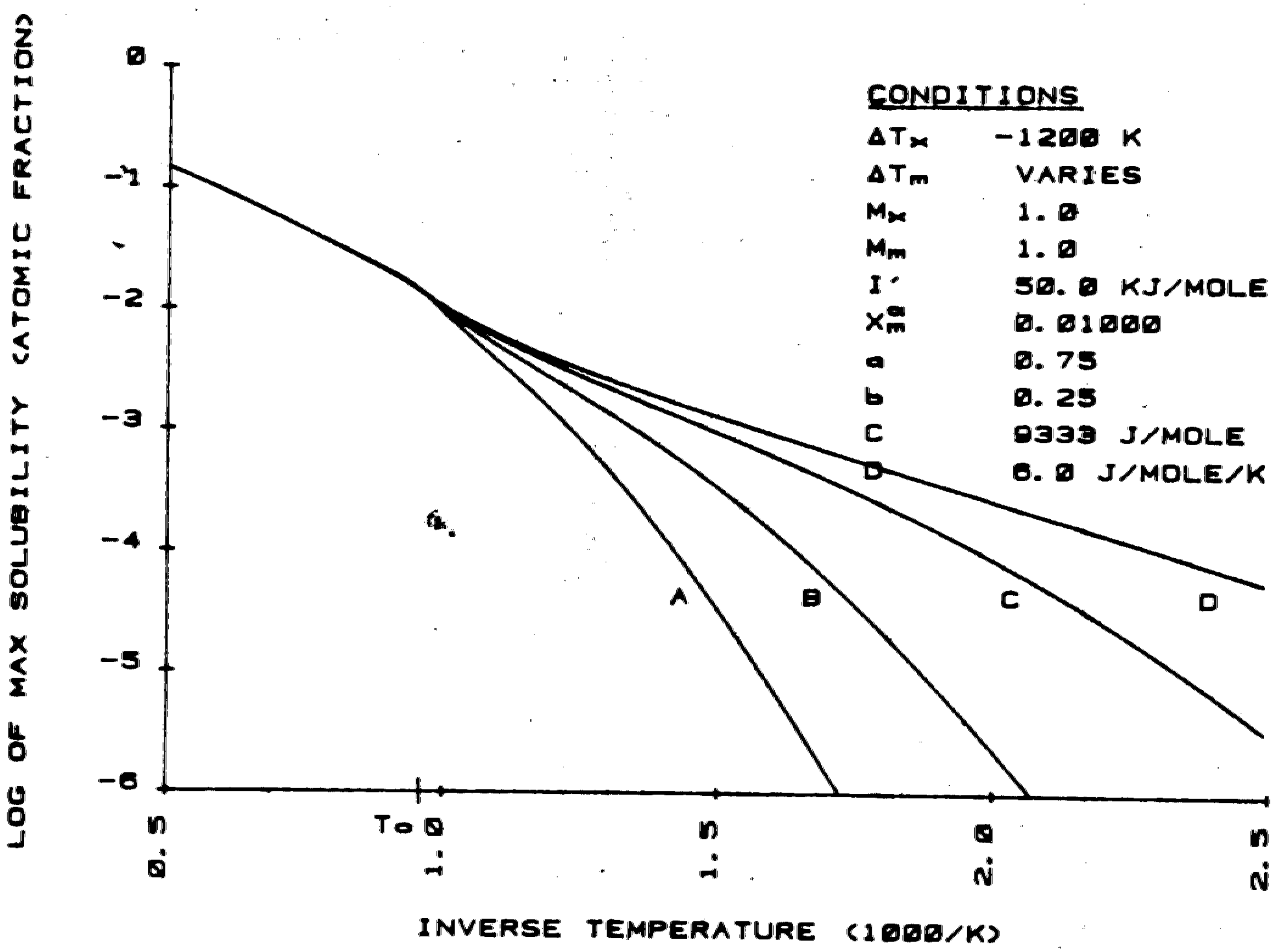

Figure 4.36
The effect of the magnetic parameter of M on phosphorus solid solubility in alpha Fe-0.01M-P (A = -2000 K, B = -1000 K, C = 0 K, D = 1000 K).

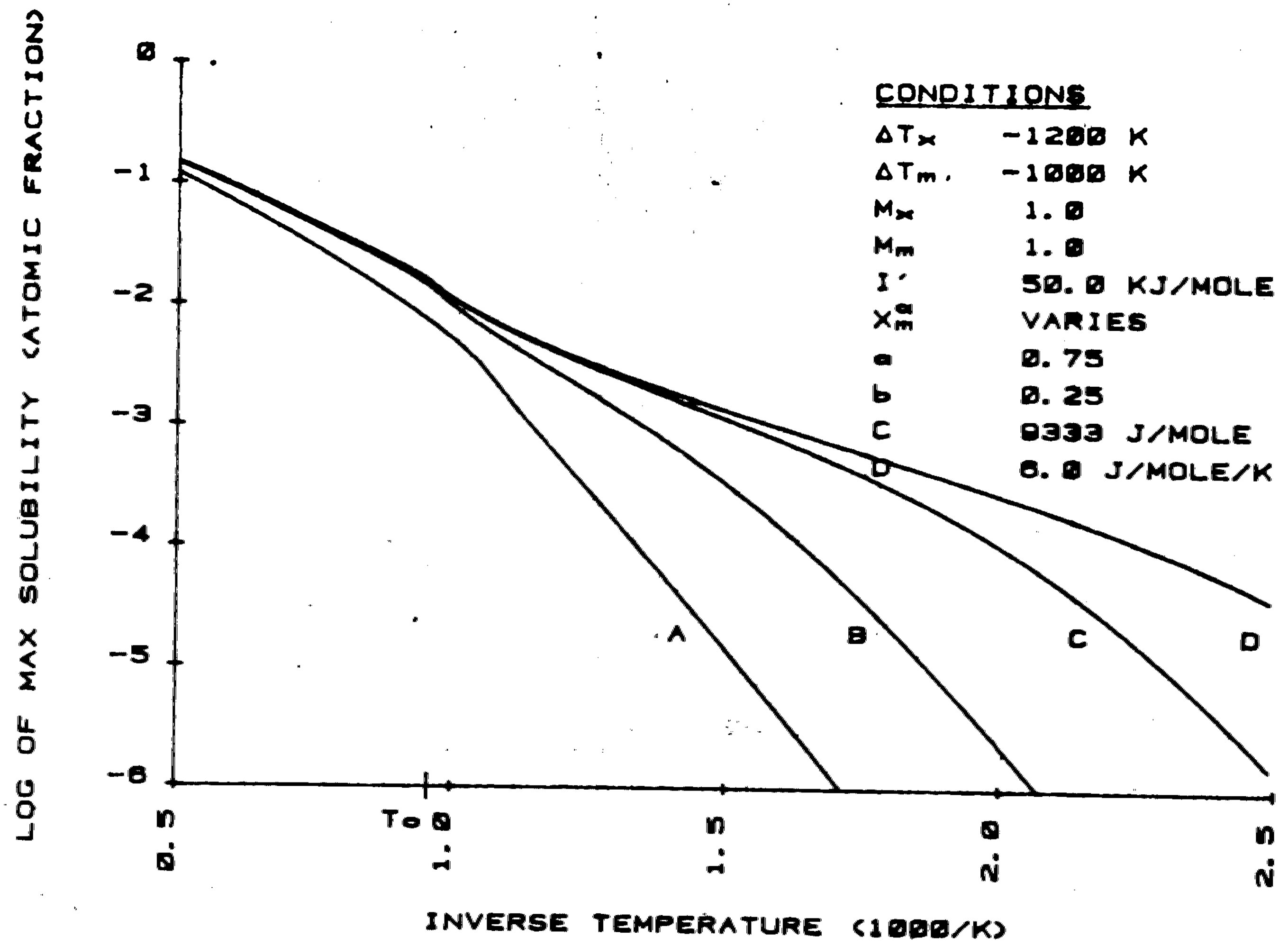

Figure 4.37
The effect of the content of solute M on phosphorus solid solubility in alpha Fe-M-X (A = 0.1, B = 0.01, C = 0.001, D = 0.0001).

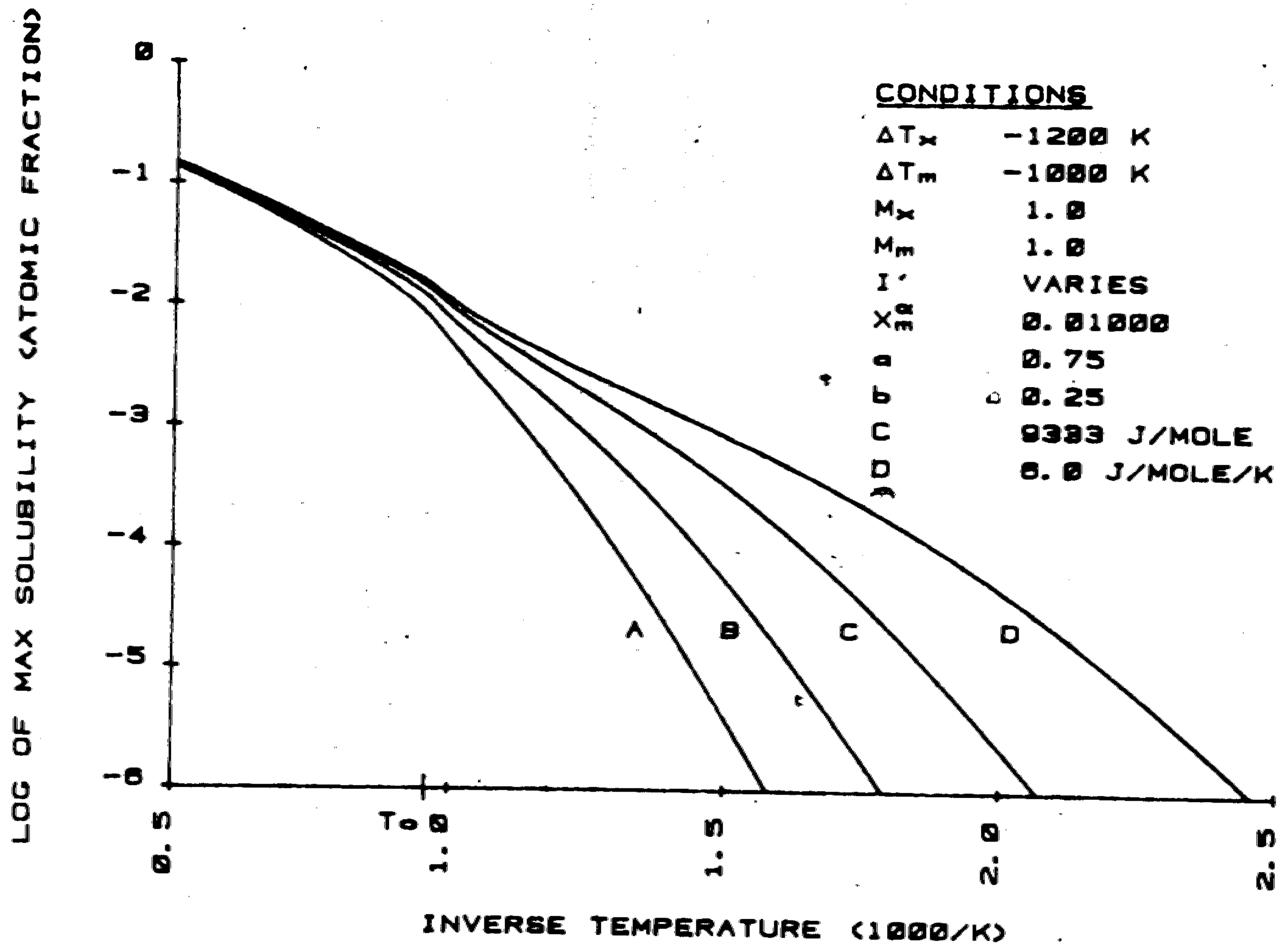

Figure 4.38
The effect of I' on the solubility of phosphorus in alpha Fe-0.01M-P (A = 100 KJ/mole, B = 75 KJ/mole, C = 50 KJ/mole, D = 25 KJ/mole).

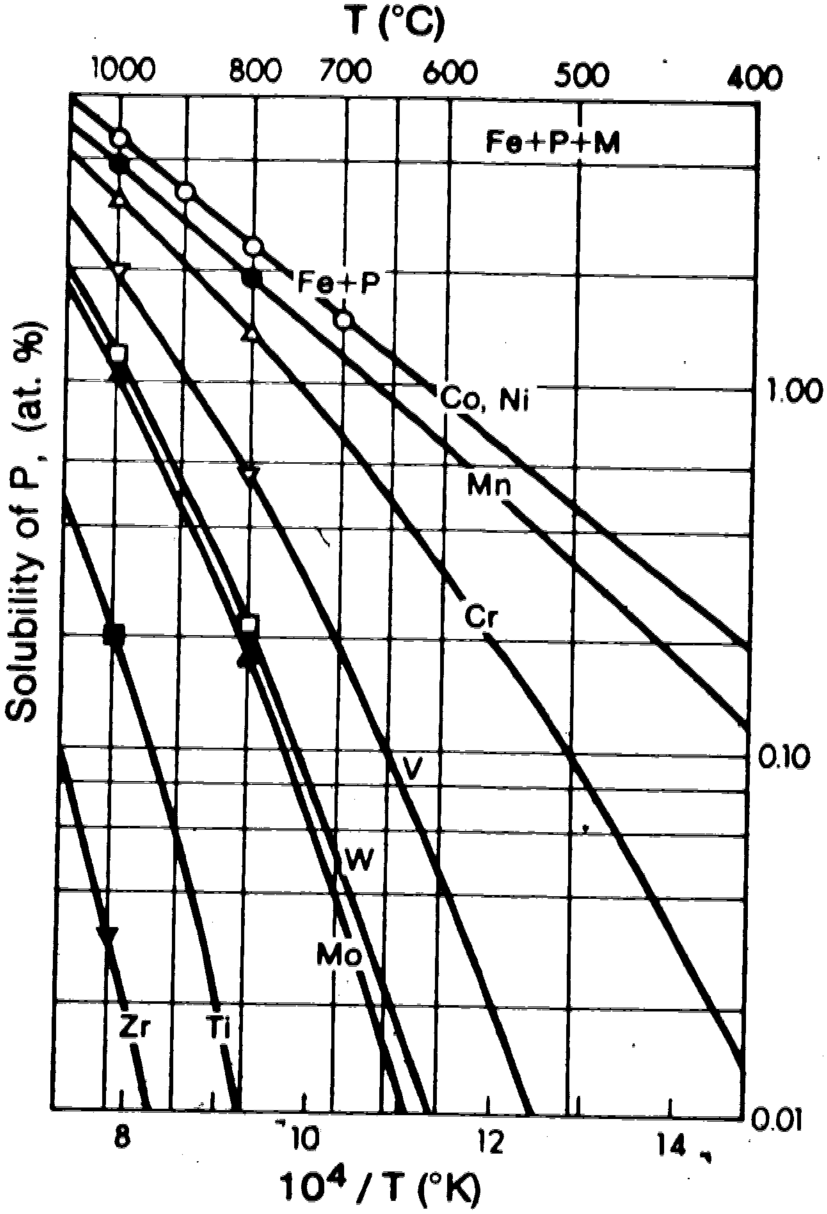

Figure 4.39 The experimental solid solubility of phosphorus for selected ternaries [23].

parameters (where available) for the metals. There is no direct relationship between I' and the magnetic parameter.

When considering Figure 4.39, it should be noted that all solubility determinations lie above the Curie temperature. Therefore, a calculated $\Delta G'$ represents a value close to its paramagnetic limit. However, there are still some short range magnetic interactions taking place. In general, the magnetic component of $\Delta G'$ raises the total value of $\Delta G'$. The calculated values of I' should be therefore considered high. A paramagnetic I' being defined constant is, in fact, a type of zeroth approximation with respect to temperature. A future consideration may be the determination of an I' that is linear with system temperature (i.e. a first approximation). In the present work, Guttmann's values of I' will be used when combining magnetic and chemical effects in real systems. Figure 4.40 shows the calculated solid solubility of P in selected alpha Fe-0.01M-P systems. At temperatures above the system Curie temperature, the solubility curves are very similar to those in Figure 4.39. However, below the Curie temperature, the predicted curves deviate greatly.

Of special interest is the Fe-V-P system. The magnetic parameter for small amounts of vanadium should be approximately +1000 K. A positive magnetic parameter raises the solubility limit of P. Therefore, although the Cr curve depends on a smaller I', it also depends on a smaller magnetic parameter, and at some low temperature actually

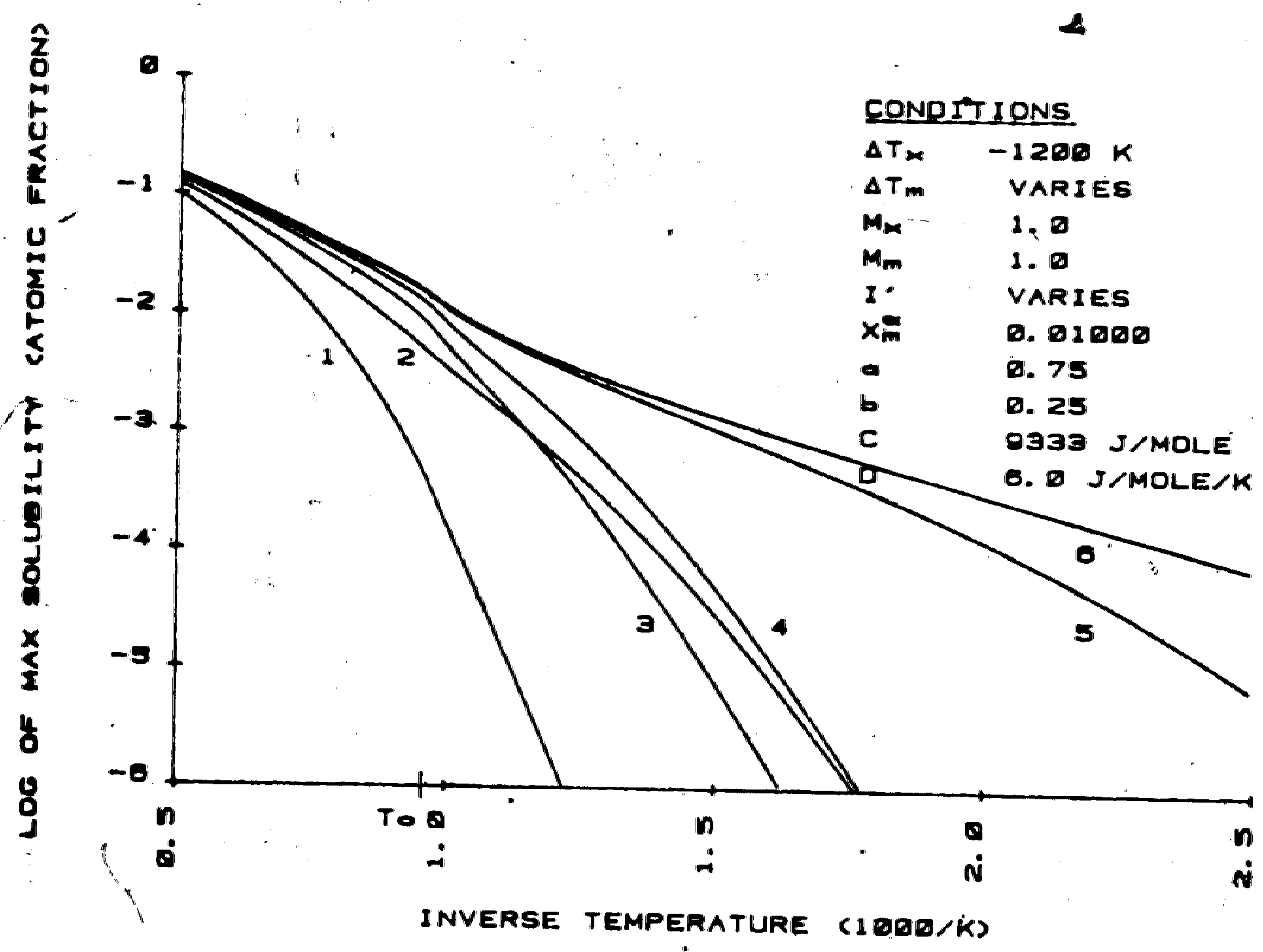

Figure 4.40
The predicted solubility of P in selected alpha Fe-0.01M-P ternaries (1 = Fe-Mo-P, 2 = Fe-V-P, 3 = Fe-Cr-P, 4 = Fe-Mn-P, 5 = Fe-Ni-P, 6 = Fe-P).

crosses below the V curve. Two specific examples of alpha Fe-M-P systems are now shown. Dashed lines in the next two figures represent the paramagnetic limits of solid solubility. Figure 4.41 exhibits the predicted alpha Fe-Mo-P systems and Figure 4.42 the predicted Fe-V-P system. It is clear that ferromagnetism can either raise or lower the solubility depending on the magnetic parameter.

4.12 Vacancy Concentration in alpha Fe-X

The following treatment for ternary systems corresponds to that found in section 4.5 for binaries. That is, consider a hypothetical alpha Fe-X solid solution, denoted A, that contains no vacancies at any temperature. Now, assume that vacancies introduced into the solution may be treated like a solute species. Therefore, one has an alpha Fe-X-v ternary solid solution. By analogy with an alpha Fe-M-X regular solid solution, the free energy of alpha Fe-X-v may be written as

$$\begin{aligned} G^T = {} & X_A {}^oG^A_{nm} + X_v {}^oG^v_{nm} + X_X {}^oG^X_{nm} + X_A X_X I^{AX}_{nm} + X_X X_v I^{Xv}_{nm} \\ & + X_A X_v I^{Av}_{nm} + RT[X_A \ell n X_A + X_X \ell n X_X + X_v \ell n X_v] \\ & + [1-M_v X_v][1-M_X X_X][G^{Fe}_{mag}(T^T)-[\Delta T_X X_X+\Delta T_v X_v]^u S^{Fe}_{mag}] \quad (4.143) \end{aligned}$$

The equilibrium vacancy concentration occurs where the ternary free energy is a minimum with respect to the vacancy concentration. Again, a dilute bulk approximation may be applied, $X_A \sim 1-X_X$, and the free energy of the alpha Fe-X

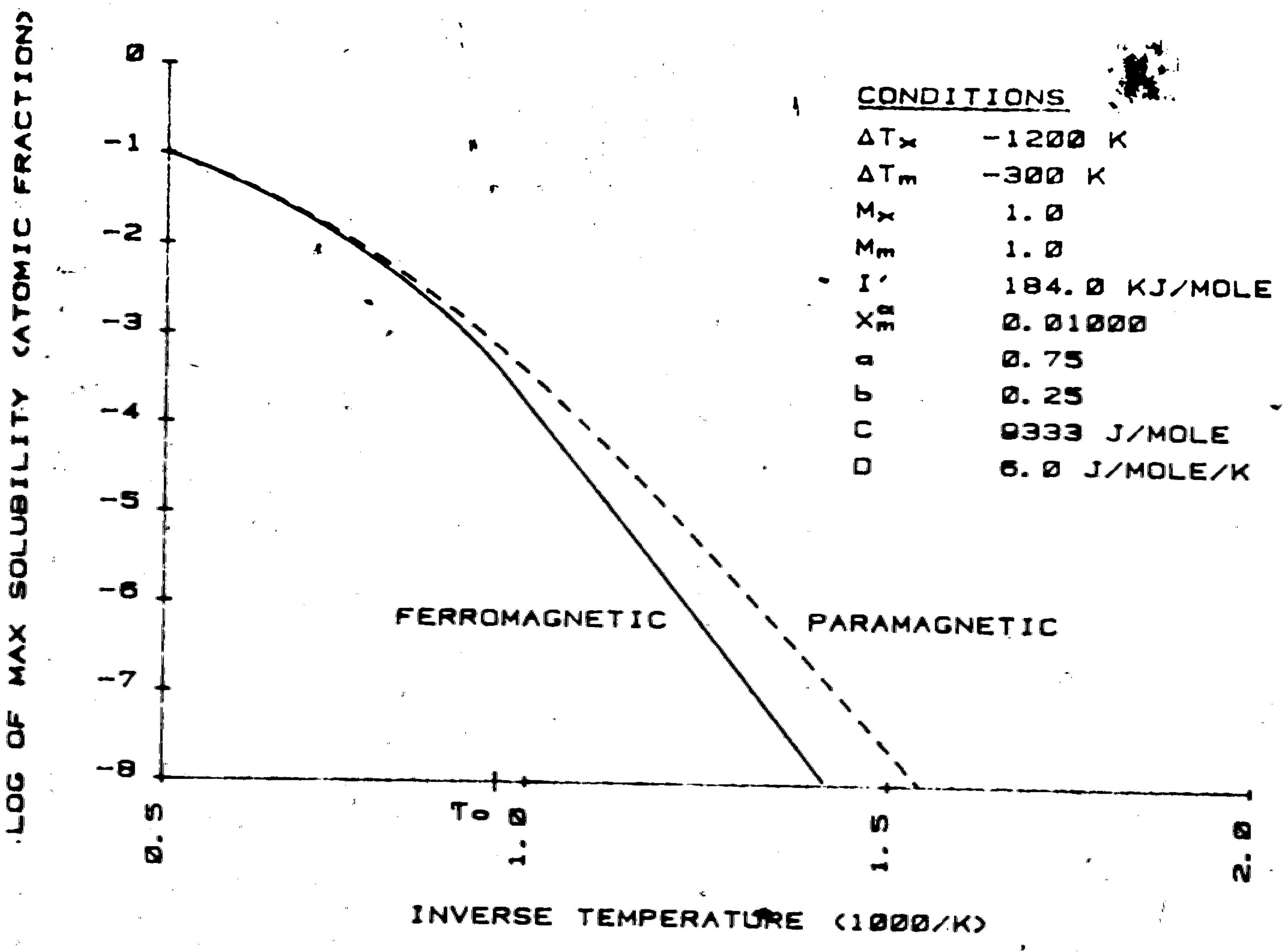

Figure 4.41
The predicted solubility of P in Fe-0.01Mo-P.

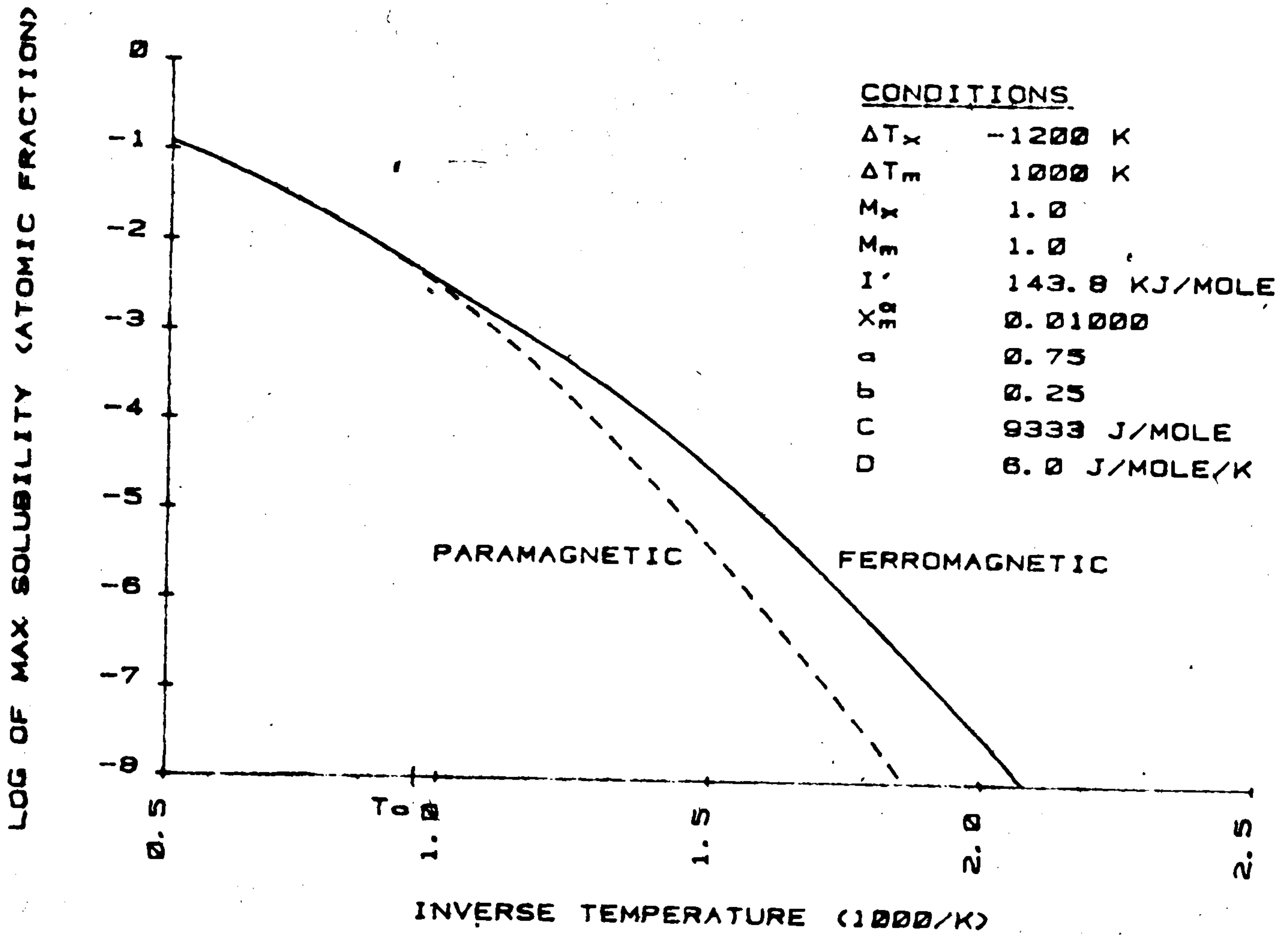

Figure 4.42
The predicted solubility of P in alpha Fe-0.01V-P.

solution approximates that of the hypothetical solution. Therefore, the derivative may be written as

$$\frac{\partial G^T}{\partial X_v} = RT\ell n X_v + RT\ell n(1-X_M) + Q_{nm} + Q_{mag} = 0 \tag{4.144}$$

where the magnetic component of Q is

$$Q_{mag} = [1-M_X X_X]\{-G^{Fe}_{mag}(T^T) + [\Delta T_v - \Delta T_X X_X][S^{Fe}_{mag}(T^T) - {}^{u}S^{Fe}_{mag}]\} \tag{4.145}$$

The equilibrium concentration of vacancies is given by

$$X_v = [1-X_M]\exp(-[Q_{nm}+Q_{mag}]/RT) \tag{4.146}$$

This equation is similar to equation (4.68). A large negative magnetic parameter for the solute X slightly increases the vacancy concentration.[13]

If the solute is substitutional, the diffusion coefficient of X in alpha iron will depend on the vacancy concentration in the bulk. Therefore, the diffusion coefficient of X will behave in a manner similar to the self-diffusion coefficient of alpha iron. This has been observed experimentally for various species in Fe [35,66]. The definition of T^T is

$$T^T = T - \Delta T_X X_X - \Delta T_v X_v$$

---

[13] There is a solute-vacancy attraction.

4.13 Grain Boundary Segregation in Alpha Fe-M-X Solid Solutions

The thermodynamic analysis of section 4.6 is now applied to ternary solutions of alpha iron. The segregation free energy as defined in equation (4.85) depends on the standard free energies of the solute components and their interaction parameters. Guttmann [17] proposed that the segregation free energies for an alpha Fe-M-X system may be approximated by

$$\Delta G^X = {}^o\Delta G^X + I'[X_M^\phi - X_M^\alpha]$$

$$\Delta G^M = {}^o\Delta G^M + I'[X_X^\phi - X_X^\alpha] \qquad (4.147)$$

in a competitive model.[14] I′ is a preferential interaction parameter for solute X and M such that

$$I' = I^{MX} - I^{FeX} - I^{FeM} \qquad (4.148)$$

The effect of an attractive I′ interaction (positive I′) is to increase the segregation free energy and therefore the tendency of a solute to segregate. The effect of I′ on segregation free energy (in absence of magnetic interactions) is shown in Figure 4.43 for alpha Fe-M-X. The corresponding calculated grain boundary solute concentration curves for competitive segregation are given in Figure 4.44 These curves were produced by the program developed in the present work and they correspond exactly to Guttmann's

---

[14] In a non-competitive model, I′ is modified by the composition of an M-X compound.

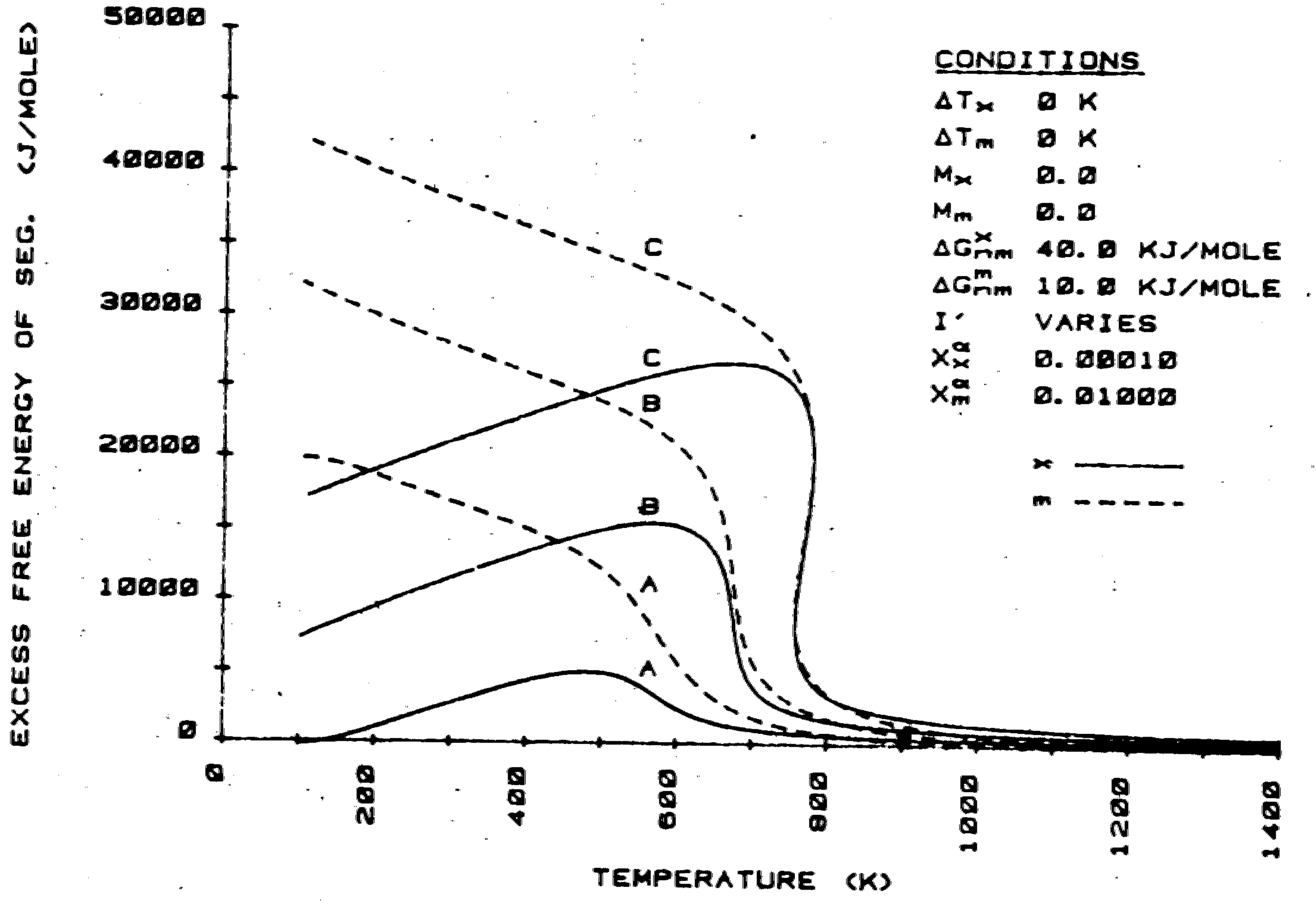

Figure 4.43
The effect of I′ on the segregation free energy for alpha Fe-0.01M-P (A = 20 KJ/mole, B = 40 KJ/mole, C = 60 KJ/mole).

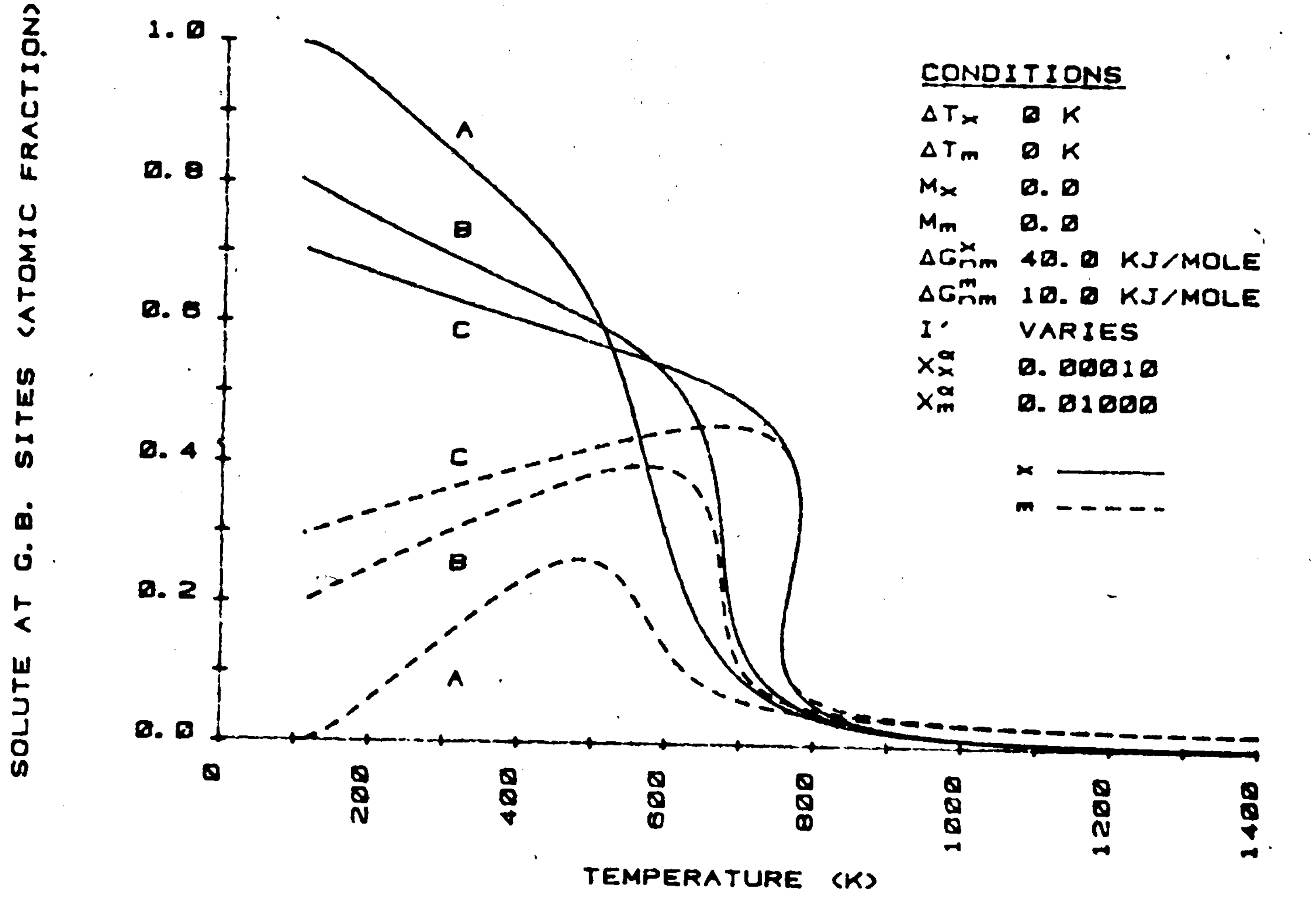

Figure 4.44
The effect of I' on the boundary solute content for alpha Fe-0.01M-P (A = 20 KJ/mole, B = 40 KJ/mole, C = 60 KJ/mole).

curves.

The assumption that the segregation free energies vary linearly with boundary solute content should allow I′ and standard segregation free energies to be determined experimentally. This, in fact, has been investigated by Guttmann [60] who determined that the standard segregation free energy for phosphorus is between 40 and 45 KJ/mole and for transition metals between 0 and 10 KJ/mole. These values will be used here for convenience. However, as is shown in the present analysis, segregation free energy does not vary linearly with boundary solute content. This is evident upon inspecting the magnetic component of segregation free energy. This affects the experimental determinations of both I′ and the standard free energies. Guttmann's free energy of segregation is approximately equivalent to a paramagnetic component of segregation free energy and is used as such in this work.

Guttmann's analysis is now applied to ternary alpha Fe-M-X solid solutions using the chemical potentials obtained in section 4.10. Chemical interactions are taken into consideration when examples of specific systems are exhibited.

4.13.1 Case I: Grain Boundary Free Energy Without Magnetic Terms

This approximation is considered for the same reasons stated in section 4.7.1, i.e. to obtain trends. The grain boundaries will be considered non-magnetic, i.e. they cannot take part in any magnetic interactions and there are no magnetic terms in the boundary free energies. Direct analytic solutions were therefore calculated. To obtain an equilibrium segregation equation, the following conditions are applied for some system temperature T,

$$\begin{aligned} \mu^{\phi X} &= \mu^{\alpha X} \\ \mu^{\phi M} &= \mu^{\alpha M} \\ \mu^{\phi Fe} &= \mu^{\alpha Fe} \end{aligned} \tag{4.149}$$

The chemical potentials from section 4.10 are defined, as in section 4.7.1, to be

$$\begin{aligned} \mu^{\phi X} &= {}^{o}\mu^{\phi X}_{nm} + RT\ell n X^{\phi}_{X} - \sigma\omega_{X} \\ &= {}^{o}\mu^{\alpha X}_{nm} + RT\ell n X^{\alpha}_{X} + \mu^{\alpha X}_{mag} \\ &= \mu^{\alpha X} \end{aligned} \tag{4.150}$$

$$\begin{aligned} \mu^{\phi M} &= {}^{o}\mu^{\phi M}_{nm} + RT\ell n X^{\phi}_{M} - \sigma\omega_{M} \\ &= {}^{o}\mu^{\alpha M}_{nm} + RT\ell n X_{M} + \mu^{\alpha M}_{mag} \\ &= \mu^{\alpha M} \end{aligned} \tag{4.151}$$

$$\begin{aligned} \mu^{\phi Fe} &= {}^{o}\mu^{\phi Fe}_{nm} + RT\ell n X^{\phi}_{Fe} - \sigma\omega_{Fe} \\ &= {}^{o}\mu^{\alpha Fe}_{nm} + RT\ell n X^{\alpha}_{Fe} + \mu^{\alpha Fe}_{mag} \\ &= \mu^{\alpha Fe} \end{aligned} \tag{4.152}$$

Again, by eliminating the surface tension terms and assuming the atomic structure of the grain boundary is not altered (all partial molar areas are equal), segregation equations are obtained,

$$\begin{aligned} RT\ell n(X_X^{\phi}X_{Fe}^{\alpha}/X_X^{\alpha}X_{Fe}^{\phi}) &= \Delta G_{nm}^{X} + {}^{I}\Delta G_{mag}^{X} \\ &= {}^{o}\mu_{nm}^{\alpha X} - {}^{o}\mu_{nm}^{\phi X} - {}^{o}\mu_{nm}^{\alpha Fe} + {}^{o}\mu_{nm}^{\phi Fe} + \mu_{mag}^{\alpha X} - \mu_{mag}^{\phi Fe} \qquad (4.153) \end{aligned}$$

$$\begin{aligned} RT\ell n(X_M^{\phi}X_{Fe}^{\alpha}/X_M^{\alpha}X_{Fe}^{\phi}) &= \Delta G_{nm}^{M} + {}^{I}\Delta G_{mag}^{M} \\ &= {}^{o}\mu_{nm}^{\alpha M} - {}^{o}\mu_{nm}^{\phi M} - {}^{o}\mu_{nm}^{\alpha Fe} + {}^{o}\mu_{nm}^{\phi Fe} + \mu_{mag}^{\alpha M} - \mu_{mag}^{\phi Fe} \end{aligned} \qquad (4.154)$$

The magnetic segregation free energy of solute X is given by

$$\begin{aligned} \Delta G_{mag}^{X} &= -M_X[1-M_M X_M^{\alpha}][G_{mag}^{Fe}(T^{\alpha}) - [\Delta T_X X_X^{\alpha} + \Delta T_M X_M^{\alpha}]{}^{u}S_{mag}^{Fe}] \\ &\quad + [1-M_M X_M^{\alpha}][1-M_X X_X^{\alpha}]\Delta T_X[S_{mag}^{Fe}(T^{\alpha}) - {}^{u}S_{mag}^{Fe}] \end{aligned} \qquad (4.155)$$

The segregation free energy of M is perfectly symmetrical to this expression (subscript X is replaced by subscript M, and vice versa). If the amount of non-magnetic solute X in the bulk is small, and applying the approximation in equation (4.35), then the segregation free energy becomes

$$\begin{aligned} \Delta G_{mag}^{X} &= -\,[1-M_M X_M^{\alpha}]\{G_{mag}^{Fe}(T) \\ &\quad + [\Delta T_M X_M^{\alpha} - \Delta T_X][S_{mag}^{Fe}(T^{\alpha}) - {}^{u}S_{mag}^{Fe}]\} \end{aligned} \qquad (4.156)$$

Therefore, unless the bulk content of M is very high, the magnetic segregation free energy of X is not very dependent on the magnetic parameter of M. An example of this situation is shown in Figure 4.45. These curves have the same shapes

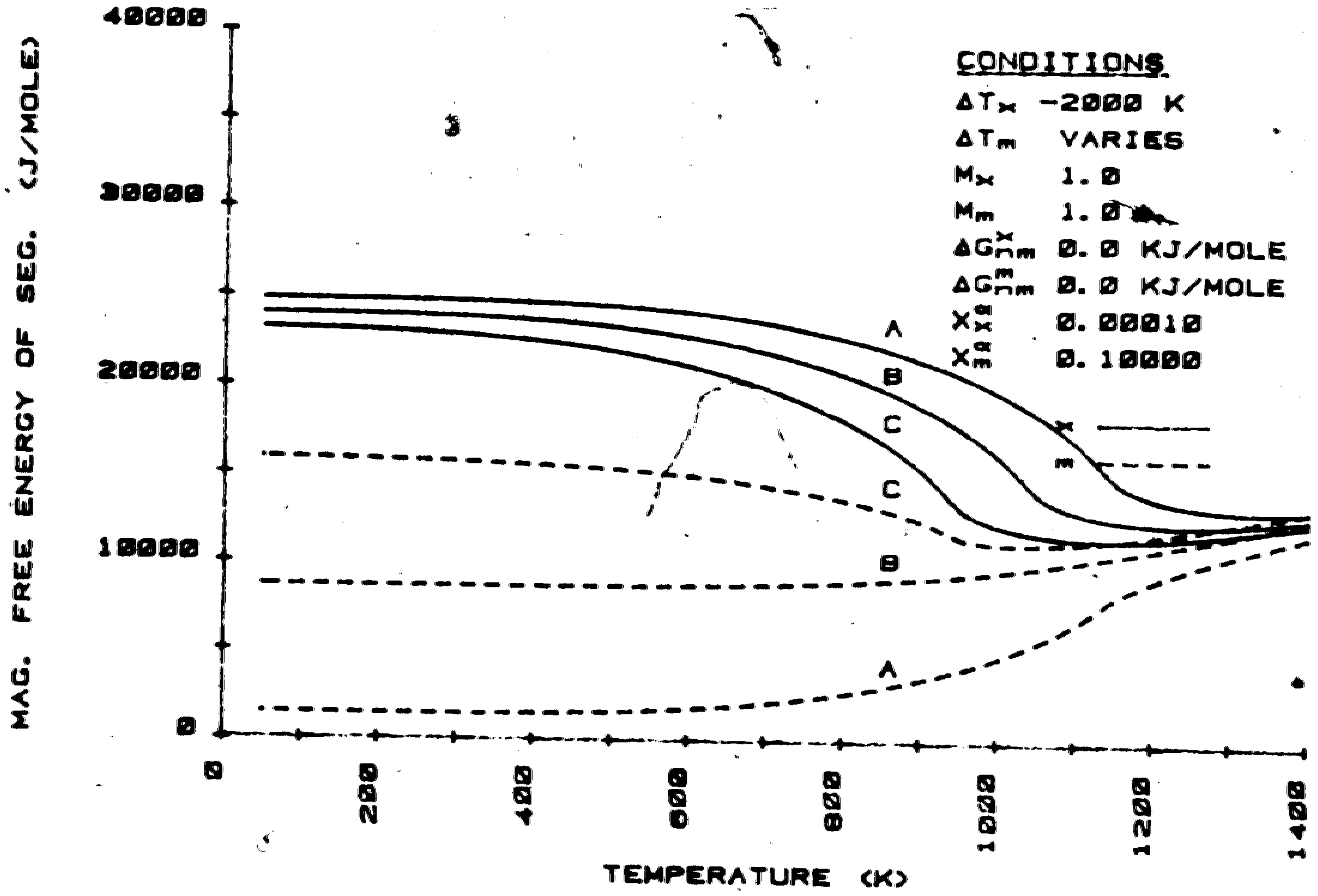

Figure 4.45
The effect of the magnetic parameter of M on the magnetic segregation free energy of X according to Case I (A = -1000 K, B = 0 K, C = 1000 K).

as observed in the analysis of binary solid solutions. The competitive boundary segregation curves corresponding to Figure 4.45 are shown in Figure 4.46. For the sake of comparison, the bulk solute content of M is set higher than that of X, simulating the situation where M is a transition metal alloying element and X is an impurity element. Due to competition, an M species with a large negative magnetic parameter will depress the grain boundary content of X. As the magnetic parameter of M becomes larger, the segregation curve for X approaches a limit which corresponds to the equivalent segregation curve in the alpha Fe-X binary.

The bulk content of one solute may also drastically affect the grain boundary concentration of the other. Figure 4.47 shows the behavior of predicted grain boundary solute concentrations with varying bulk content of M. A large amount of solute M in the bulk may reduce the grain boundary concentration of X especially at higher temperature. This may occur even if M has little effect on the magnetic properties of the solution (magnetic parameter of M is zero). This situation could be encountered where M is a metal alloying element and X an impurity element.

Case I, as outlined, points out the general trends of the effect of ferromagnetism on segregation. However, the shortcomings of Case I discussed for binary solutions are likewise present here. Therefore, Case II will now be considered.

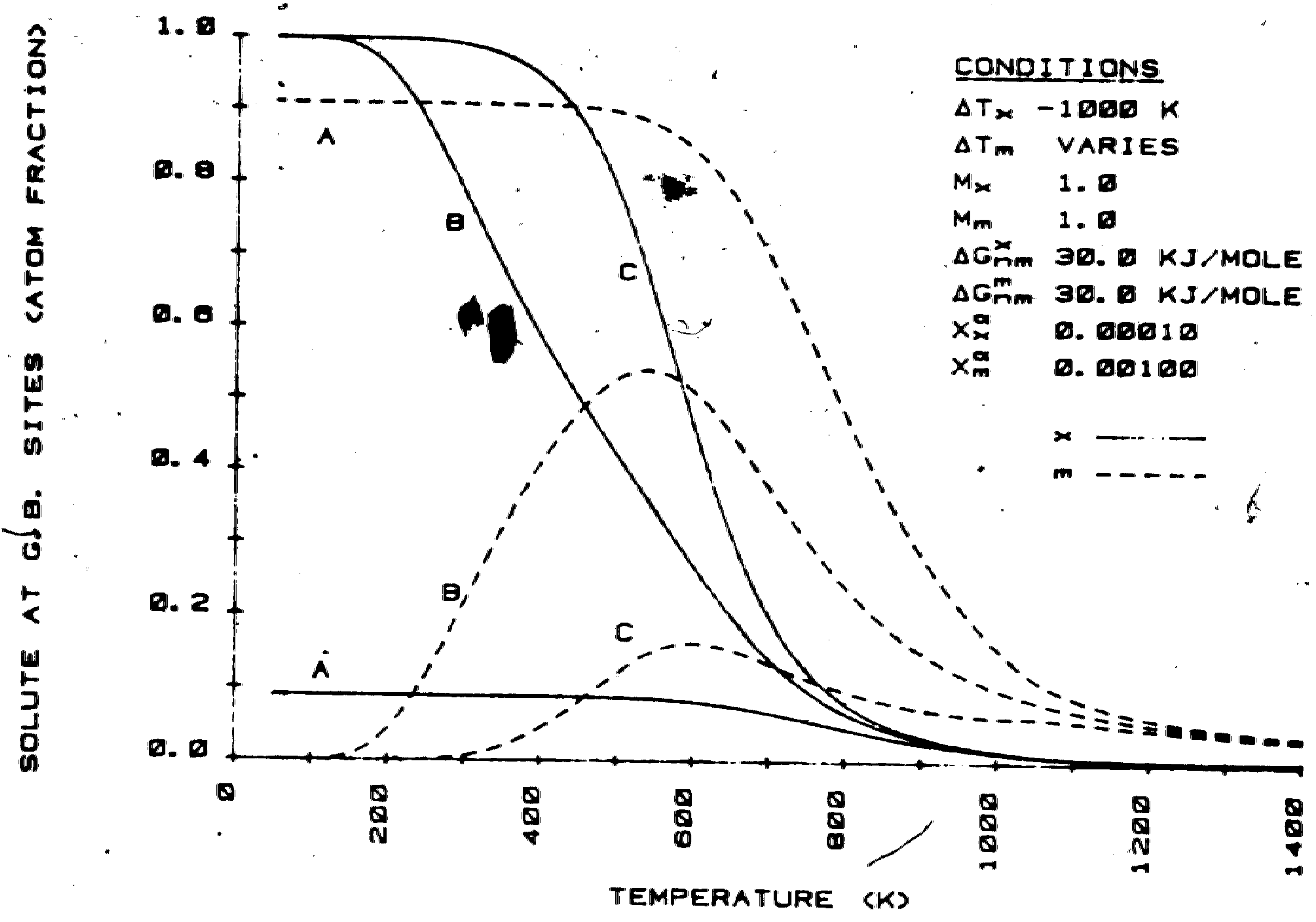

Figure 4.46
The effect of the magnetic parameter of M on boundary solute contents (A = -1000 K, B = 0 K, C = 1000 K).

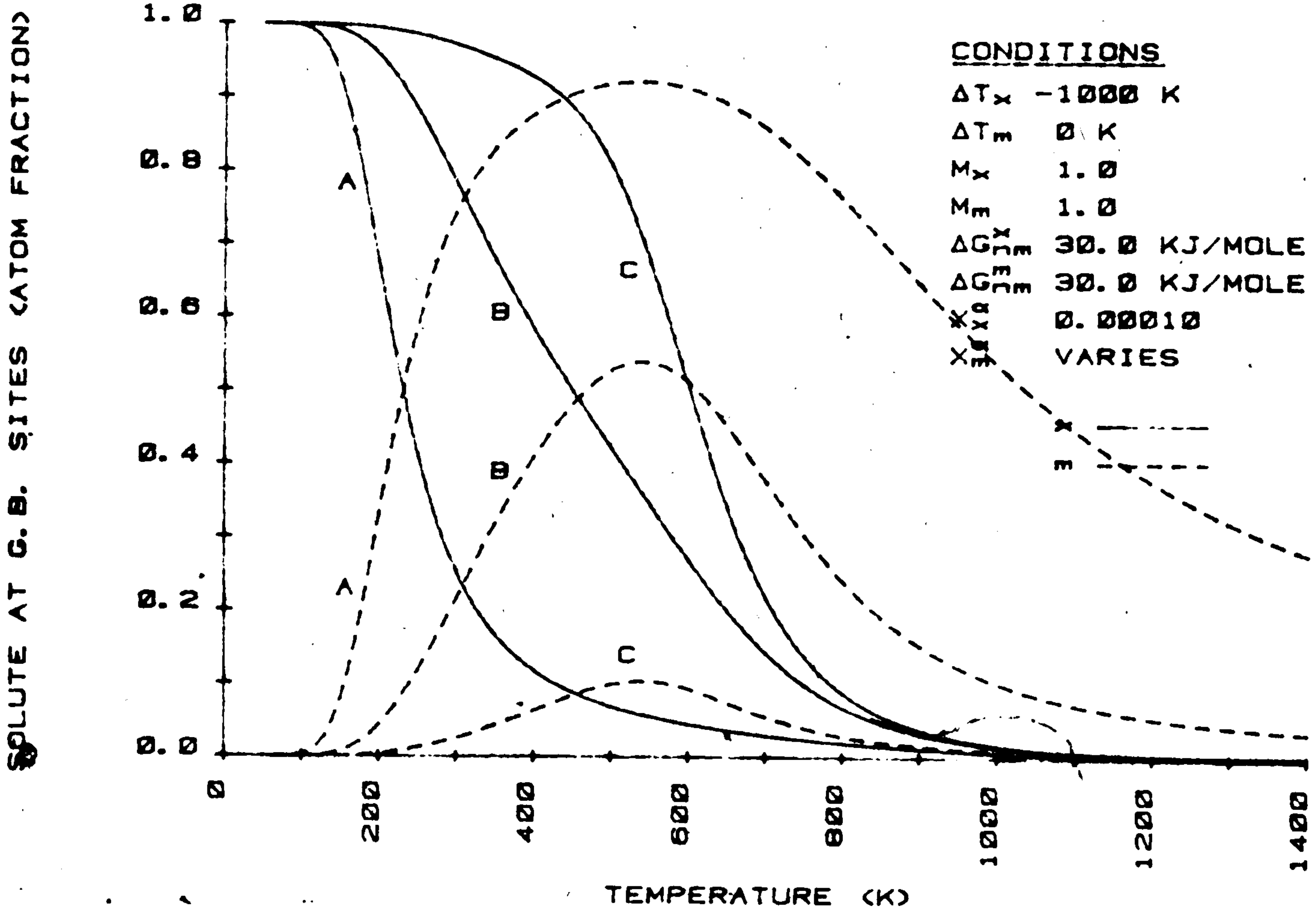

Figure 4.47
The effect of bulk content of M on the boundary solute contents according to Case I (A = 0.1, B = 0.01, C = 0.001).

4.13.2 Case II: Grain Boundaries May Be Ferromagnetic

As described in section 4.7.2, the only difference between a 2-d and a 3-d phase is the 2-d surface tension. The chemical potentials of the grain boundary species would have magnetic components and would be written analogously to the chemical potentials in section 4.10. The Guttmann analysis is again applied[15] and for a system temperature T, the equilibrium segregation equations result, from the conditions

$$\begin{aligned}\mu^{\phi i} &= {}^{o}\mu^{\phi i}_{nm} + RT\ell n X^{\phi}_{i} - \sigma\omega_{i} + \mu^{\phi i}_{mag}\\ &= {}^{o}\mu^{\alpha i}_{nm} + RT\ell n X^{\alpha}_{i} + \mu^{\alpha i}_{mag}\\ &= \mu^{\alpha i}\end{aligned} \qquad (4.157)$$

The magnetic segregation of solute X is given by

$$\begin{aligned}RT\ell n(X^{\phi}_{X}X^{\alpha}_{Fe}/X^{\alpha}_{X}X^{\phi}_{Fe}) &= \Delta G^{X}_{nm} + {}^{II}\Delta G^{X}_{mag}\\ &= {}^{o}\mu^{\alpha X}_{nm} - {}^{o}\mu^{\phi X}_{nm} - {}^{o}\mu^{\alpha Fe}_{nm} + {}^{o}\mu^{\phi Fe}_{nm}\\ &\quad + \mu^{\alpha X}_{mag} - \mu^{\alpha Fe}_{mag} - \mu^{\phi X}_{mag} + \mu^{\phi Fe}_{mag}\end{aligned} \qquad (4.158)$$

The magnetic free energy of segregation for solute M is symmetrical to the above equation with subscript X being replaced by M and vice versa. After treatment as in Case I,

---

[15] The partial molar areas for all species are equal.

$$
\begin{aligned}
{}^{II}\Delta G^{X}_{mag} = {} & M_X[1-M_M X^{\phi}_M][G^{Fe}_{mag}(T^{\phi})-[\Delta T_X X^{\phi}_X+\Delta T_M X^{\phi}_M]{}^{u}S^{Fe}_{mag}] \\
& - M_X[1-M_M X^{\alpha}_M][G^{Fe}_{mag}(T^{\alpha})-[\Delta T_X X^{\alpha}_X+\Delta T_M X^{\alpha}_M]{}^{u}S^{Fe}_{mag}] \\
& - [1-M_M X^{\phi}_M][1-M_X X^{\phi}_X]\Delta T_X[S^{Fe}_{mag}(T^{\phi})-{}^{u}S^{Fe}_{mag}] \\
& - [1-M_M X^{\alpha}_M][1-M_X X^{\alpha}_X]\Delta T_X[S^{Fe}_{mag}(T^{\alpha})-{}^{u}S^{Fe}_{mag}]
\end{aligned}
\tag{4.159}
$$

This equation cannot be evaluated directly but equation (4.85) must be considered for X and M, such that

$$
\begin{aligned}
X^{\phi}_X &= \frac{X^{\alpha}_X \exp({}^{II}\Delta G^{X}/RT)}{1-X^{\alpha}_X-X^{\alpha}_M+X^{\alpha}_X\exp({}^{II}\Delta G^{X}/RT)+X^{\alpha}_M\exp({}^{II}\Delta G^{M}/RT)} \\
X^{\phi}_M &= \frac{X^{\alpha}_M \exp({}^{II}\Delta G^{M}/RT)}{1-X^{\alpha}_X-X^{\alpha}_M+X^{\alpha}_X\exp({}^{II}\Delta G^{X}/RT)+X^{\alpha}_M\exp({}^{II}\Delta G^{M}/RT)}
\end{aligned}
\tag{4.160}
$$

are solved simultaneously for roots. This is a somewhat more difficult numerical analysis than performed in the binary case.

Figure 4.48 shows the magnetic segregation free energies of alpha Fe-M-X as a function of temperature and magnetic parameter of M. As in Case I, large negative magnetic parameters lead to larger segregation free energies. The general shapes of the binary curves are retained. However, since X and M interact and are competitive, a reduced magnetic segregation free energy for M (due to a larger magnetic parameter of M) reduces the magnetic segregation free energy for X. These curves may have steps and a complex behavior (due to magnetic

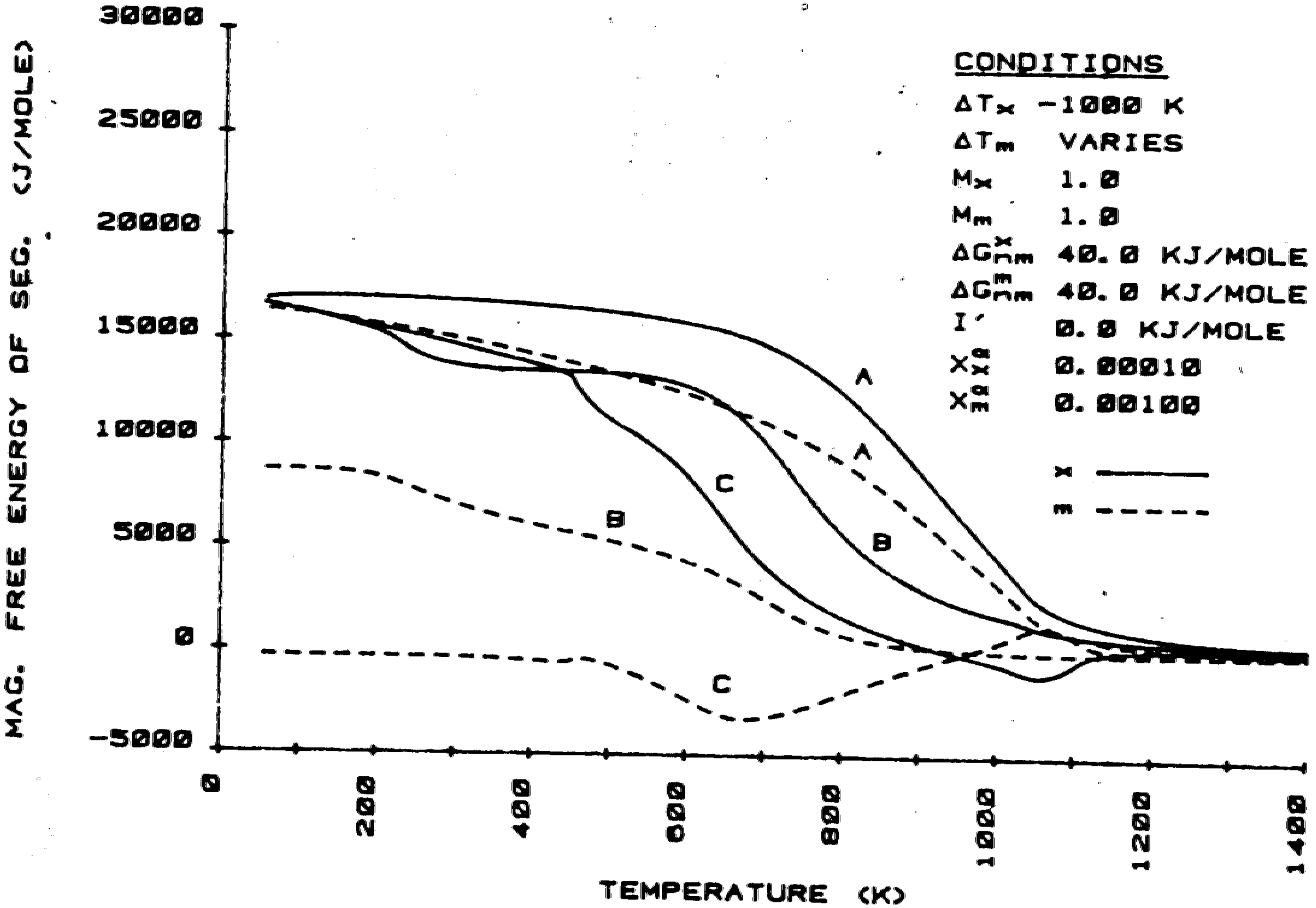

Figure 4.48
The effect of the magnetic parameter of M on the magnetic segregation free energy according to Case II (A = -1000 K, B = 0 K, C = 1000 K).

interaction and site competition). Figure 4.49 is the corresponding grain boundary solute content curve. Curves A show that similar solute share grain boundary sites. A large difference in segregation free energies usually allows one solute species to 'win out' over the other. The effect of bulk content of M on the magnetic segregation free energies is shown in Figure 4.50 and the corresponding grain boundary segregation curves in Figure 4.51. It is evident that in a competitive model even solute M with a zero magnetic parameter but large bulk content may reduce the boundary content of X. A similar effect from the non-magnetic segregation free energy of M is shown in Figure 4.52.

In a noncompetitive situation, the grain boundary segregation curves are similar to the binary segregation curves. That is, the segregation curve for each solute is shifted when the segregation free energy for that solute is modified by considering magnetic terms. The effect of one solute on the other is small unless there is a strong (usually chemical) interaction between the solute. In such a case, the strongly segregating solute 'drags' the other solute to the boundary, so that the segregation of the weakly segregating solute is enhanced.

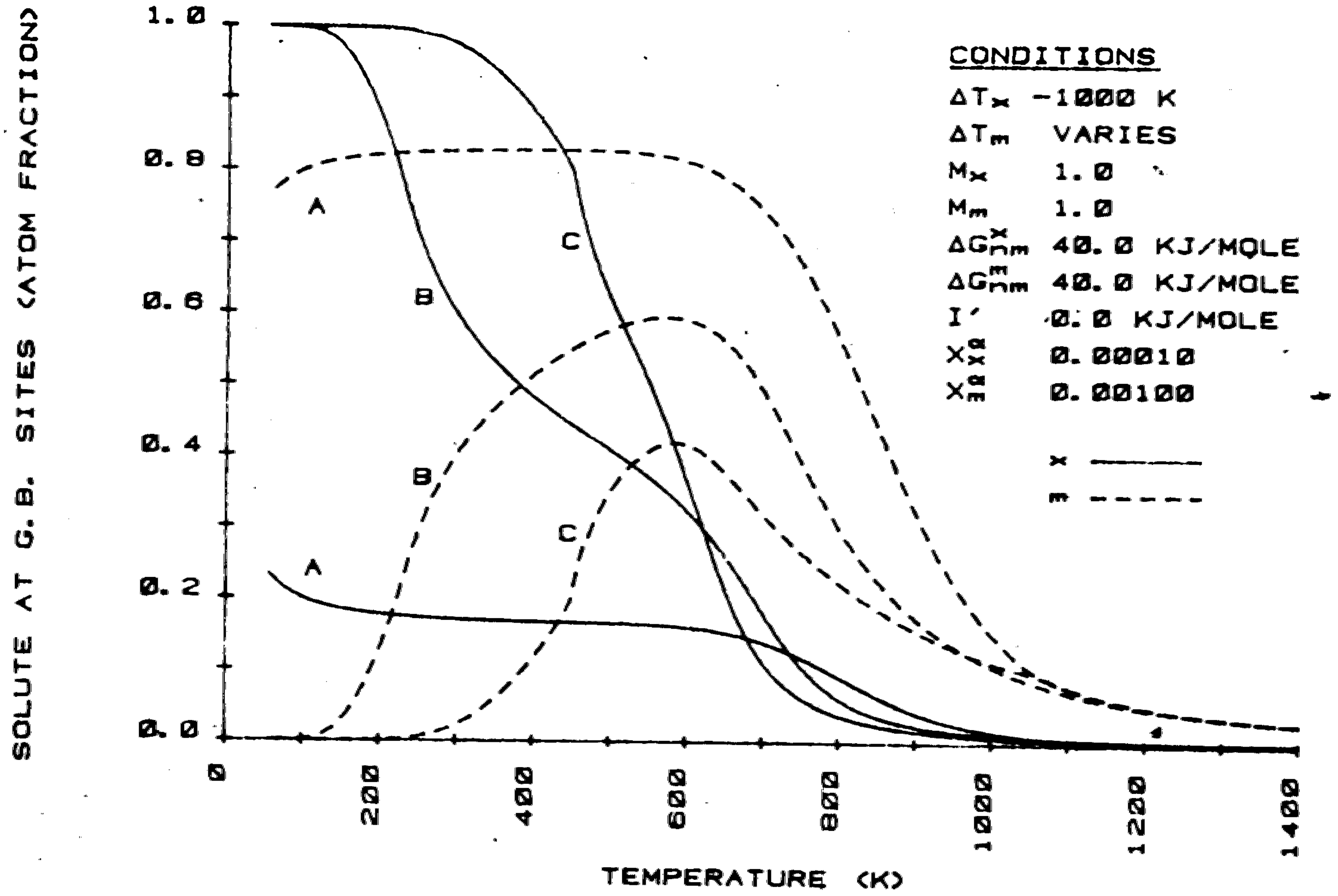

Figure 4.49
Predicted grain boundary solute contents for alpha Fe-0.01M-X according to Case II (A = -1000 K, B = 0 K, C = 1000 K).

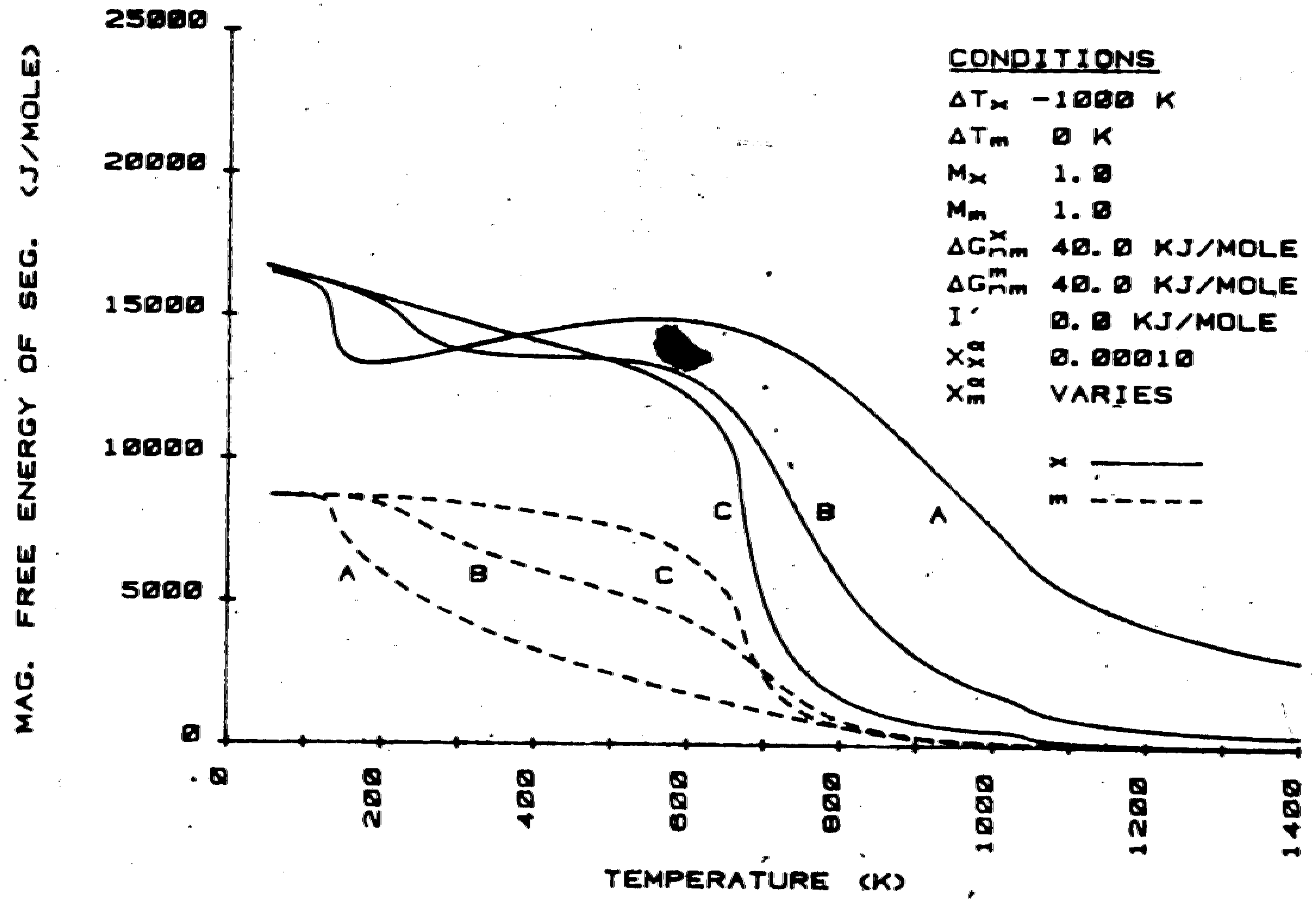

Figure 4.50
The effect of bulk content of solute M on the magnetic segregation free energies according to Case II (A = 0.1, B = 0.01, C = 0.001).

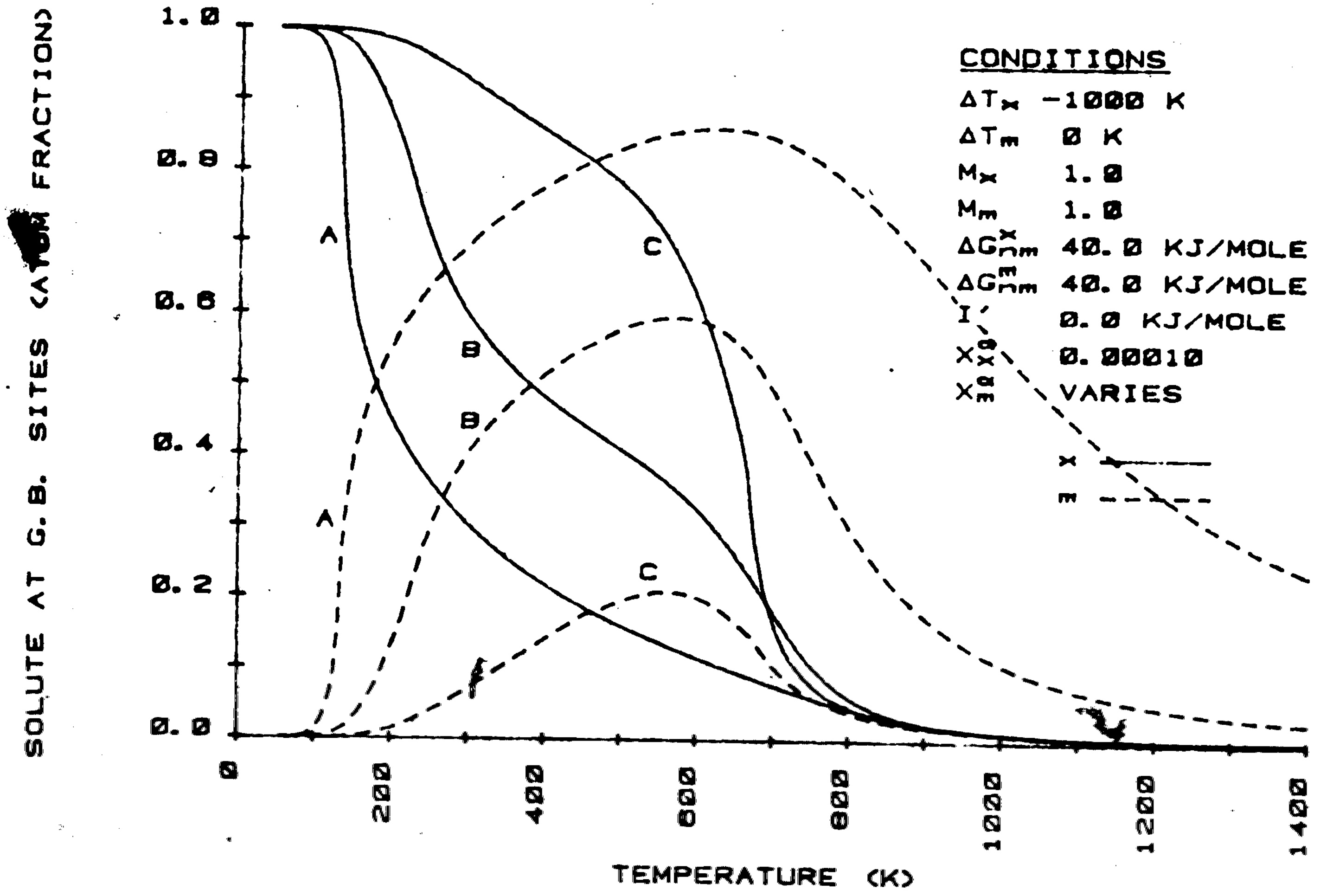

Figure 4.51
The effect of bulk content of M on grain boundary segregation according to Case II (A = 0.1, B = 0.01, C = 0.001).

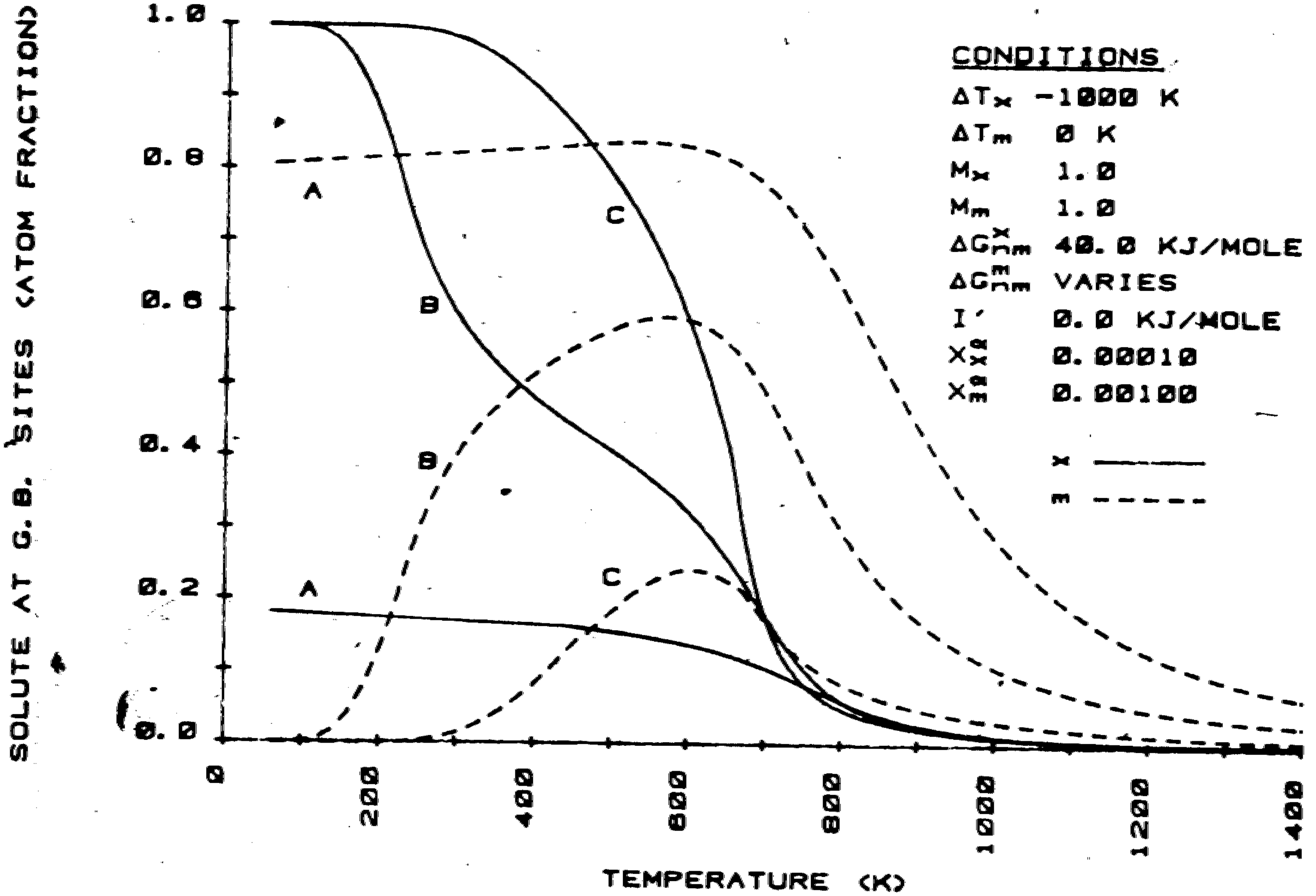

Figure 4.52
The effect of the non-magnetic segregation free energy of M on grain boundary solute content acccording to Case II (A = 50 KJ/mole, B = 40 KJ/mole, C = 30 KJ/mole).

4.14 Predicted Grain Boundary States in Certain Ternary Systems

As outlined in section 4.8, the state of a grain boundary is dependent on its solute content. The same possibility exists that boundaries rich in solute can achieve a transition to the paramagnetic state as segregation causes the Curie temperature of the boundary to fall below the system temperature. The grain boundary Curie temperature for an alpha Fe-M-X is

$$T_c^{\phi} = T_c^{Fe} + \Delta T_X X_X^{\phi} + \Delta T_M X_M^{\phi} \qquad (4.161)$$

No simple criteria for transition may be applied to ternary segregation curves as was the case in the binary model. This is due to the complex relationship between the various grain boundary solute concentrations.

It is possible, however, to represent the transitions as was done for binaries in Figure 4.33. Figure 4.53 shows the equilibrium grain boundary segregation curves equivalent to the segregation curves in Figure 4.52. With lowering temperatures, the paramagnetic to ferromagnetic to paramagnetic transitions are easily seen.

Three specific competitive alpha Fe-.01M-P systems are now considered. Figure 4.54 shows the predicted grain boundary concentration of P for alpha Fe-.01Ni-.0001P under chemical, magnetic or both types of interactions. As is immediately evident, the magnetic interaction significantly shifts the segregation curve to higher temperatures

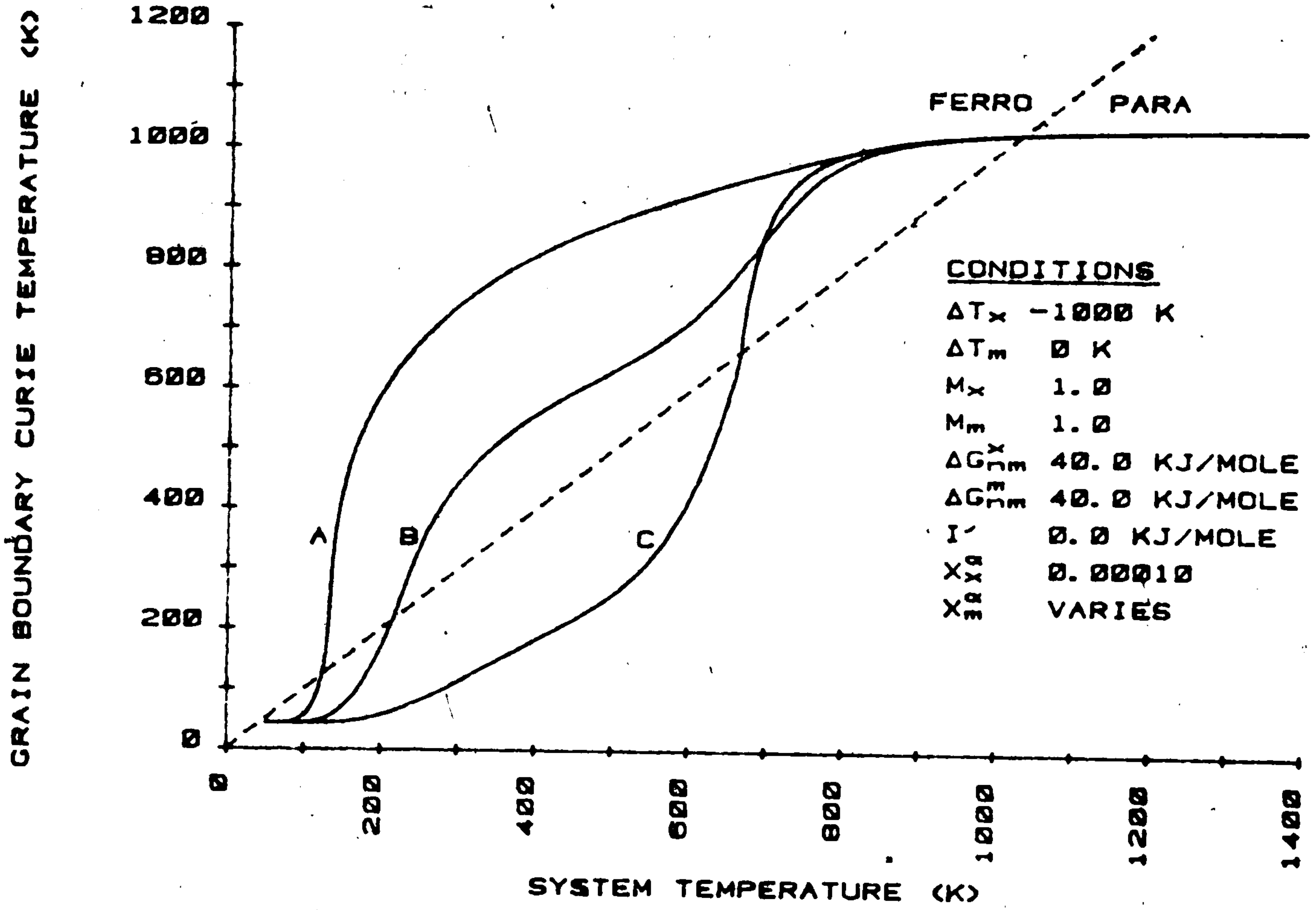

Figure 4.53
The effect of bulk content of M on the equilibrium grain boundary Curie temperature (A = 0.1, B = 0.01, C = 0.001).

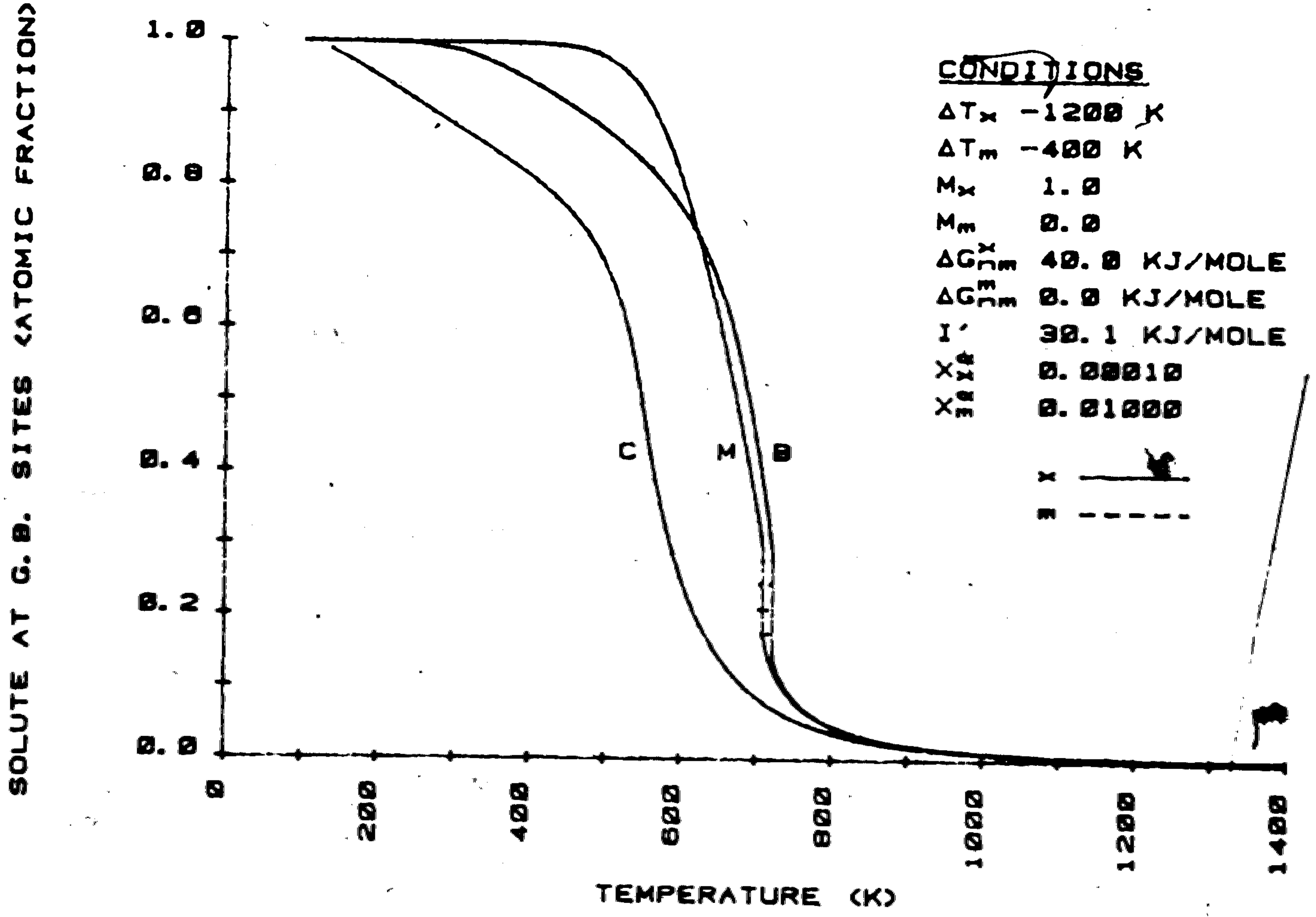

Figure 4.54
Predicted grain boundary content of P in alpha Fe-Ni-P according to Case II (C = chemical only, M = magnetic only, B = chemical and magnetic).

(increases segregation). In this situation, the magnetic interaction is stronger than the chemical interaction.

The second example concerns alpha Fe-.01[illegible]-.0001P. Figure 4.55 shows the predicted grain boundary concentration of P under the various interaction possibilities. The magnetic and chemical interactions are of the same order of strength. The combination of both interactions shifts the segregation to significantly higher temperatures.

However, the third example shows an alpha Fe-.01Cr-.0001P system. Figure 4.56 indicates that the excess chemical segregation free energy has more impact on the grain boundary composition than the magnetic segregation free energy. The calculated segregation curve is still significantly shifted to higher temperatures (dotted line) but the step or transition temperature is not as affected. Figure 4.57 shows the corresponding equilibrium Curie temperature curves. This indicates that strong chemical effects may also reduce the range over which the grain boundary may be ferromagnetic.

A word must be said about the steps occurring in the previous figure. When the segregation curve shows a non-function relation, that is, when there is more than one grain boundary composition possible for a system temperature, the solid solution becomes metastable. The stable configuration requires two solid solutions with a transition occurring at the inflection in the segregation curve. This point occurs at the mid-point of the S-shaped